TECHNISCHE UNIVERSITÄT MÜNCHEN

FAKULTÄT FÜR CHEMIE

MOLEKULARE KATALYSE

Abnormal *N*-Heterocyclic Carbene Ligands in Heterobimetallic Complexes and Ruthenium Catalyzed Hydrogen Transfer Reactions

LORENZ PARDATSCHER

Vollständiger Abdruck der von der Fakultät für Chemie der Technischen Universität München

zur Erlangung des akademischen Grades eines

Doktors der Naturwissenschaften (Dr. rer. nat.)

genehmigten Dissertation.

Vorsitzender: Prof. Dr. Tom Nilges

Prüfer der Dissertation: 1. Prof. Dr. Fritz E. Kühn

2. Prof. Dr. Walter Baratta

Die Dissertation wurde am 11.07.2019 bei der Technischen Universität München eingereicht und durch die Fakultät für Chemie am 02.09.2019 angenommen.

Die vorliegende Arbeit wurde am Arbeitskreis für Molekulare Katalyse der Technischen Universität München im Zeitraum von Dezember 2016 bis Juli 2019 angefertigt.

Ich danke meinem Doktorvater **Prof. Dr. Fritz E. Kühn** für die unkomplizierte Aufnahme in seine Arbeitsgruppe, für die finanziell sorgenfreie Arbeit in einem äußerst angenehmen Arbeitsumfeld und für die Möglichkeit mein Forschungsthema frei gestalten und meine Ziele uneingeschränkt verfolgen zu können.

Genauso danken möchte ich **Prof. Dr. Walter Baratta** für seinen fachlichen Rat, die vielen guten Ideen und die schöne und fruchtbare Zeit an der Università degli Studi di Udine. Mit seiner herzlichen Art hat er mich stets motiviert, mich kurzfristig in sein Labor aufgenommen und sich mit viel Zeit und Geduld meiner Forschung gewidmet.

Zu den wohl wichtigsten Menschen gehören meine Studienfreunde: **Fabi**, **Gitti**, **Jens**, **Annika**, **Kathi**, **Michl**, **Lara**, **Gerdi**, **Mara**, **Sebi**, **Christina** und **Zani**. Danke, dass ihr mich sofort in euren Freundeskreis mit aufgenommen habt. Dank euch war und ist meine Zeit in München einfach wunderbar. Ich hoffe und bin zuversichtlich, dass diese Freundschaften auch nach unserer gemeinsamen Zeit an der TUM fortbestehen.

Ich danke meinen **Eltern** für den Rückhalt und das große Vertrauen, das ich seit meiner Kindheit genieße. Ihr habt mir immer jede Freiheit gegeben und mich bei allem unterstützt. Ihr habt mir das Durchhaltevermögen vermittelt, das mich durch das Studium begleitet hat und mich schließlich zu dem gemacht, der ich heute bin. Genauso danke ich dafür meinen Geschwistern **Stefanie**, **Franz** und **Sophie**. Ihr wart und seid jederzeit völlig bedingungslos für mich da.

Zuletzt und am allermeisten danke ich **Anna**. Du machst mich glücklich. Zusammen mit dir blicke ich sorglos in eine wundervolle Zukunft.

Table of Contents

List of Abbreviations

aNHC	abnormal *N*-heterocyclic carbene
Ar	aromatic
cod	cyclooctadiene
conv	conversion
CV	cyclic voltammetry
DFT	density functional theory
DIPP	2,6-Diisopropylphenyl
Dppe	diphenylphosphano ethane
DPV	differential pulse voltammetry
eq	equivalent
et al.	et alii, et aliae (and others)
GC	gas chromatography
M	metal
Me	methyl
Mes	2,4,6-trimetylphenyl (Mesityl)
MPV	Meerwein-Ponndorf-Verley reduction
NHC	*N*-heterocyclic carbene
NHDC	*N*-heterocyclic dicarbene
NMR	nuclear magnetic resonance
OAc	acetate
ORTEP	Oak Ridge thermal ellipsoid plot
Ph	phenyl
ppm	parts per million
RT	room temperature (25 °C)
TH	transfer hydrogenation
TM	transition metal
TOF	turnover frequency
VT	variable temperature

Zusammenfassung

Die Entwicklung von Katalysatoren, um den Energieaufwand chemischer Prozesse zu verringern, ist die beste Investition in eine nachhaltige Zukunft im Einklang mit einem ausgeprägten Wohlstand für breite Teile der Weltbevölkerung. Ein wichtiger chemischer Prozess ist die Reduktion von ungesättigten Verbindungen durch die Hydrierung. Obwohl Wasserstoff das häufigste Element im Universum ist, tritt dieser auf der Erde nicht natürlich auf und muss in äußerst energieaufwändigen Prozessen hergestellt werden. Alternativ, können chemische Wasserstoffdonoren als Reduktionsmittel in der sogenannten Transferhydrierung verwendet werden. Ein ähnlicher Ansatz kann auch für die Rückreaktion, der oxidativen Dehydrierung von funktionellen Gruppen angewandt werden. Aceton ersetzt als Oxidationsmittel dabei Mangan- und Chromsalze, welches die Erzeugung großer Mengen an toxischen Abfallprodukten vermeidet. Diese Oxidations- und Reduktionsreaktionen laufen zudem unter sehr milden Reaktionsbedingungen ab und sind demnach tendenziell umweltfreundlich. Eine ganze Reihe von Übergangsmetallkomplexen ist in den letzten Jahren entwickelt worden, welche entweder die Oxidation von Alkoholen oder die Reduktion von Carbonylverbindungen katalysieren. Im Rahmen dieser Arbeit wurden Ruthenium- und Iridiumkomplexe auf Basis N-heterocyclischer Carbenliganden (NHC) synthetisiert und in beiden katalytischen Wasserstofftransferreaktionen untersucht.

Eine generell anwendbare Syntheseroute hin zu heterobimetallischen N-heterocyclischen Dicarbenkomplexen (NHDC) ausgehend von abnormalen NHC-Komplexen (aNHC) wurde im Laufe dieser Dissertation entwickelt. Die positive Ladung der Komplexe spielt dabei eine zentrale Rolle für die Reaktivität gegenüber Ag$_2$O und ein stark ins Tieffeld verschobenes Signal für das NCHN Proton im ^{1}H NMR-Spektrum weist auf diese Reaktivität hin. Die elektronischen Eigenschaften der Komplexe wurden durch voltammetrische Experimente analysiert und bestätigten die vorhandenen elektronischen Wechselwirkungen zwischen den beiden Metallen. Alle neuen Komplexe wurden katalytisch getestet, um den Einfluss des zweiten Metalls auf die katalytische Reaktivität zu bestimmen. Das zweite Metall hat einen positiven Einfluss auf die Stabilität der Katalysatoren, aber keinen oder negativen Einfluss auf dessen Aktivität. Kooperative Interaktionen zwischen den Metallen wurden demnach nicht gefunden.

Die Einführung eines zweiten aNHC Liganden führte zu einem außerordentlich aktiven di-aNHC Ruthenium Katalysator für Wasserstofftransferreaktionen. Der C_2-symmetrische Komplex ist der derzeit aktivste NHC Ruthenium Komplex für die Transferhydrierung von Ketonen und erreicht Umsatzraten bis zu $1{,}3 \cdot 10^6$ h^{-1}. Noch bemerkenswerter ist dessen Aktivität in der Oppenauer Oxidation, bei der für die Dehydrierung von Alkoholen Umsatzraten bis zu $5{,}5 \cdot 10^5$ h^{-1} bei einer Katalysatorbeladung von nur 0,01 mol% und dem Einsatz von lediglich zwei Äquivalenten Aceton erreicht werden. Diese Aktivität

übertrifft alle bisherigen Katalysatoren um eine Größenordnung. Auf Basis stichhaltiger NMR-spektroskopischer Daten und DFT-Rechnungen wird ein bifunktioneller Katalysemechanismus postuliert, welcher eine C-H Aktivierung an den Phenylgruppen der Phosphanliganden miteinbezieht. Zudem wird ein Deaktivierungsmechanismus vorgestellt, welcher die Notwendigkeit abnormaler Koordination der NHC Liganden für eine hohe katalytische Aktivität ist. Die Änderung des Koordinationsmodus hin zur normalen Koordination führt zur nahezu vollständigen sterischen Abschirmung des reaktiven Zentrums durch die Mesitylgruppen am NHC.

Abstract

Catalysis is the research area that continuously contributes to a more sustainable future with a steadily increasing wealth for an increasing share of the world's population by reducing the energy input necessary for chemical transformations. One of the most fundamental transformations in organic synthesis is the reduction of unsaturated compounds by hydrogenation. Despite being the most abundant element in the universe, dihydrogen is not naturally available on earth and must be synthesized in energy intensive processes. As an alternative, chemical hydrogen donors can be used as reducing agents in the so-called transfer hydrogenation (TH). Typical donor molecules are ^{i}PrOH, which is oxidized to acetone, and formic acid, which upon dehydrogenation releases CO_2. A similar approach of hydrogen transfer from one molecule to another can be used for the reverse oxidation of functional groups by dehydrogenation. Therefore, oxidants like acetone, which is reduced to ^{i}PrOH, replaces the usually applied manganese and chromium salts that produce high amounts of toxic waste products. These two transformations based on hydrogen transfer reactions represent environmentally friendly oxidation and reduction strategies and a myriad of transition metal complexes have been reported to catalyze either the one or the other reaction. In this work, ruthenium and iridium complexes bearing highly powerful *N*-heterocyclic carbene (NHC) ligands were successfully employed in both hydrogen transfer reactions.

A general synthesis route towards heterobimetallic *N*-heterocyclic dicarbene (NHDC) complexes starting from abnormal *N*-heterocyclic carbene (aNHC) ruthenium compounds was established. Thus, the cationic nature of the aNHC precursors is crucial to achieve the desired reactivity against Ag_2O and the electronic requirements might correlate with a strongly down-field NC*H*N proton in the ^{1}H NMR spectra of these precursors. Heterobimetallic ruthenium iridium species were synthesized and their electronic properties were examined by means of voltammetry experiments. Electronic interactions between the metal centers were found. All monometallic and bimetallic species obtained throughout the synthesis were tested in catalytic TH to compare their performances. The introduction of a second metal center positively influences the catalyst stability but has either no or a decelerating effect on the catalyst activity. No hints towards a cooperative interaction of the metal centers could be found.

By introduction of a second aNHC-phosphane ligand a very active catalyst for both, the hydrogenation and the dehydrogenation reactions, was obtained. The C_2-symmetric compound is the first di-aNHC Ru complex reported and is the most active NHC Ru complex in TH known to date, reaching TOFs up to $1.3 \cdot 10^6$ h^{-1}. Its activity in Oppenauer-type oxidation of alcohols is unprecedented. The catalyst oxidizes α-tetralol as a model substrate with a rate of $5.5 \cdot 10^5$ h^{-1} at a catalyst loading of 0.01 mol% and with only two equivalents of acetone, outperforming all known systems by an order of magnitude. According

to NMR spectroscopic data and DFT calculations a bifunctional mechanism is proposed, suggesting a C-H activation reaction at the phenyl substituents of the phosphane ligands. Furthermore, a possible catalyst deactivation pathway is presented based on NMR, SC-XRD and DFT calculational data, involving an NHC isomerization from their abnormal to their normal coordination mode. The pronounced steric shielding of the metal center by the mesityl wingtip substituents in the normal mode highlights the necessity for abnormal coordination to gain high catalytic activities.

1. Introduction

1.1 General Introduction to Catalysis

The last century is characterized by a huge growth of the world's population that came along with a drastically increasing demand for food.[1] In 1898, in his speech in front of the British Association for the Advancement of Science, Sir William Crookes pointed out that food production based on natural nitrogen containing fertilizers would soon not suffice to nourish "*multiplying mouths*".[2] He emphasized that chemical nitrogen fixation and thus synthetic fertilizers will be the only way to escape starvation:

"*It will be through laboratory that starvation may ultimately be turned into plenty*."[2]

And indeed, it was the discovery of an Os containing catalyst, that ultimately led to the industrial synthesis of ammonia from molecular nitrogen and hydrogen.[3] Ammonia is the basis for all nitrogen-based synthetic fertilizers and the Haber-Bosch process has become the largest chemical process world-wide.[3] The mentioned example is only one out of many for catalysts being the basis of our todays standard of living. Nearly all consumables have their origin in catalytic refining of oil and gas feedstocks and in polymer chemistry. Today, more than 90% of all products from chemical industry are produced in catalytic processes being reflected in a catalyst market of 25.0 billion USD (2018).[4]

About 20% of the catalyst market is used in petroleum refining processes, another 20% in the synthesis of polymers and petrochemicals and about 27% is applied in chemical synthesis. However, catalysts are not only used for the synthesis of value-added products, but also for the withdrawal of hazardous pollutants from the environment, for example by decomposition.[5] About 32% of the global catalyst market is applied for environmental belongings and is predicted to expand further. The global catalyst market size share regarding the respective application of the catalysts is depicted in Figure 1.[4]
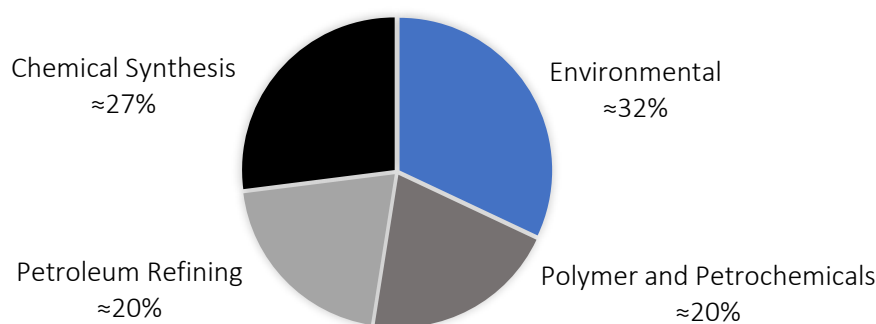

Figure 1: Global catalyst market size share by application of the catalysts.[4]

Generally, a catalyst forms chemical bonds to substrates and activates them by weakening intramolecular bonds or/and by facilitating the spatial approach of the substrates. In the initial example of ammonia synthesis, molecular nitrogen adsorbs to the surface of a heterogeneous catalyst and the N-N triple bond is weakened. Dihydrogen adsorbs as well to the catalyst surface, and the H-H bond is split. The surface-H atoms approach the adsorbed nitrogen and reduce it to ammonia step-by-step.[6] Therefore, catalysts accelerate chemical reactions by intervening in the reaction mechanism and thus lowering the activation energy that must be overcome. They substantially reduce the necessary energy input and are not consumed themselves.

Most industrial processes are catalyzed heterogeneously, where the catalyst is usually in solid state and the substrates are either liquid or gaseous. Activation and reaction of the substrates occur at the catalyst surface. In this regard, the catalysis does not take place on flat, idealized surfaces but at defect sites like steps or edges and it is difficult to state, which defined moieties are the active centers since such atom arrangements on a surface are challenging to investigate or mimic experimentally.[7] The reaction conditions in heterogeneously catalyzed transformations are generally rougher than in homogeneous catalysis. Ammonia synthesis for example is performed at 500 °C and pressures above 20 MPa. Detailed mechanistic investigations under realistic reaction conditions are therefore not feasible.

Homogeneous catalysis, by contrast, takes place at single metal centers with well-defined surroundings and under comparably mild circumstances.[8] This allows mechanistic investigations and detailed studies of the bonding situation between the catalytically active center and the substrates. In turn, deep knowledge about the reactions in a catalytic cycle allow for target modifications in the ligand scaffold to improve the catalysts performance. Today, homogeneous organometallic catalysts allow chemo- and even enantioselective transformations according to a chiral ligand system which is crucial for the synthesis of fine-chemicals and pharmaceuticals. Another major advantage of homogeneous catalysis is the applicability of very low catalyst loadings. In contrast to heterogeneous catalysts, every single metal atom is a potentially active center resulting in a higher catalytic efficiency regarding the applied amount of metal. As a result, the costs for homogeneous catalysts are not primarily determined by the prices for the applied metals, but by the arising expenses from the ligand and catalyst synthesis.[9] Table 1 summarizes the advantages and disadvantages of homogeneous and heterogeneous catalysis.

Table 1: Advantages and disadvantages of homogeneous over heterogeneous catalysis.[9]

	Homogenous catalysis	Heterogeneous catalysis
Efficiency	✔ High	✘ Varying
Selectivity	✔ Chemo- and enantioselectivity	✘ Varying
Steric and electronic variability	✔ High	✘ None
Mechanism clarification	✔ Possible	✘ Not possible
Diffusion problems	✔ None	✘ Possibly limiting
Reaction conditions	✔ Mild	✘ Harsh
Sensitivity towards poisoning	✔ Varying	✘ High
Catalyst lifetime	✘ Varying	✔ High
Catalyst recycling	✘ Difficult	✔ Easy

The main drawback and the reason for the predominant use of heterogeneous catalysts is the tedious separation from the reaction mixture while heterogeneous catalysts can be recycled by simple filtration.[8] Furthermore, many homogeneous catalysts cannot be recycled and reused several times.[9] Nevertheless, a number of industrial transformations are nowadays catalyzed homogeneously.[8, 9] The first application of an organometallic homogeneous catalyst goes back to Otto Roelen (Ruhrchemie) who in the late 1930s established Co tetracarbonyl hydride as catalyst in hydroformylation.[10] Since then, numerous processes applying organometallic catalysts have been developed, the most prominent examples being the Ziegler/Natta polymerization for low-pressure polyethylene synthesis and the Shell Higher Olefin Process (SHOP) for the synthesis of linear longer-chained olefins.[9] The net chemical reactions of these three processes are depicted in Scheme 1.
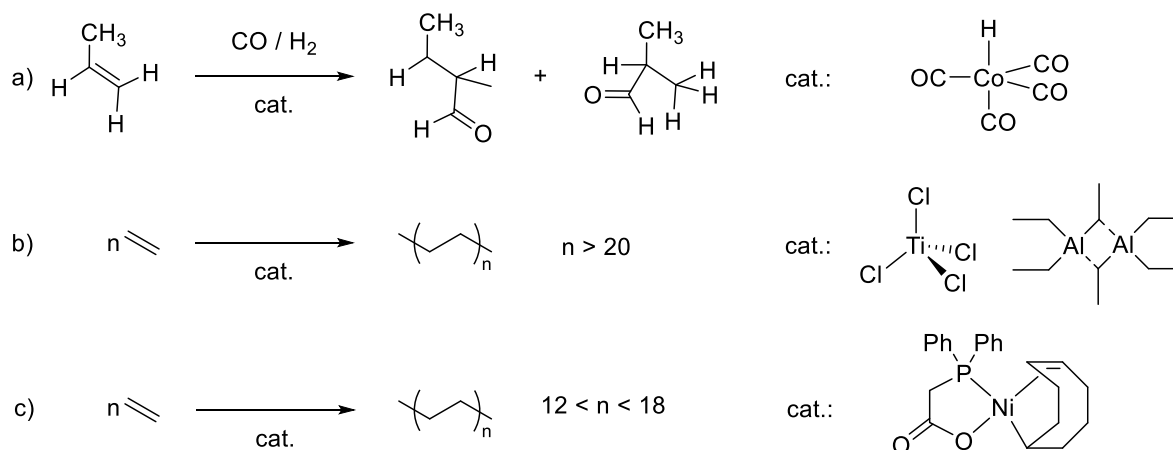
Scheme 1: a) Hydroformylation with Co^I tetracarbonyl hydride; b) Ziegler-Natta polymerization with Ti^{IV} chloride and triethyl aluminum as promoter; c) Shell Higher Olefin Process with Ni^{II} phosphane complexes.

The possibility of tailoring a homogeneous catalyst appropriately to its application according to the used ligands, led to chiral catalysts for fast enantioselective synthesis. In 2001, Ryoji Noyori, William S. Knowles and K. Berry Sharpless received the Nobel prize in chemistry for their contribution to the advances in asymmetric catalysis by application of organometallic homogeneous catalysts. The work of Noyori had a particular impact on the development of catalytic hydrogen transfer reactions. He established Ru complexes bearing chiral amine ligands for the asymmetric transfer hydrogenation (TH) of ketones and imines and for the oxidative kinetic resolution of secondary alcohols.[11]

In summary, catalysis might be considered the research area with the greatest potential for leading into a sustainable future in prosperity as they reduce the necessary energy input for chemical transformations, can be applied to reduce environmental pollution and allow for (enantio-)selective synthesis of fine-chemicals and chiral molecules for medicinal applications.

1.2 *N*-Heterocyclic Carbenes as Ligands in TM Catalysis

1.2.1 General Aspects of *N*-Heterocyclic Carbenes

In the last decades a new, very powerful type of ligands for organometallic compounds arose: *N*-heterocyclic carbenes (NHCs). Carbenes are neutral compounds featuring a divalent C atom with six valence-electrons.[12] The incomplete electron octet renders carbenes highly reactive and they were considered momentary intermediates in organic transformations.[13] After the first isolation attempts in the early 19th century, Bertrand *et al.* reported the first isolable carbene species only in 1988.[14] In 1991, Arduengo et. al. presented a bench-stable crystalline carbene that was inductively and mesomerically stabilized being incorporated in a nitrogen containing heterocycle.[13, 15] Bulky adamantyl substituents on the N atoms additionally prevent the carbene from dimerization.[16] Already two decades earlier Wanzlick and Öfele demonstrated that NHCs can be used as ligands to form transition metal complexes.[17, 18] Although NHCs found some applications as organocatalysts,[21] they are still mostly used as ligands in transition metal catalysis. In this context, their extraordinarily strong σ-donating and relatively weak π-accepting properties are of high relevance for both, the stability of the complex and the basicity of the metal center.[19-29] In contrast to tertiary phosphane ligands that are also strong σ-donors, the strong metal-C bonds render NHC complexes thermally and chemically stable against oxygen and moisture.[13] In this regard, spectacular discoveries were the palladium NHC catalyzed Heck coupling reaction by Herrmann *et al.* and the Ru catalyzed metathesis reaction with the Grubbs catalyst (Scheme 2).[30-32]
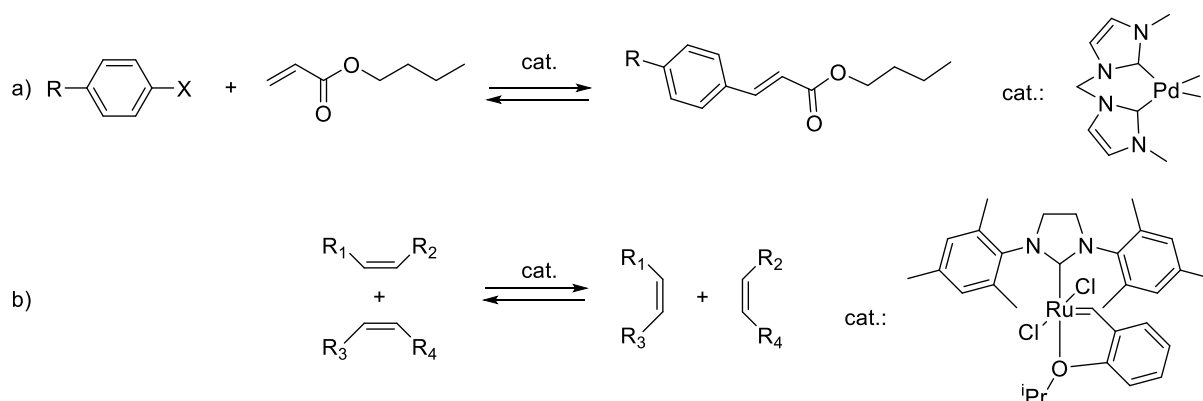
Scheme 2: Most prominent reactions catalyzed by NHC TM complexes: a) NHC Pd catalyzed Heck-coupling reaction; b) NHC Ru catalyzed olefin metathesis reaction.[30, 33]

The definition of NHCs is relatively wide and includes many different ring-sizes and numbers and types of heteroatoms. The most prominent NHC in organometallic chemistry is the imidazolylidene where the carbene is adjacent to two N atoms and the backbone is unsaturated. The discussion within this work will be restricted to this particular type of NHCs.

The rapid success of NHCs is not only based on their electronic properties, but also relies on their versatility and the ease for their synthesis and modification of steric and electronic properties.[34] The steric demand of NHCs is predominantly determined by the wingtip substituents (Figure 2, green), which in most cases are simply introduced *via* nucleophilic substitution reactions.[35]

● Heteroatoms: Electronic properties

● Wingtip substituents: Steric (and electronic) properties

● Backbone: Electronic (and steric) properties
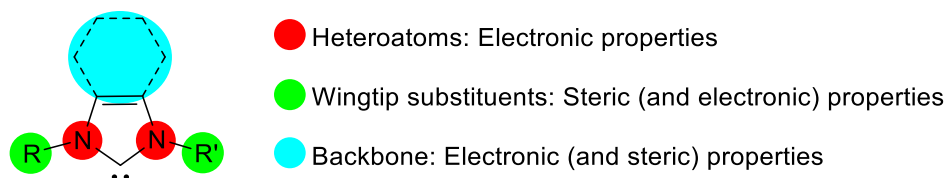
Figure 2: General structure of an imidazolylidene based NHC.

The electronic properties are strongly dependent on the NHC backbone (Figure 2, blue) and the wingtips (Figure 2, green), but are primarily determined by the nature of the heterocycle and the type of the heteroatoms (Figure 2, red).[36] Moreover, the properties of NHC ligands are determined by the coordination mode, namely the position of the carbenic carbon. If the NCC carbons are coordinated to a TM instead of the N*C*N carbon, a so-called abnormal NHC (aNHC) is obtained, which exhibits a higher σ-donor strength.[13, 37]

1.2.2 Functionalized *N*-Heterocyclic carbenes

The synthetic ease for the introduction of different wingtip substituents allows the design of NHC ligands with additional functional groups that either also coordinate to the metal resulting in a chelate ligand or that influence other properties of the corresponding complexes like the solubility. The former is mostly achieved by introduction of C, O, P, N or S moieties, the latter mainly by ionic groups like SO_3^-.[38] More than one NHC can be coupled to give bis, tri or tetra NHC ligands.[39] Therefore, endlessly structural diverse NHC ligands can be designed fitting the respective application (Figure 3).
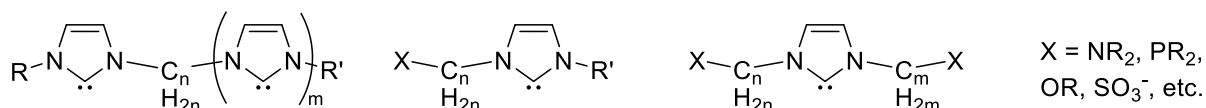
Figure 3: General examples for multi-NHCs (left), monofunctionalized NHCs (center) and difunctionalized NHCs (right).

Functionalization further has some more general advantages[40]: NHC complexes with a hydride ligand tend to reductively eliminate imidazolium salts, which in most cases leads to catalyst decomposition. An additional anchor connected to the NHC moiety helps preventing such decomposition pathways leading to an increased catalyst stability.[41] For this purpose, strongly coordinating functionalities are coupled to the NHC ligand leading to a highly stable ligand environment. In this regard, our group reported multidentate NHC and phosphane functionalized NHC Ru complexes that show excellent activities in TH.[42-46] Functional groups are further introduced to achieve hemilability, which is also associated with an increased catalyst stability: the strong donor ligand acts as fixed anchor while the labile moiety can easily dissociate from the metal center and yield free coordination sites for substrate-catalyst interaction. The dangling ligand, however, remains close to the metal center because it is tethered to the strongly bound moiety. It can therefore stabilize the complex by occupying the resulting free coordination site, when the substrates leave the catalyst (Scheme 3). [47]
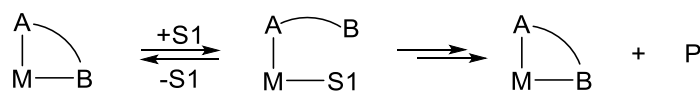
Scheme 3: Schematic representation of hemilability.

Depending on the combination of NHC, functional group and central metal atom one ligand can act as anchor or hemilabile ligand, respectively. In combination with hard donors like amines or oxos, the NHC itself can act as a hemilabile ligand when the metal center is an s-block element or an early transition metal.[48, 49] On the other hand, NHCs form strong bonds to late transition metals, and thus, the functional group must be chosen properly to gain a hemilabile ligand.[50] This concept was studied in our group on a pyrido functionalized NHC Ir complex.[51]

1.2.3 Abnormal Coordination Mode and Bimetallic *N*-Heterocyclic Dicarbene Complexes

With regard to imidazolylidene based NHCs, not only the C adjacent to two N atoms can coordinate to the metal center, but alternatively also a C adjacent to one N and one C atom. These types of NHCs are called abnormal, remote or mesoionic NHCs, because no mesomeric structure can be drawn without charge separation.[21] Different types and coordination modes of NHCs are depicted in Figure 4.
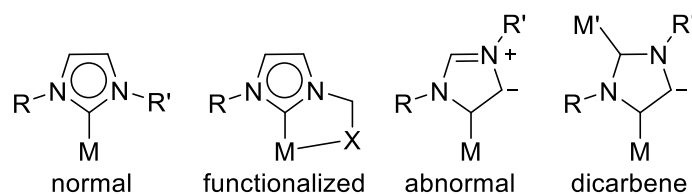
Figure 4: Different types of imidazolylidene based NHCs: normal NHC (left), functionalized NHC (center-left), aNHC (center-right), anionic *N*-heterocyclic dicarbene (right).

The two most frequently applied synthesis routes for imidazolylidene based NHC transition metal complexes include a deprotonation step of the imidazolium salt. This is true for the so-called Ag-transfer-route, where the ligand precursor is converted with Ag_2O as the base and Ag^I source (Scheme 4, I_A). The resulting NHC Ag complexes are used to transfer the carbene ligand to other transition metal precursors that usually contain halide (X^-) ligands to simultaneously precipitate AgX (Scheme 4, I_B). Moreover, NHC complexes can be synthesized directly, reacting imidazolium salts with a base and a TM precursor or even only a TM precursor bearing a basic ligand (Scheme 4, II).
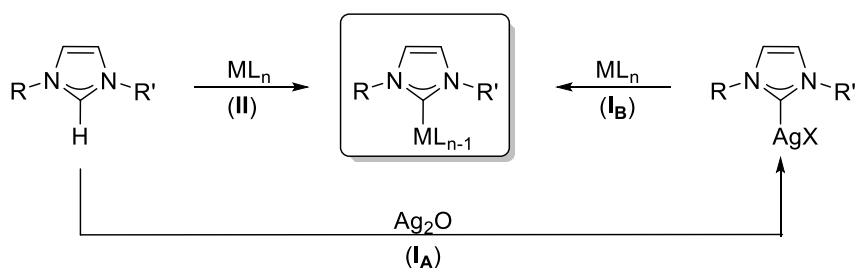
Scheme 4: Most prominent synthesis routes for NHC TM complexes.

The strongly σ-accepting N atoms stabilize the free carbenic electron pair.[13] Therefore, the NC*H*N proton exhibits the lowest pK_A value and is abstracted first. For this reason, most NHCs coordinate the metal center at the NCN position. Alternative coordination modes can be obtained, if the NCN position is protected by an alkyl group or if the steric demand of the wingtip substituents hinders the coordination to the NCN carbon. In the latter case, H migration from the backbone to the deprotonated NCN carbon might occur, allowing coordination of a NCC carbon to the metal center.[20]

The first aNHC complex was reported in 2001 by Crabtree *et al.*, who introduced a bidentate 2-pyridylmethylimidazolylidene ligand to an Ir hydride complex (Scheme 5, top).[25] The abnormal

coordination might result from the steric repulsion of the isopropyl- or *n*-butyl substituents with the PPh$_3$ ligands. The first crystalline aNHC was isolated in 2009 by Betrand *et al.* who used a NCN-alkylated imidazolium precursor with a phenylsubstituent on the C4 position (Scheme 5, bottom).[52] The resulting abnormal or mesoionic NHCs are electronically stabilized by one single N atom.[22]
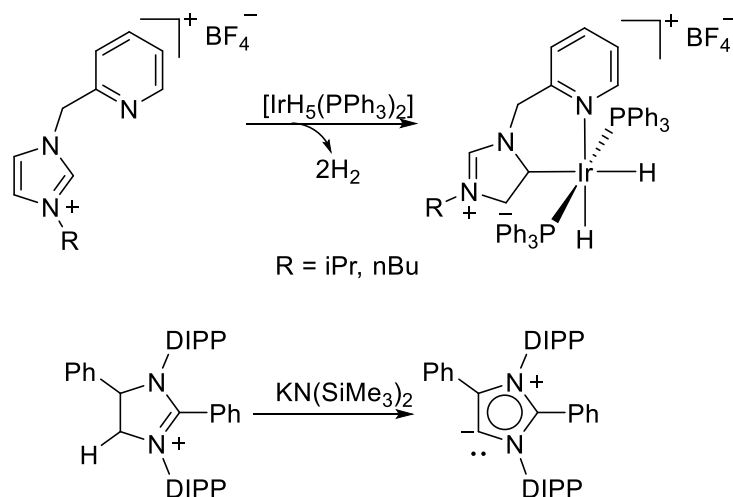
Scheme 5: Synthesis of the first aNHC ligand by Crabtree *et al.* (top) and the first crystalline aNHC reported by Bertrand *et al.* (bottom).

aNHCs are therefore generally considered stronger σ-donors than normal NHCs which is of high relevance for potential catalytic applications.[19-29] For instance, aNHC ligands have been applied in C-C cross-coupling reactions, in hydrogenation and hydrosilylation as well as in olefin metathesis.[22] Furthermore, an aNHC complex reported by Baratta *et al.* in 2013 is the most active NHC complex in TH today (Figure 5, left). Its activity is further enhanced by addition of a diamine, which presumably acts as *in-situ* amine ligand for which in turn the Noyori outer-sphere mechanism applies.[46] A related mixed normal/abnormal NHC complex also showed good activity in TH (Figure 5, right).[44, 45]
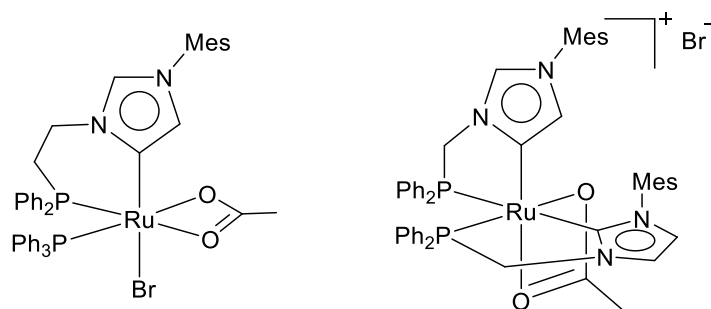
Figure 5: Ru-aNHC complexes reported by Kühn and Baratta *et al.*: Mono aNHC with C$_2$-backbone (left) and mixed NHC/aNHC with C$_1$ backbone (right).

Such NCN-unsubstituted aNHCs potentially exhibit a free coordination site for a second metal center. Upon deprotonation of the coordinated aNHC ligand at the NCN position, another type of NHC ligands

arises, namely, *N*-heterocyclic dicarbenes (NHDC). These ditopic carbanionic carbenes can be considered bridging ligands, so far mainly in relation with main group elements and lanthanides.[53-56] However, NHCD complexes including two transition metals are relatively rare.[57-67] They show great potential as ligands in homogeneous tandem catalysis since two catalytically active centers with distinct functionalities can be combined. The properties of the metal centers are furthermore potentially varied by electronic interactions across the NHC's π-system.[23] Peris *et al.* reported triazolyl derived heterobimetallic complexes, with application in catalytic tandem reactions.[68-79] Electronic interactions where established *via* voltammetry experiments.[69] The first heterobimetallic imidazolyl-based transition metal NHDC complexes were published in 2015 by Kühn *et al.* who synthesized Ru-Ag (Figure 6, left) and Ru-Au NHDC complexes.[44] By transmetalation of the Ag^I complex with PdCl$_2$(cod) (cod = 1,5-cyclooctadiene) a Ru-Pd heterobimetallic NHDC complex (Figure 6, right) was obtained, which was successfully applied in the tandem TH and Suzuki-Miyaura coupling reaction.[43]
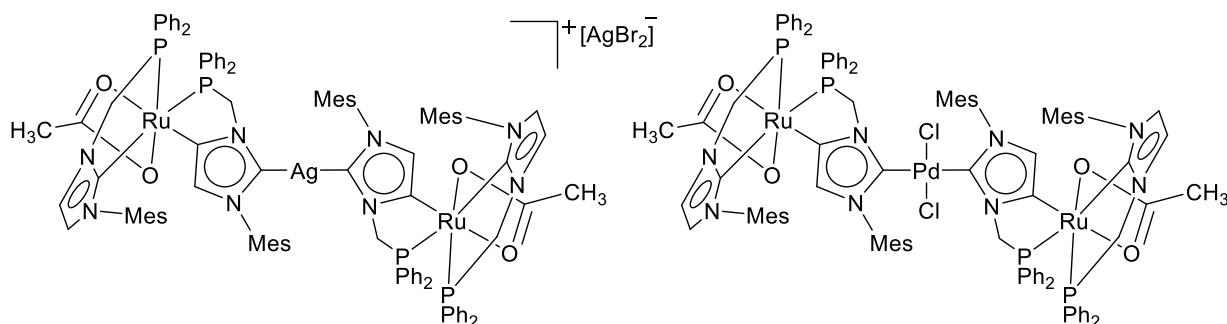
Figure 6: First heterobimetallic TM NHDC complexes reported by Kühn and Baratta *et al.*

NHCs have shown to be powerful ligands in homogeneous catalysts for many different reaction types.[80,][81] Regarding TM catalyzed hydrogen transfer reactions, many different ligand systems were thoroughly investigated.[82] However, NHCs are less explored and the performance of NHC containing catalysts features significant room for improvement.[83]

1.3 Transfer Hydrogenation

1.3.1 General Aspects of Transfer Hydrogenation

A thoroughly studied reaction in organometallic catalysis is the TH of carbonyl compounds.[82] Unlike the hydrogenation with pressurized dihydrogen, TH uses hydrogen containing molecules as chemical hydrogen source (Scheme 6).

$$R{-}C(R')({=}X) \;+\; DH_2 \;\rightleftharpoons\; R{-}CH(R')({-}XH) \;+\; D$$
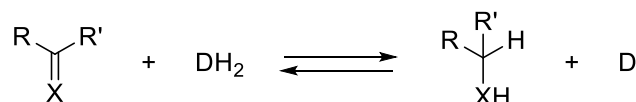
Scheme 6: General reaction scheme of the reversible TH.

Most popular examples for chemical hydrogen donors are ^{i}PrOH that is reduced to acetone and formic acid that upon oxidation releases CO_2 as the side-product. TH exhibits some major advantages compared to the hydrogenation with dihydrogen:

- Chemical H-donors like ^{i}PrOH are readily available, inexpensive, non-toxic, environmentally friendly and easy to handle.
- The use of pressurized, hazardous and highly flammable dihydrogen is replaced by easy-to-handly liquids. Therefore, challenging dihydrogen storage is avoided and a much simpler reaction setups can be applied, which is of high interest in laboratory use.
- According to the relatively low boiling points, H-donors and side-products (e.g. acetone) are easily removed from the reaction mixture.

However, the simple fact of producing stochiometric amounts of byproducts like acetone is a huge drawback regarding large-scale applications compared to the clean hydrogenation with dihydrogen gas. Therefore, in industry hydrogenation under high-pressure dihydrogen is preferably performed.

TH was first reported in 1925 by Meerwein[84], Ponndorf[85] and Verley[86], who used aluminum alkoxides as reaction promoters. The TH protocol is therefore called the Meerwein-Ponndorf-Verley (MPV) reduction. Since the discovery of hydrogen transfer reactions, many promoters based on different elements were established, but only some could be applied in catalytic amounts.[82] The major drawback of the initial MPV protocols was the stochiometric need for aluminum salts.[87] Despite this drawback, MPV reduction found some larger-scale applications, especially in the synthesis of fine chemicals and in fragrance industry.[82] However, it was highly desirable to replace the MPV promoters by catalysts that promote the reaction at lower loadings. In the 1960s, the first late-transition metal complex was used as a catalyst for the MPV reduction. Henbest and Mitchell *et al.* found that chloroiridic acid catalyzed the reduction of α,β-unsaturated ketones and cyclohexanones to the corresponding alcohols with ^{i}PrOH as the reducing agent.[88, 89] In the 1970s, Sasson and Blum provided evidence that $RuCl_2(PPh_3)_3$ also

catalyzed the TH of α,β-unsaturated ketones.[90, 91] A real breakthrough, however, was the discovery that catalytic amounts of base enhance the reaction rate by a factor of 10^3 - 10^4 which was reported in the 1990s by Bäckvall *et al.*[92] Nowadays, a myriad of TM complexes catalyzing TH of carbonyl compounds are known. Despite Ru which is the most widely applied TM for catalytic TH, the most prominent metals are Ir and Rh.[82] A true milestone was the work of Noyori on the asymmetric TH in the late 1990s. He reported Ru complexes bearing a primary or secondary amine functionality as well as an arene ligand that weakly occupies three coordination sites of the octahedral Ru(II) center (Figure 7, left). These complexes catalyze TH with *i*PrOH or formic acid even at RT and excellent enantiomeric excess of up to 99%.[11] In 2001, Ryoji Noyoris contribution to asymmetric catalysis was rewarded with the Nobel Prize in chemistry together with K. Barry Sharpless and William S. Knowles. Pincer Ru complexes were found to efficiently catalyze TH reactions.[93] The work of Baratta *et al.* on CNN pincer complexes RuCl(CNN)(PP) led to today's most efficient systems (Figure 7, right)[94-96], showing highest rates (TOF up to 10^6 h^{-1}) at very low catalyst loadings (down to 0.001 mol%) for the enantioselective transformation of a broad substrate scope.[82, 96, 97]
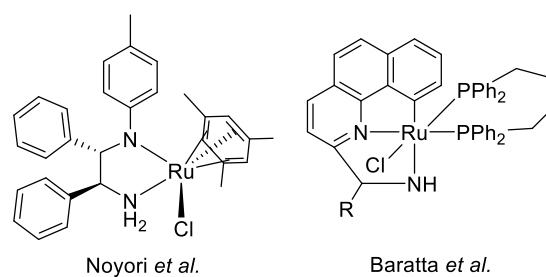
Figure 7: Most prominent TH catalysts reported by Noyori *et al.* (left) and Baratta *et al.* (right).

1.3.2 NHC Ligands in Catalytic TH

Numerous catalysts have been reported mostly with Rh, Ru and Ir as the active metal centers combined with ligands based on N, P, O, C and S elements.[82] However, NHCs as ligands in TH catalysts were only introduced in the last two decades. Nolan *et al.* were the first to successfully apply an Ir NHC complex in catalytic TH in 2001 (Figure 8, left).[98] One year later, Crabtree *et al.* presented an air and moisture stable Ir bis-NHC complex active in catalytic TH (Figure 8, mid-left).[99] The first Ru NHC complexes as TH catalysts were presented by Danopoulos *et al.* (Figure 8, mid-right)[100] and Peris *et al.* (Figure 8, right)[101].
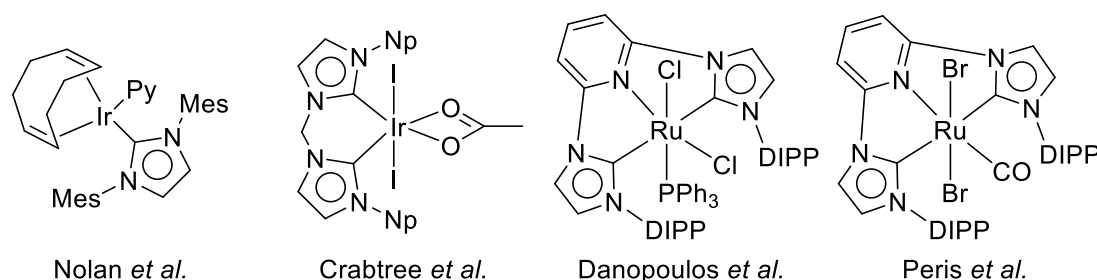
Figure 8: Early NHC Ir and Ru complexes.

One of the most active NHC Ru complexes in TH was reported by Baratta *et al.* in 2005 (Figure 9, left),[102] who applied a 1,2,4-triazolyl-5-ylidene based NHC precursor for the synthesis of an *ortho*-metalated Ru NHC complex that reaches TOFs up to $120\,000$ h^{-1}. The most active Ru NHC complex to date was reported by Kühn and Baratta *et al.* in 2013, which is a phosphane functionalized aNHC Ru complex based on the usual imidazolylidene motif (Figure 9, right).[46]
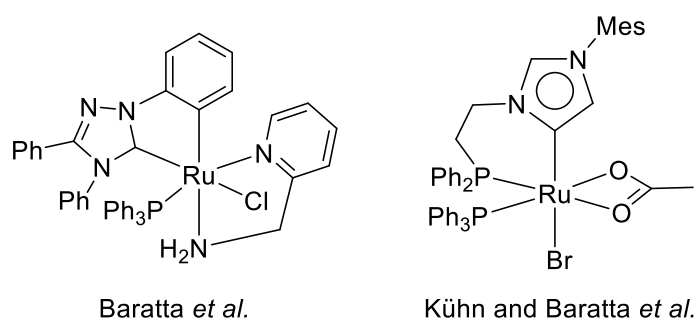
Figure 9: Most active NHC Ru catalysts for the TH of carbonyl compounds.

However, this complex only reaches the maximal TOF of $140\,000$ h^{-1} by the *in-situ* addition of amine ligands. Therefore, both complexes only reach high rates in TH when an amine ligand enters the coordination sphere and induces an outer-sphere mechanism as will be described in the following section.

1.3.3 Reaction Mechanism

Mechanistic investigations led to two majorly proposed reactions pathways of Ru catalyzed TH: The more general and longer-known inner-sphere or hydric route (Scheme 7)[103] and the outer-sphere or dihydride pathway (Scheme 8)[11] that applies only for Ru complexes with bidentate ligands and one coordinating group being a primary or secondary amino group. Bifunctional catalysis was also reported with other functional groups, i.e. O-H, S-H or C-H, with the N-H functionality being the most prominent for catalytic TH.[81]
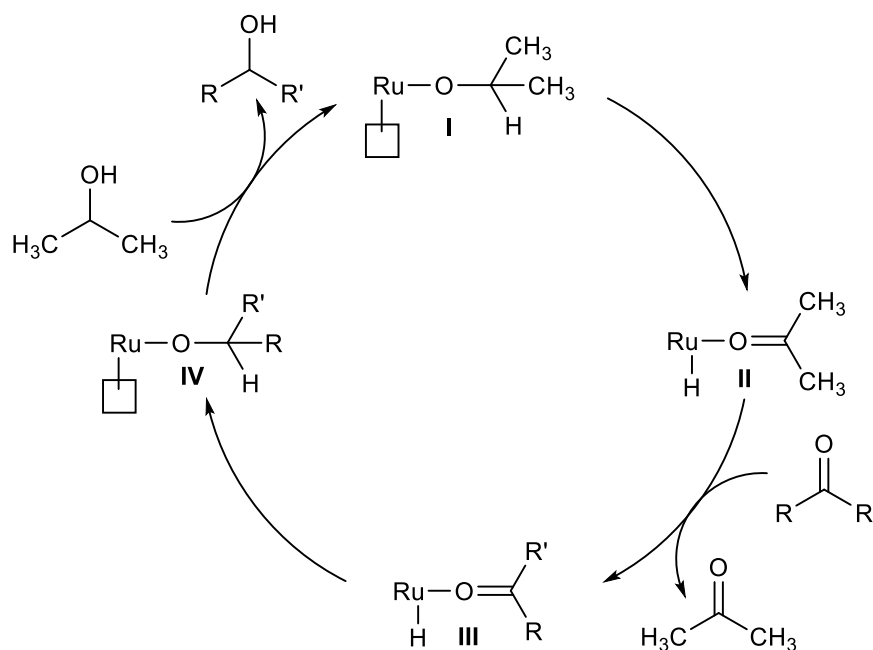
Scheme 7: Inner-sphere mechanism for the Ru catalyzed TH of ketones with ^{i}PrOH.

Following the inner-sphere mechanism, ^{i}PrO⁻ coordinates to the Ru center (**I**) and a metal-hydride is formed according to β-H-elimination (**II**). The resulting coordinated acetone is replaced by the substrate carbonyl compound (**III**) followed by the transfer of the hydride to the carbonyl carbon (**IV**). By protonation and release of the product and coordination of another ^{i}PrO⁻, the initial complex (**I**) is rebuilt. Following this route, the substrates have to directly coordinate to the metal center. Two vacant coordination sites on the metal are necessary that must be created in the initial catalyst activation step.
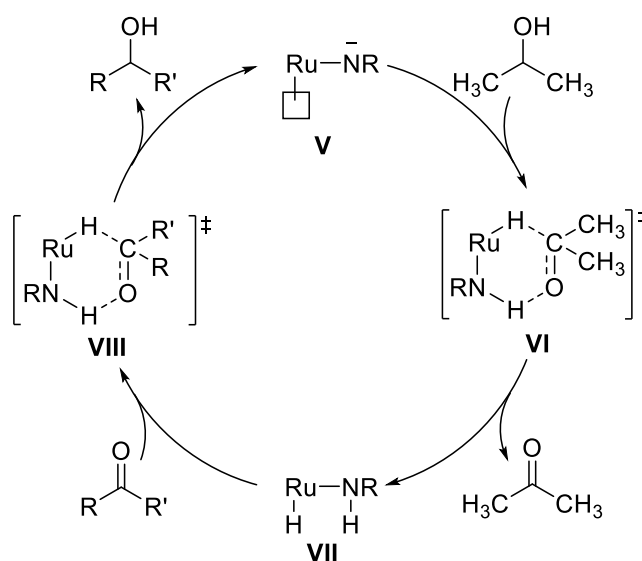
Scheme 8: Outer-sphere mechanism for the Ru catalyzed TH of ketones with ^{i}PrOH.[11, 104]

The outer-sphere mechanism was first proposed by Noyori in 1997.[11, 104] He proposed a bifunctional metal-ligand catalysis where dihydrogen is formally transferred from the H-donor to the catalyst in one step, and then to the substrate in another step. The starting complex (**V**) forms a pericyclic transition state with ^{i}PrOH (**VI**). Two H atoms are formally transferred to the catalyst, forming the active species (so-called "dihydride") (**VII**). Both H atoms transferred to the carbonyl substrate in another pericyclic transition state (**VIII**) where the amine-moiety stabilizes the out-of-plane attack of the Ru-hydride by H-bonding. Upon transfer of both H atoms to the substrate the initial complex (**V**) is rebuilt. This species **V** is stabilized by π-backdonation from the negatively charged amine into the empty d-orbital of the Ru center.[105] As stated above, this mechanism applies for Ru complexes bearing chelating ligands with a primary or secondary amino group. Furthermore, the complex must allow a *syn*-periplanar geometry of the Ru-amine fragment with the hydrogen donor. Following this route only one vacant coordination site on the metal is necessary and the catalytic reaction involves less reaction steps. Therefore, catalysts following this mechanism usually work faster than those following the inner-sphere route. This discovery is also called the N-H effect, which can further be exploited by the *in-situ* addition of chelating amines like ethylene diamine or 2-(aminomethyl)pyridine (ampy).[105]

However, several other pathways and side-reactions might be expected to apply for different catalysts. For RuCl$_2$(PPh$_3$)$_3$ it was shown that not the monohydride species [RuH(PPh$_3$)$_3$]$^+$ but the dihydride species RuH$_2$(PPh$_3$)$_3$ is the active species in catalysis.[106, 107]. To activate the catalyst, a dihydride (**IX**) must be formed first by two subsequent base-assisted β-H-eliminations (Scheme 9).
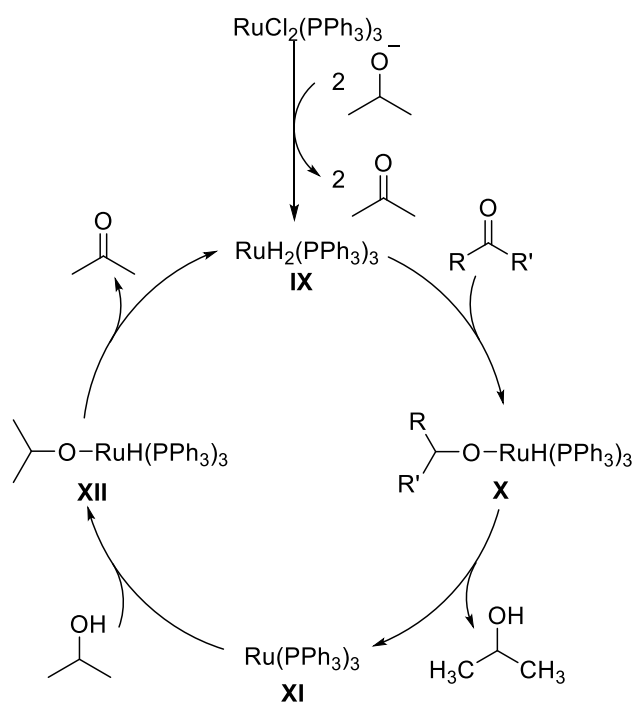
Scheme 9: Dihydride route for TH with RuCl$_2$(PPh$_3$)$_3$ proposed by Bäckvall *et al.*

According to deuteration experiments, both hydrides are transferred to the substrate upon ketone coordination (**X**). Since formally two H atoms are transferred similar to a reductive elimination of dihydrogen, the resulting intermediate has a Ru(0) center (**XI**).[108] The dihydride is rebuilt by transfer of both, a proton (**XII**) and a hydride (**IX**), from ^{i}PrOH to the Ru center.[108] This step therefore is similar to a oxidative addition resulting in the active Ru(II) dihydride species. In order to obtain two subsequent β-H-eliminations during the activation process, at least three vacant coordination sites are necessary. In this particular case two chlorides can act as leaving groups and the coordination environment can be extended from the five-fold square pyramidal to six-fold octahedral coordination geometry. In this regard, a TH test reaction with pure RuH$_2$(PPh$_3$)$_3$ without further addition of base could clarify whether this reaction mechanism could apply. In summary, the catalytic TH of carbonyl compounds involves TM hydride species that are either generated in an inner-sphere or an outer-sphere process. Identification of such hydridic intermediates could give indications about the catalytic mechanism.

1.4 Oppenauer-type Oxidation Catalysis

As accounts for the hydrogenation of carbonyl compounds, also the oxidation of alcohols is a fundamental transformation in organic synthesis. Therefore, multiple oxidation strategies have been developed, however, largely using stochiometric amounts of metal-based oxidants like $Cr_2O_7^{2-}$, RuO_4^- or MnO_4^- that produce huge amounts of toxic waste-products.[109] More sustainable oxidation routes are therefore highly desirable. In 1930, Oppenauer presented an alternative oxidation method for the synthesis of ketones and aldehydes.[87, 110-112] The Oppenauer oxidation is the opposite reaction to the MPV reduction: An H-accepting molecule, such as acetone, is used in excess as oxidizing reagent to which two H atoms are transferred from the oxidized substrate (Scheme 10).
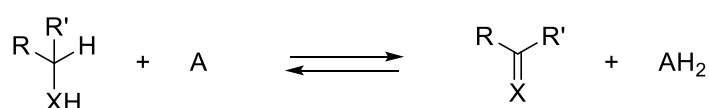
Scheme 10: General reaction scheme of the reversible Oppenauer oxidation reaction.

Oppenauer oxidized steroidal compounds bearing a secondary alcohol function using acetone as oxidant and $Al(O^tBu)_3$ as the promoter. Similar to the MPV reduction, the Oppenauer oxidation proceeds *via* a 6-membered cyclic transition state involving Al^{III} (Scheme 11).
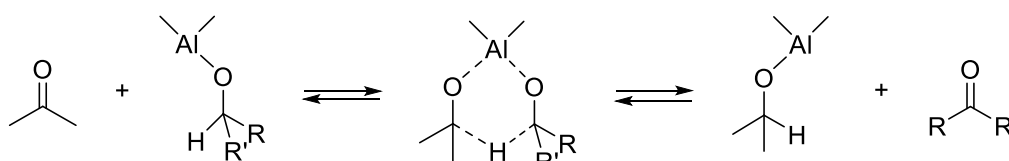
Scheme 11: Reaction mechanism for the Oppenauer oxidation of alcohols with acetone promoted by Al^{III}.

The major drawback of the protocol presented by Oppenauer is the same as for MPV reduction: the stochiometric use of aluminum salts. However, the reaction proceeds under very mild conditions, which is interesting for the synthesis of natural products. A major benefit of the Oppenauer oxidation over other oxidation methods, is selectivity towards ketones and aldehydes, because over-oxidation towards carboxylic acids is prohibited.[87]

In order to overcome the use of stochiometric amounts of Al salts, a lot of effort has been put into the development of catalytic versions of the Oppenauer oxidation. Nowadays, a number of TM complexes that catalyze the Oppenauer-type oxidation are known (Figure 10). Most of them are based on $Ru^{92, 113-124}$, but also Rh, Ir and $Fe^{116, 125-133}$ have been reported. Bäckvall *et al.* used $RuCl_2(PPh_3)_3$ in the Oppenauer-type oxidation of cholesterols, which is of high interest for the synthesis of pharmaceuticals based on steroid hormones.[115] Enantioselective Oppenauer-type oxidation with $RuCl_2(PPh_3)(PN)$ was furthermore effectively applied for the kinetic resolution of chiral alcohols.[134] Hartwig *et al.* recently

reported a Ru-phosphane catalyst that displays high chemoselectivity in the oxidation of polyols and applied it in natural product transformations.[124]
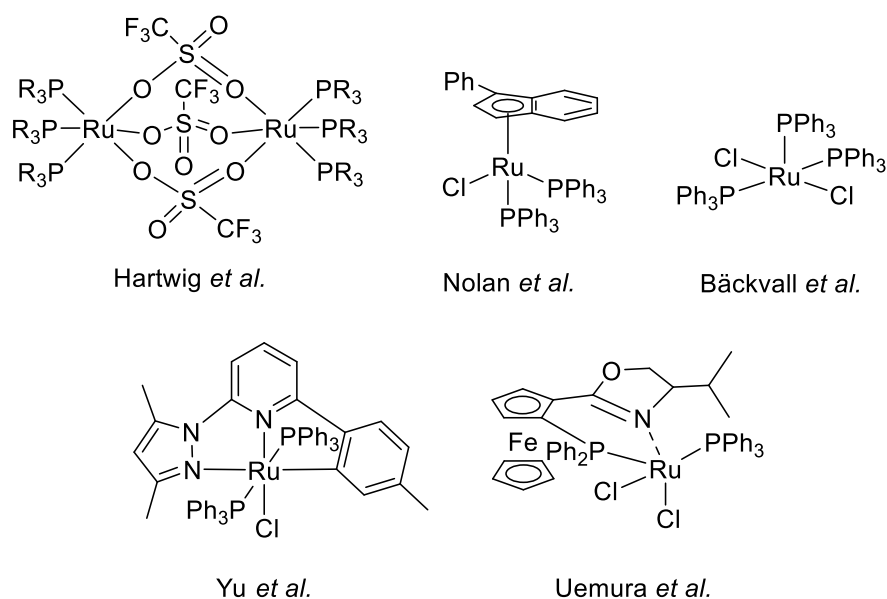
Figure 10: Selected Ru based Oppenauer-type oxidation catalysts reported by Hartwig *et al.* (top left)[124], Nolan *et al.* (top center)[119], Bäckvall *et al.* (top right)[115], Yu *et al.* (bottom left)[118] and Uemura (bottom right).[134]

As observed for the Noyori catalysts for asymmetric TH, most catalysts are more efficient for the reduction than for the oxidation pathway.[11] Necessary catalyst loadings are still relatively high (>>0.01 mol%) and the reaction rates are comparably low. To the best of my knowledge, the highest TOF for Oppenauer oxidation of 11 880 h^{-1} was reported by Yu *et al.*[118], for the kinetic resolution of alcohols a TOF of 80 000 h^{-1} was reached.[134] Compared to catalytic TH that works at catalyst loadings of 0.001 mol% and reaction rates >10^6 h^{-1}, there is still potential in the catalyst optimization for this reaction, also regarding the substrate scope. Furthermore, when acetone is used as solvent, strong bases should not be applied as reaction promoters due to the formation of aldol condensation products causing a tedious work-up process. This side reaction was already observed in the early state of Oppenauer oxidation.[87] However, relatively soft bases like K$_2$CO$_3$ are not always able to activate the catalyst as the substrate alcohols have to be deprotonated. The low boiling point of acetone and therefore the limited reaction temperature of 56 °C could further hinder a proper catalyst activation because of its energy barrier. Therefore, in many protocols inert solvents like toluene are used and acetone is added in high excess.[119]

In summary, the catalytic Oppenauer-type oxidation represents a very mild pathway to oxidize alcohols to carbonyl compounds. The protocol allows for chemoselective transformations and no over-oxidation towards carboxylic acids is observed. Further catalyst optimization is necessary for a potential larger scale application.

2. Objective

Phosphane functionalized aNHC Ru complexes have shown to be efficient catalysts for the TH of carbonyl compounds. However, NHCs and especially NHC-P ligands are relatively unexplored in TH catalysis with respect to other ligand systems. Despite being powerful ligands for catalytic TH, aNHC ligands can coordinate to a second metal center and therefore act as ditopic NHDC ligands. The scope of this work is to elaborate a more general route towards heterobimetallic complexes. The previously reported protocol[44] is to be extended to another aNHC Ru complex[46] which is highly active in TH catalysis (Scheme 12).
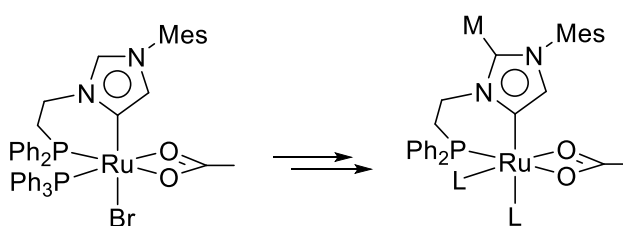
Scheme 12: General synthesis of heterobimetallic complexes starting from an aNHC Ru complex.

Since the analogous heterobimetallic Ru-Pd complex catalyzes the tandem TH / Suzuki-Miyaura coupling reaction, both metal centers might be active in catalysis. Therefore, potential cooperative effects between two metal centers with similar catalytic properties (e.g. Ru and Ir) in catalytic TH will be investigated. Electronic interactions of the two metal centers across the π-system of the NHDC ring should be evaluated by investigation of their redox-properties. Thus, cyclic voltammetry and differential pulse voltammetry experiments will be conducted to determine the respective redox potentials.

The previously published aNHC Ru complex (Scheme 12) exhibits high activity in TH of acetophenone, which is further enhanced when an ampy is added *in-situ* to the reaction mixture. The amine might therefore coordinate to the metal center and replace other ligands. Furthermore, it shows fast catalyst deactivation reaching high initial TOFs but only slowly completing the reaction. Therefore, this complex shows great potential for optimization of the catalytic properties by introduction of more suitable ligands like chelating diphosphanes or bidentate NHC-phosphanes (Scheme 13).
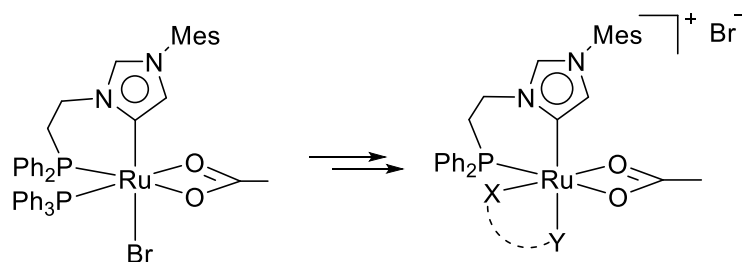
Scheme 13: Possibility for the catalyst optimization by introduction of (bidentate) ligands replacing the bromide (and the PPh₃).

Finally, the NHC precursor Ru(OAc)₂(PPh₃)₂ is to be functionalized with an amine group instead of the phosphane. Thus, the amine necessary for fast bifunctional TH catalysis according to the NH-effect would be intrinsically provided (Scheme 14). Although bidentate NHC-amine ligands have been previously reported, aNHC-amine Ru complexes are completely unexplored.[81]
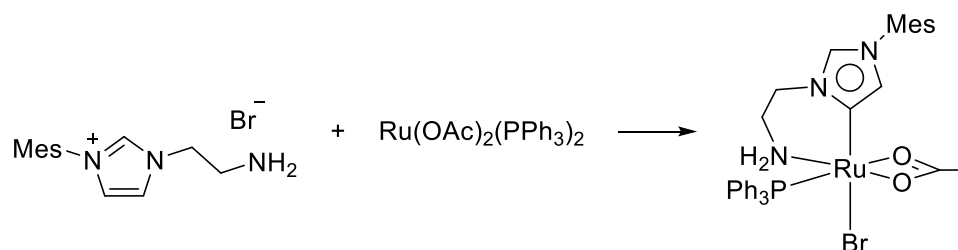
Scheme 14: Synthesis of aNHC-amine Ru complexes.

3. Results and Discussion

3.1 Transforming aNHC Ru Complexes into Suitable Precursors for Heterobimetallic NHDC Compounds

Parts of this chapter where published in L. Pardatscher, M. J. Bitzer, C. Jandl, J. W. Kück, R. M. Reich, F. E. Kühn and W. Baratta, *Dalton Trans.*, 2019, **48**, 79-89.[45]

In the following chapter, a synthesis route towards heterobimetallic NHDC complexes starting from aNHC Ru complexes will be presented. It will be shown that the cationic nature of the aNHC precursor is of high importance for further metalation reactions. Electronic properties of the mono- and heterobimetallic species will be described by means of voltammetry experiments. Finally, all complexes will be tested as catalysts for the TH of acetophenone in ^{i}PrOH to investigate the influence of the second metal center on the performance of the catalysts.

3.1.1 Synthesis of the Ruthenium Iridium Heterobimetallic NHDC Complex with a C_1 backbone

3.1.1.1 Synthesis of **1**-**8**

The Ru-Ag NHDC complex **8**, which is used as the precursor for the synthesis of the heterobimetallic Ru-Ir NHDC complex **9**, is synthesized *via* multiple literature known procedures. 1-(2,4,6-Trimethylphenyl)-1H-imidazole (**1**) was synthesized in 50% (lit. 75%) yield according to a modified literature procedure[135]. Column chromatography as work-up process was replaced by resublimation at 10^{-3} mbar and 200 °C. Hydroxymethyldiphenylphosphineoxide (**2**) was synthesized from chlorodiphenylphosphane and formaldehyde in 90% (lit.: 90%) yield following a literature procedure (Scheme 15, a).[136] Bromomethyldiphenylphosphineoxide (**3**) was synthesized from **2** and thionylbromide in 32% (lit.: 30%) yield following a literature procedure (Scheme 15, b).[44] 1-(Methyldiphenylphosphinoxide)-3-(2,4,6-trimethylphenyl)-imidazolium bromide (**4**) was synthesized from **3** and **1** in 90% (lit.: 94%) yield following a literature procedure (Scheme 15, c).[44] 1-(Methyldiphenylphosphine)-3-(2,4,6-trimethylphenyl)-imidazolium bromide (**5**) was synthesized by reduction of **4** with trichlorosilane in 85% (lit.: 78%) yield following a literature procedure (Scheme 15, d).[44] Ru(OAc)$_2$(PPh$_3$)$_2$ (**6**) was synthesized in 74% (lit.: 71%) yield following a literature procedure.[137] Complex **7** is obtained by reaction of **5** with **6** in presence of an excess of NaOAc in 70% (lit.: 88%) yield following a literature procedure (Scheme 15, e).[44] Complex **8** was synthesized from **7** and Ag$_2$O in 60% (92%) yield following a literature procedure (Scheme 15, f).[44] The formation and purity of **1** - **8** was confirmed by ^{1}H, ^{13}C and ^{31}P NMR spectroscopy, ESI-MS and elemental analysis.
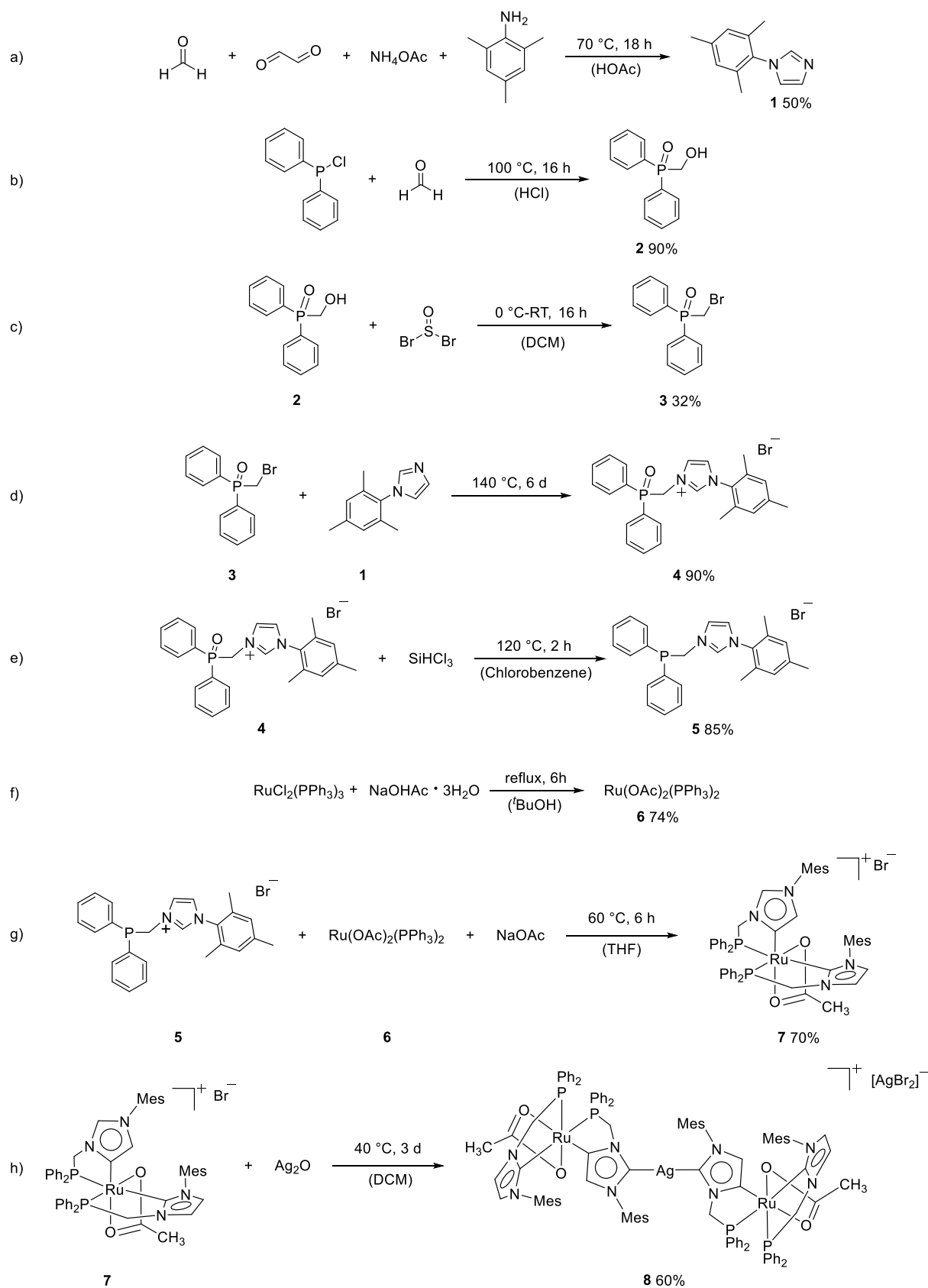
Scheme 15: Synthesis of **1** - **8**.

3.1.1.2 Synthesis of **9**

9 was synthesized by transmetalation of the Ru-Ag NHDC **8** with [Ir(cod)Cl]$_2$ in DCM in presence of Ag$_2$O to prevent the formation of the monometallic Ru aNHC complex **7** as inferred by ^{1}H NMR spectroscopy (Scheme 16).
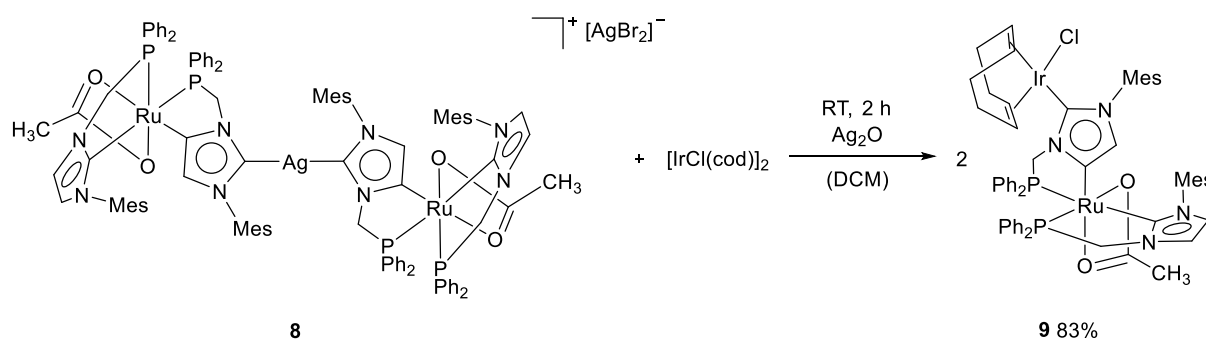
Scheme 16: Synthesis of **9**.

In the ^{31}P{^{1}H} NMR spectrum of **9** in CD$_2$Cl$_2$, four doublets (80.8 ppm, 80.3 ppm, 58.6 ppm and 57.1 ppm; $^2J_{PP}$ = 24.0 Hz) are observed corresponding to two isomers of **9** in a 4 : 5 ratio, as observed for related species[43, 44]. In toluene-d$_8$ the isomer ratio is 1 : 3, which indicates a dynamic equilibrium that depends on the applied solvent. Even in the ^{13}C NMR spectrum both isomers are observed, indicating a slow interconversion of the two species. In toluene-d$_8$ the ratio is 1 : 3 indicating again a solvent dependent equilibrium reaction of the two isomers. VT-NMR studies do not show any influence of the temperature on the peak sizes or shapes and therefore reveal that the isomer ratios are not temperature dependent. This behavior was attributed to different conformations of the five-membered metallacycles including the C$_1$ backbone between the N and P atoms.[43, 44] In order to investigate the potential interconversion of the two isomers, NOESY NMR experiments were performed to see if exchange-signals are observed (Figure 11).
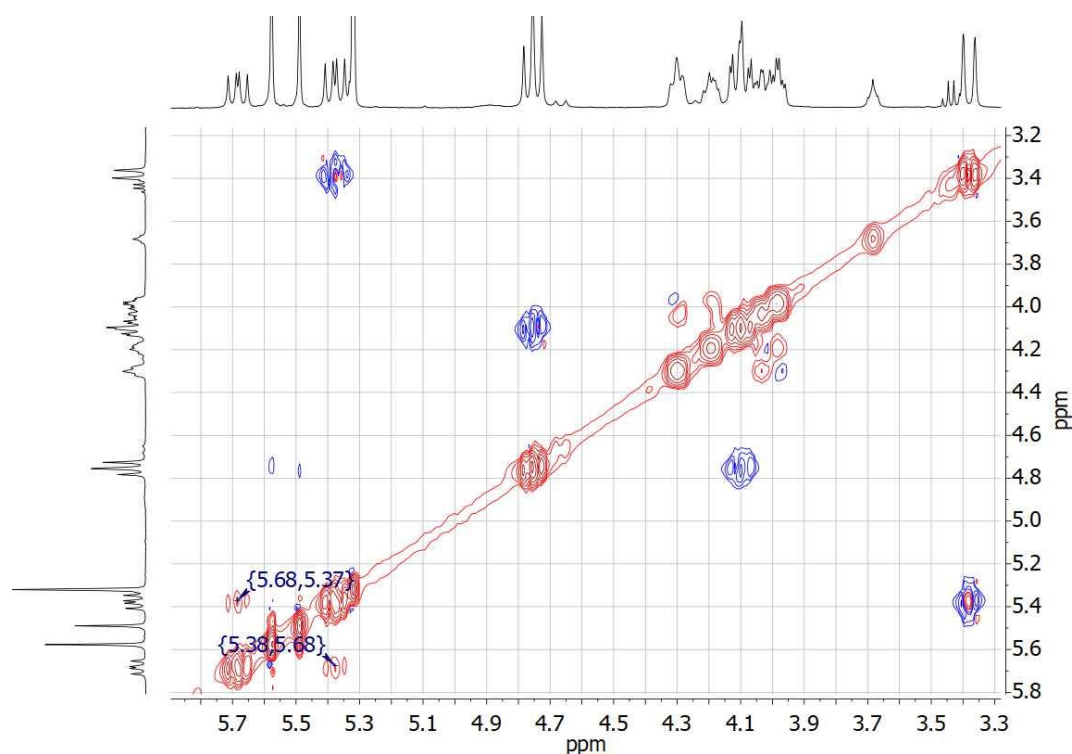
Figure 11: NOESY NMR spectrum (CD$_2$Cl$_2$, 400 MHz) of **9**. The marked peaks resemble cross peaks between the two isomers. [L. Pardatscher, M. J. Bitzer, C. Jandl, J. W. Kück, R. M. Reich, F. E. Kühn and W. Baratta, *Dalton Trans.*, 2019, **48**, 79-89] – Reproduced by permission of the Royal Society of Chemistry.

NOESY NMR measurements clearly show cross peaks for the NC*H*$_2$P protons at 5.68 ppm for the major isomer and 5.38 ppm for the minor isomer. These peaks indicate that the interconversion of the two species involves conformational changes in the five-membered metallacycles, as these are the only protons that show an exchange process.

In the ^{1}H NMR spectrum, the cod-moiety exhibits four distinct signals for the olefinic protons with integrated peak areas that correspond to one proton, which indicates the overall low symmetry of the heterobimetallic species and an asymmetric coordination of the cod. In the ^{13}C{^{1}H} NMR spectrum, the normal carbene is at 193.7 ppm for the one and 193.4 ppm for the other isomer. The signals appear as doublet of doublets with $^2J_{CP}$ constants of 102 Hz and 13 Hz for couplings with the P atoms in *trans* and *cis* positions, respectively. The abnormal carbene appears as a multiplet at 152.0 ppm, because the peaks for the two isomers overlap. The $^2J_{CP}$ constants are 20.5 Hz and 11.0 Hz for couplings with two P atoms in *cis* position. The NC*N* carbene of the NHDC ring bound to the Ir center gives two doublets at 177.7 ppm and 175.9 ppm. Single crystals suitable for SC-XRD were grown by layering a solution of **9** in DCM with *n*-pentane (Figure 12).
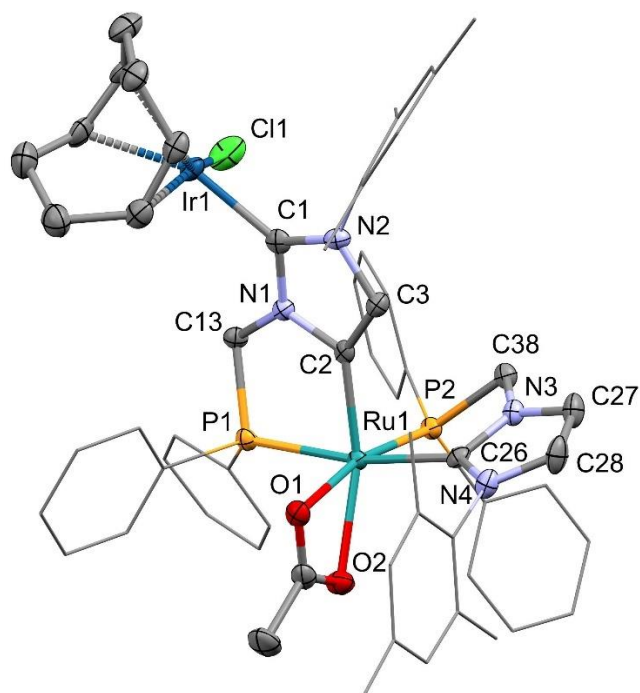
Figure 12: ORTEP-style presentation of the molecular structure of **9**. Thermal ellipsoids are shown at a 50% probability level. H atoms are omitted for clarity. Grey = C, blue = N, purple = P, red = O, dark red = Ru, yellow = Ir, green = Cl. Ru1-C2 2.026(3), Ru1-C26 2.071(3), Ru1-P1 2.2908(9), Ru1-P2 2.2092(8), Ru1-O1 2.214(2), Ru1-O2 2.248(3), Ir1-C1 2.059(3), Ir1-Cl1 2.3693(9), P1-Ru1-C26 169.14(8), O1-Ru1-O2 58.73(9), O2-Ru1-C2 159.28(11), O1-Ru1-P2 167.61(7), P1-Ru1-P2 98.78(3), C26-Ru1-P2 78.87(9), C2-Ru1-P1 81.16(10), C1-Ir1-Cl1 90.68(9). [L. Pardatscher, M. J. Bitzer, C. Jandl, J. W. Kück, R. M. Reich, F. E. Kühn and W. Baratta, *Dalton Trans.*, 2019, **48**, 79-89] – Reproduced by permission of the Royal Society of Chemistry.

SC-XRD confirms the coordination of an Ir(cod)Cl moiety to the N*C*N position. Unfortunately, no further insight into the different isomers present in solution are obtained, as no disordered fragments are present and only one isomer crystallized. The Ru1-C2 distance is 2.026(3) Å is shorter than the Ru1-C26 distance with 2.071(3) Å corresponding to the Ru-aNHC and Ru NHC distances, respectively. The Ir fragment is coordinated in a distorted square planar geometry with an Ir1-C1 distance of 2.059(3) Å. The C1-Ir1-Cl1 angle of 90.68(9) ° differing only slightly from the ideal 90 ° underlines the square planar coordination. The distance between the Ru center and the P atom *trans* to the acetate (Ru1-P2 = 2.2092(8) Å) is smaller than the distance to the P *trans* to the NHC (Ru1-P1 = 2.2908(9) Å). The Ru1-O1 and Ru1-O2 distances are 2.214(2) Å and 2.248(3) Å, respectively. According to the overall similar coordination geometry around the Ru centers of **7**, **8** and **9**, the heterobimetallic **9** can be considered as a hybrid of a cationic Ru fragment and an Ir(cod)Cl-NHC moiety.

3.1.2 Synthesis of the Ruthenium Iridium Heterobimetallic NHDC Complex with a C_2 backbone

3.1.2.1 Synthesis of **10-12**.

1-(2-hydroxyethyl)-3-(2,4,6-trimethylphenyl)-imidazolium bromide (**10**) was synthesized according to a literature procedure in 86% (lit.: 90%) yield.[138] 1-(2-bromooxyethyl)-3-(2,4,6-trimethylphenyl)-imidazolium bromide (**11**) was obtained according to a literature procedure in 81% (lit.: 78%) yield.[138] 1-(2-diphenylphosphanoethyl)-3-(2,4,6-trimethylphenyl)-imidazolium bromide (**12**) was obtained in 90% (lit.: 91%) yield according to a literature procedure.[139] The formation and purity of **10** - **12** was confirmed by ^{1}H, ^{13}C and ^{31}P NMR spectroscopy, ESI-MS and elemental analysis. All transformations are depicted in Scheme 17.
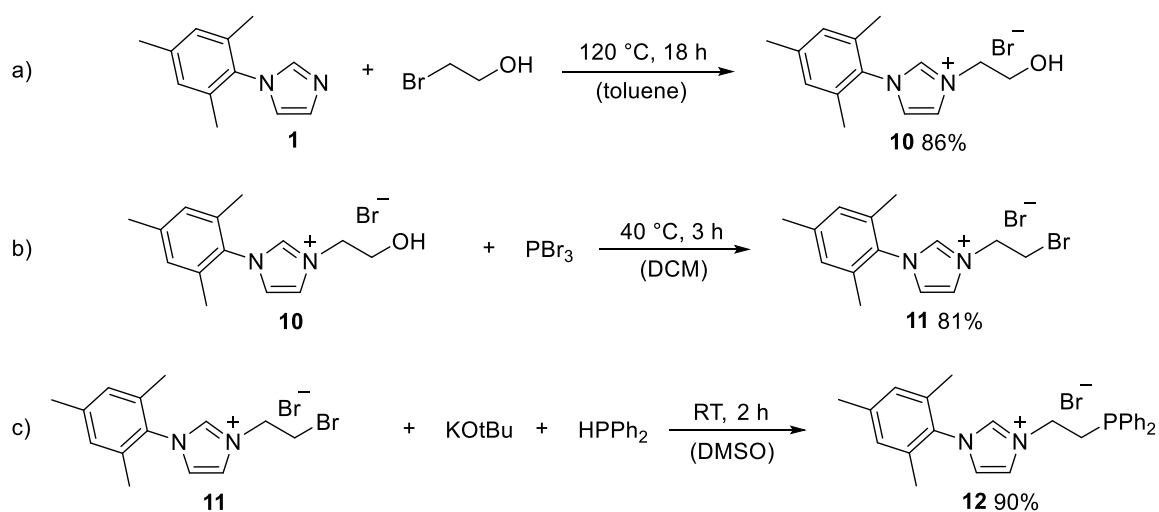
Scheme 17: Synthesis of **10** - **12**.

3.1.2.2 Synthesis of the monometallic aNHC Ru precursor **14**

The Ru aNHC complex **13**, which was previously published by Kühn and Baratta *et al.* is available in 85% yield by conversion of **12** with **6** (Scheme 18).[46] In contrast to the procedure described in literature, no base was added to the reaction mixture. The leaving acetate of the Ru precursor acts as an internal base for the deprotonation of the imidazolium salt. When the synthesis is performed in presence of a base, the formation of a side product is observed which will be described in the chapter 3.2.

Starting from **13**, it was envisioned that the second metal center could be introduced *via* reaction with Ag_2O as the base and the metal source following the protocol reported for the analogous complex **7** (Scheme 18).[44] However, reaction of **13** with Ag_2O only led to a non-characterizable mixture of decomposition products.
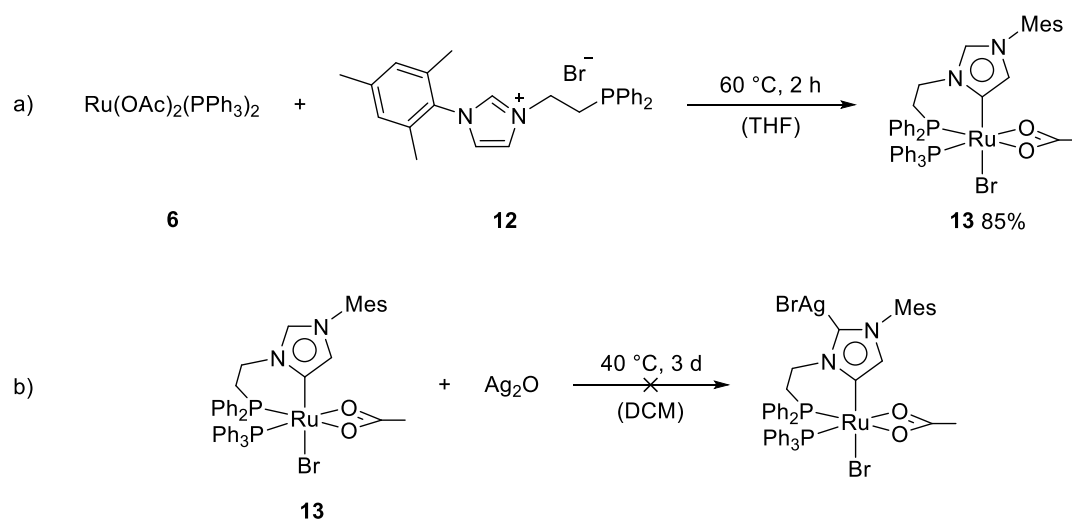
Scheme 18: Synthesis of **13** (a) and envisioned introduction of a second metal center (b).

The deprotonation of at the N*C*N position seems to be hampered for **13**, which is in clear contrast to the reactivity of **7**. The NC*H*N proton of **13**, which must be abstracted by Ag_2O, appears at 7.89 ppm in the ^{1}H NMR spectrum. The analogous NC*H*N proton of **7** is at 9.75 ppm, which is in the region of imidazolium salts that usually readily react with Ag_2O. It is noteworthy that **13** is a neutral compound, while **7** is cationic. The charge of the aNHC complexes might have a strong influence on the electronic situation of the NHC ligands. A change in the reactivity could be achieved by the replacement of the anionic bromide by neutral ligands as e.g. bidentate 1,2-bis(diphenylphosphano) ethane (dppe). Substitution of the anionic bromide with a neutral phosphane leads to a cationic compound with bromide as the counter ion (Scheme 19).
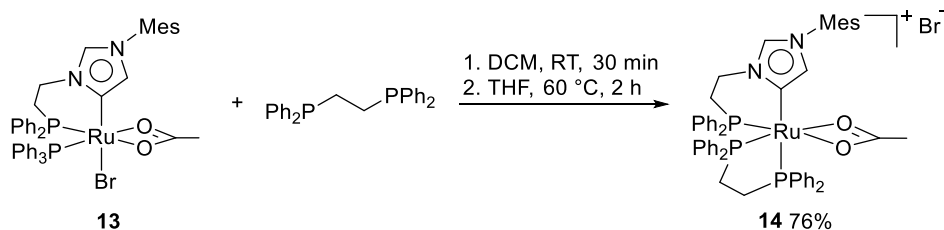
Scheme 19: Synthesis of **14**.

Thus, **13** and dppe were dissolved in DCM and stirred at RT for 30 min. Solvent removal leads to a bright yellow solid, which according to ^{31}P{^{1}H} NMR spectroscopy consists of several different species. Subsequently, the solid was dissolved in THF and the mixture was stirred at 60 °C. After 2 h, **14** precipitated as a bright yellow powder. After washing with diethyl ether and *n*-pentane **14** was isolated in 76% yield. Interestingly, neither the synthesis in THF nor in DCM solely leads to the selective formation of **14**.

The ^{1}H NMR spectrum of **14** shows a strongly down-field shifted signal for the NC*H*N proton (9.93 ppm) compared to **13** (7.89 ppm). This confirms the strong impact of the overall charge of the complex on the chemical shift of the NC*H*N proton. The chemical shift is very similar to the respective shift for complex **7** (9.75 ppm) suggesting a similar electronic situation on the NHC ring. The signal of the backbone proton of the aNHC is down-field shifted as well (6.72 ppm) compared to the respective resonance of **13** (5.82 ppm). The signals in the aromatic region account to 30 protons, which confirms the displacement of the PPh$_3$ and bromide ligand by the bidentate dppe ligand. Four distinct signals between 2.87 and 1.00 ppm represent the diastereotopic protons of the ethylene bridge of the dppe ligand.

The abnormal carbene gives a *pseudo*-triplet at 155.8 ppm in the ^{13}C{^{1}H} NMR spectrum with a large $^2J_{CPtrans}$ of 89.5 Hz and two small $^2J_{CPcis}$ of 11.4 Hz. This confirms the presence of two equatorial and one axial phosphane ligand. The ^{31}P{^{1}H} NMR spectrum of **14** shows three signals as doublets of doublets at δ = 72.0, 56.9 and 42.4 ppm. The coupling constants of $^2J_{PP}$ = 8.8 Hz, 38.8 Hz and 23.5 Hz indicate their *fac* arrangement of the P atoms. The small coupling constant of 8.8 Hz is attributed to the *trans* influence of the strongly σ-donating aNHC on the axial phosphane P atom and therefore to a presumably elongated Ru-P bond and a distorted C-Ru-P angle. FAB-MS shows an *m/z* value of 955.5 which corresponds to the molecular mass of **14** without the bromide counter ion. Single crystals were obtained by layering a solution of **14** in THF with *n*-pentane. The molecular structure was confirmed by SC-XRD (Figure 13).

Figure 13: ORTEP-style presentation of the molecular structure of **14**. Thermal ellipsoids are shown at a 50% probability level. H atoms and the bromide counter ion are omitted for clarity. Grey = C, blue = N, yellow = P, red = O, turquoise = Ru. Ru1-P3 2.2569(9), Ru1-P2 2.3813(10), Ru1-P1 2.2789(9), Ru1-C2 2.073(3), Ru1- Ru1-O2 2.177(2), O1 2.235(2), C2-Ru1-P3 93.18(7), C2-Ru1-P2 165.92(8), P2-Ru1-P3 84.67(3), P1-Ru1-P2 103.14(3), P1-Ru1-P3 92.90(3) O1-Ru1-O2 59.28(7). [L. Pardatscher, M. J. Bitzer, C. Jandl, J. W. Kück, R. M. Reich, F. E. Kühn and W. Baratta, *Dalton Trans*., 2019, **48**, 79-89] – Reproduced by permission of the Royal Society of Chemistry.

14 displays a distorted octahedral coordination geometry around the Ru center with a Ru1-C2 distance of 2.073(8) Å, which is in the typical range for Ru-carbene distances and slightly longer than reported for **13**.[46] This is in accordance with the presence of a phosphane, which is a stronger σ-donor than the bromide, in *trans* position to the carbene.[12] The Ru1-P2 distance is 2.3813(10) Å and longer than the other Ru1-P distances in *trans* to the acetate which are 2.2789(9) Å and 2.2569(9) Å, respectively. The C2-Ru1-P2 angle is 165.92(8) ° and therefore significantly distorted from the 180 ° expected for a regular octahedral coordination geometry. Also, the P1-Ru1-P2 and O1-Ru1-O2 angles (103.14(3) ° and 59.28(7) °, respectively) deviate from the ideal 90 °.

3.1.2.3 Synthesis of the heterobimetallic Ag-Ru NHDC complex **15**

The deprotonation of **7** at the NCN position and subsequent Ag coordination yielding the heterobimetallic **15** can be achieved by conversion of cationic **14** with Ag_2O. Therefore, **14** and Ag_2O were suspended in THF and stirred at 40 °C for 3 d. After filtration and solvent removal, the crude product was recrystallized from diethyl ether at −31 °C and obtained in 90% yield (Scheme 20).
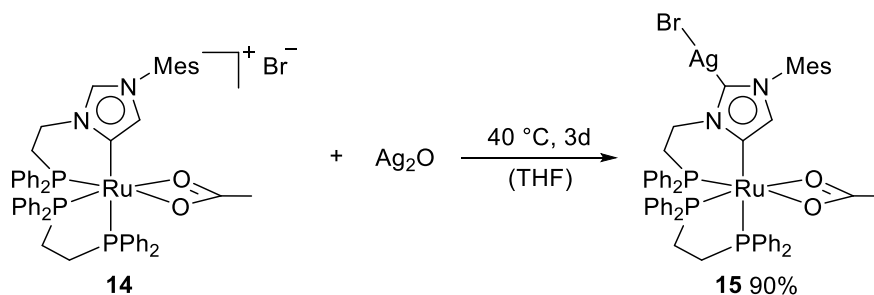
Scheme 20: Synthesis of **15**.

The deprotonation of the NCN position is confirmed by the absence of the respective signal in the ^{1}H NMR spectrum of the **15**. In the ^{31}P{^{1}H} NMR spectrum of **15** the three expected resonances appear in similar chemical shift ranges (δ = 72.6, 57.0 and 46.1 ppm, $^2J_{PP}$ = 5.5, 7.3 and 40.2 Hz) as observed for **14**. The absence of the NCN carbene signal in the ^{13}C NMR spectrum indicates an equilibrium reaction between the monomeric, neutral structure and the dimeric, cationic analogous with a $[AgBr_2]^-$ counter ion, a behavior that was previously reported.[140, 141] Single crystals suitable for SC-XRD where obtained by cooling a saturated solution of **15** in diethyl ether to −31 °C. SC-XRD confirms the coordination of the Ag[I] to the NCN position (Figure 14).
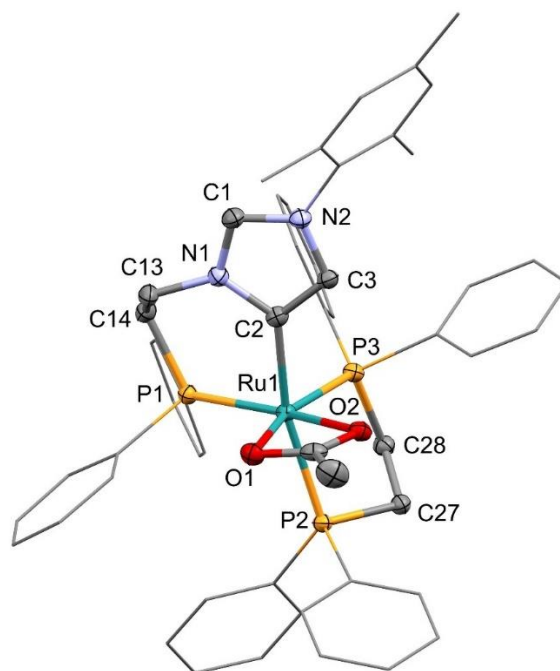
Figure 14: ORTEP-style presentation of the molecular structure of **15**. Thermal ellipsoids are shown at a 50% probability level. H atoms are omitted for clarity. Grey = C, blue = N, yellow = P, red = O, turquoise = Ru, white = Ag, brown = bromine. Ru1-P1 2.2593(12), Ru1-C2 2.118(5), Ag1-Br1 2.4172(9), Ag1-C1 2.078(5), C2- C1-Ag1-Br1 174.28(12), Ru1-P1 89.24(12). [L. Pardatscher, M. J. Bitzer, C. Jandl, J. W. Kück, R. M. Reich, F. E. Kühn and W. Baratta, *Dalton Trans.*, 2019, **48**, 79-89] – Reproduced by permission of the Royal Society of Chemistry.

The molecular structure of **15** shows a linear coordination of the Ag atom by a bromide and a Ru aNHC moiety. The Br1-Ag1-C1 angle (174.28(12) °) nearly matches the ideal 180 °. The Ag1-C1 distance is 2.078(5) Å and in the typical range of Ag carbene distances. The coordination sphere of the Ru fragment is similar to **14**. The Ru1-C2 distance is 2.118(5) Å and significantly longer than for the analogous Ru-Ag-NHDC complex with a C_1 backbone.[44] This might be due to the formation of a neutral complex bearing a negatively charged NHDC ligand.

15 is air-stable as a solid and stable in THF solution for months even without protection from light. In DCM, however, within two days a dark solid precipitates from the solution. In the ^{1}H NMR spectrum, a signal at δ = 9.75 ppm is observed, assigned to a NC*H*N proton. This indicates the formation of the precursor compound **7**, which is confirmed by ^{31}P NMR spectroscopy. Therefore, the cleavage of the Ag-carbene bond and the protonation of the aNHC ligand is assumed, which is rather surprising in an apolar and aprotic solvent like DCM.

When the metalation reaction is performed in DCM instead of THF as the solvent at 40 °C (Scheme 21), a yellow solid is obtained that exhibits the identical ^{1}H NMR spectrum as complex **15**. However, the molecular structure (Figure 15) reveals that the Ag atom is bearing a chloride instead of a bromide.

Single crystals suitable for SC-XRD were obtained by cooling of a saturated solution of **16** in diethyl ether to −31 °C.

Scheme 21: Synthesis of **16**.
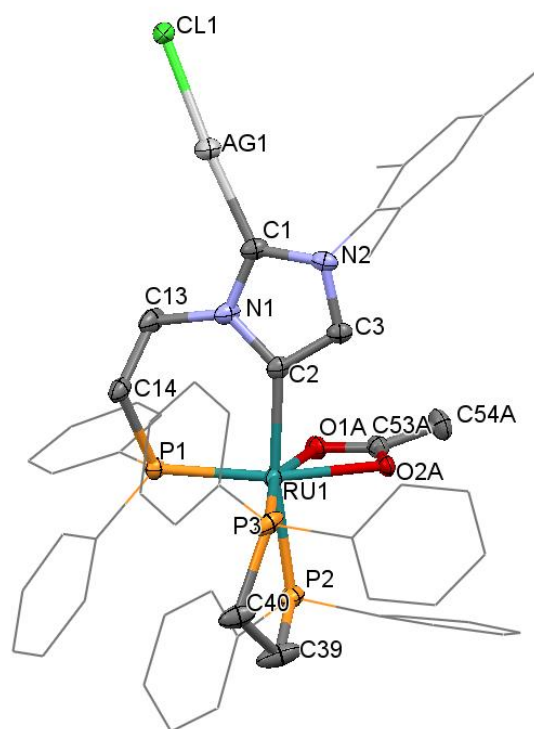

Figure 15: ORTEP-style presentation of the molecular structure of **16**. Thermal ellipsoids are shown at a 50% probability level. H atoms are omitted for clarity. Grey = C, blue = N, yellow = P, red = O, turquoise = Ru, white = Ag, green = Cl. Ag1-C1 2.074(3), Ag1-Cl1 2.3399(9), Ru1-C2 2.117(3), Ru1-P1 2.2569(8), Ru1-P2 2.3516(9), Ru1-P3 2.253(1), C1-Ag1-Cl1 174.13(9), C2-Ru1-P2 170.06(9), C2-Ru1-P3 98.93(9).

The overall molecular structures, namely bond lengths and angles, of **15** and **16** do not significantly differ from each other. Since neither the precursor complex **14**, nor Ag₂O contains Cl atoms, a Agᴵ promoted activation of DCM might occur. This could in turn possibly explain the bromide/chloride exchange observed for the synthesis in DCM and the observed instability of **16** in DCM.

3.1.2.4 Synthesis of **17**

17 was synthesized by transmetalation of **15** with [Ir(cod)Cl]$_2$ in THF in the presence of Ag$_2$O in order to suppress the formation of **14** as deduced by ^{1}H NMR spectroscopy (Scheme 22).
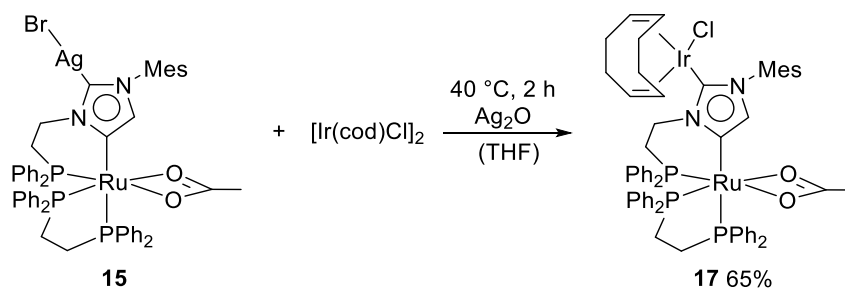
Scheme 22: Synthesis of **17**.

15 was added dropwise to a solution of [Ir(cod)Cl]$_2$ in THF at 40 °C. A grey solid is formed immediately, which indicates the precipitation of AgBr. After filtration and solvent removal, the resulting dark yellow solid is washed with a small amount of cold THF to dissolve the excess [Ir(cod)Cl]$_2$. The ^{1}H NMR and ^{31}P{^{1}H} NMR spectra of **17** in toluene-d$_8$ indicate the presence of a single species. In CD$_2$Cl$_2$ and THF-d$_8$, however, two isomers in a 1 : 2 and 1 : 4 ratio are present, respectively. The appearance of different isomers and isomer ratios is not due to different solubilities, since the NMR samples did not contain any precipitate. VT-NMR studies do not show any influence of the temperature on the peak sizes or shapes and therefore reveal that the isomer ratios are not temperature dependent. This behavior was previously observed for the analogous and mono- and heterobimetallic complexes with a C$_1$ backbone and was attributed to different conformations of the five-membered metallacycles.[43, 44] In this case, the six-membered metallacycles might be involved in the solvent dependent conformational changes. LIFDI-MS in DCM showed only one major signal at m/z = 1293 confirming the formation and purity of **17**. Single crystals suitable for SC-XRD were obtained by layering a solution of **17** in TH with n-pentane (Figure 16). SC-XRD confirms the coordination of an Ir(cod)Cl moiety to the NCN position. Unfortunately, it does not give further insight into the presence of different isomers, since only one isomer crystallized with the Ir(cod)Cl and acetate moieties being the only disordered fragments.
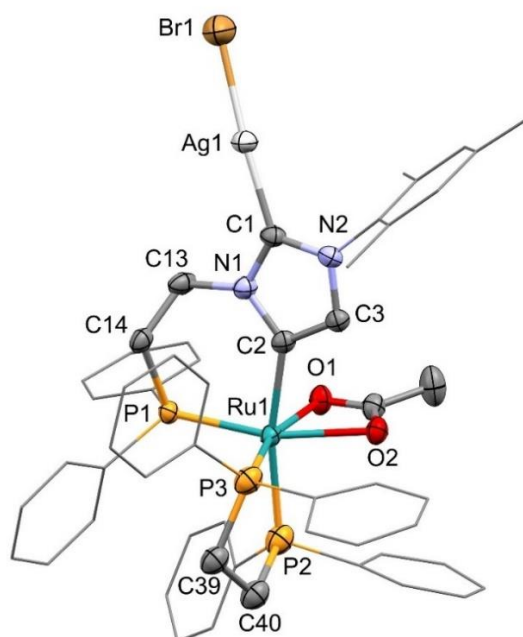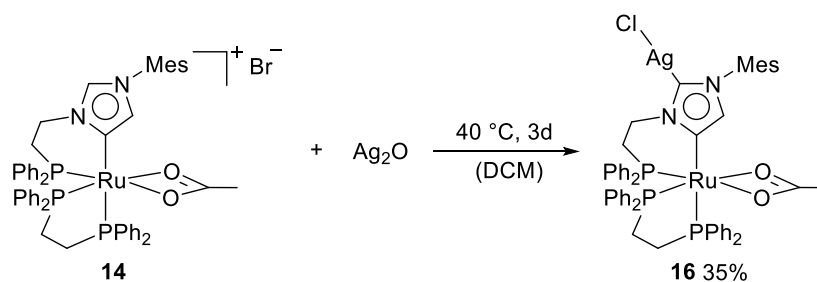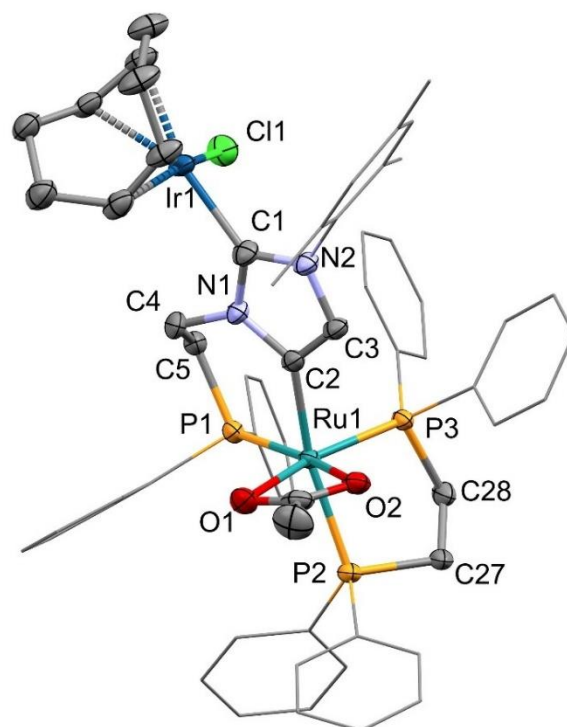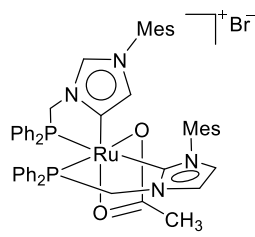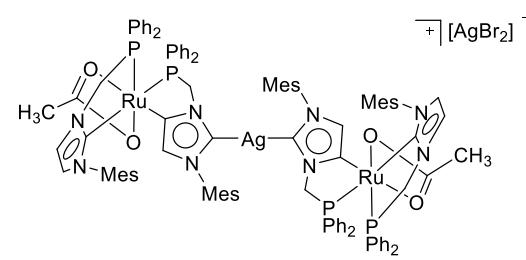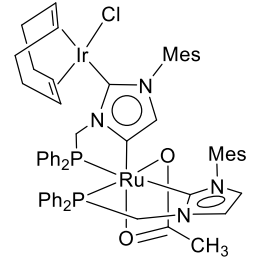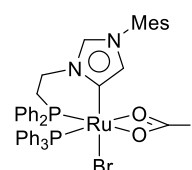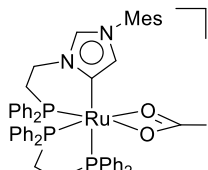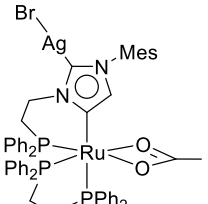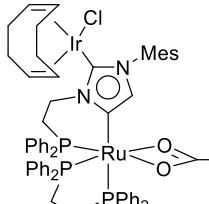
Figure 16: ORTEP-style presentation of the molecular structure of **17**. Thermal ellipsoids are shown at a 50% probability level. H atoms are omitted for clarity. Grey = C, blue = N, yellow = P, red = O, dark blue = Ir, turquoise = Ru, green = Cl. Ru1-P3 2.2384(10), Ru1-P2 2.3697(10), Ru1-P1 2.2798(11), Ru1-C2 2.085(4), C2-Ru1-P3 91.90(11), C2-Ru1-P2 166.08(11). [L. Pardatscher, M. J. Bitzer, C. Jandl, J. W. Kück, R. M. Reich, F. E. Kühn and W. Baratta, *Dalton Trans*., 2019, **48**, 79-89] – Reproduced by permission of the Royal Society of Chemistry.

The coordination geometry of the Ru fragment of **17** is very similar to that of **14**. For instance, the Ru1-C2 distance (2.085(4) Å) in complex **17** is only slightly shorter than in complex **15** (2.118(5) Å) and similar to the respective bond length in complex **14** (2.073(3) Å). The Ir atom is coordinated in a distorted square planar geometry by a chloride, a bidentate 1,5 cyclooctadiene and a Ru aNHC moiety. The bond lengths and angles cannot be determined properly due to disorder of the fragment. Since the overall octahedral coordination geometry of the Ru center is very similar for **14** and **17**, **17** can be considered as a hybrid of **14** and [Ir(cod)Cl]$_2$, which could exhibit interesting catalytic properties.

3.1.3 Evaluation of Electronic Interactions Between the Metal Centers

To investigate potential electronic interactions between the two metal centers bound to the anionic NHDC ring, cyclic voltammetry (CV), to consecutively investigate the oxidation and reduction potentials, and differential pulse voltammetry (DPV), to determine the precise first oxidation potentials in a single sweep, were conducted for the complexes **7-9** and **13-17** (except for **16**) and [IrCl(IMes)(cod)], which mimics the Ir fragment of **9** and **17**. The results are summarized in Table 2, the CVs and DPVs are depicted in Figure 17-19.

Table 2: CV and DPV results^a of monometallic and heterobimetallic complexes.

Complex	Metals	E$_{1/2}$ (V) (ΔE (mV))		Metal centered oxidation (V)^b
7	Ru	0.50^c	0.76^c	0.42
8	Ag, Ru	0.14 (100)	0.44 (70)	0.14
9	Ir, Ru	−0.09 (130)	0.40^c	−0.12
13	Ru	0.41^c	0.57	0.62
14	Ru	0.42^c	0.68 (95)	0.67
15	Ag, Ru	0.39 (100)	0.79 (160)	0.37
17	Ir, Ru	0.27^c	0.63^c	0.10
[IrCl(IMes)(cod)]	Ir	0.36 (140)		0.29

^{a}electrochemical experimetns were conducted in a 0.1 M solution of (nBu)$_4$NBF$_4$ in DCM. Working electrode: glassy carbon; counter electrode: graphite stick; reference electrode: Ag/AgCl, 3.4 M KCl, 0.200 V vs. NHE. Sample concentration: approx. 0.5 mm. Scan rate: 0.1 V s^{-1}. Potentials given relative to the *in-situ* added internal standard Fc/Fc$^+$ redox couple. ^{b} Metal centered oxidation peaks determined by DPV experiments. ^{c}Irreversible oxidation event.

Ru complex **7** bearing a normal and an abnormal NHC-P ligand shows an irreversible, presumably Ru centered transition at 0.50 V. **8** exhibits its reversible Ru^{II}/Ru^{III} redox potential at lower potential (0.14 V) than the monometallic precursor **7**. The analogous Au-Ru complex that was previously published[44] shows a very similar CV. The Ru centered oxidation is found at 0.17 V. According to SC-XRD, however, the molecular structure of the Au-Ru analogue resembles the structure of **15**, being monomeric and neutral. These results further indicate the previously mentioned equilibrium reaction between the dimeric structure like found for **8** and the monomeric structure as found for **15**, as their overall redox behavior is similar. The Ru-Ir complex **9** shows a reversible redox event at -0.09 V, which is again significantly lower than found for the precursor complexes. Thus, again substitution of Ag with Ir results in a much lower redox potential. This points towards significant coupling between the metal centers.
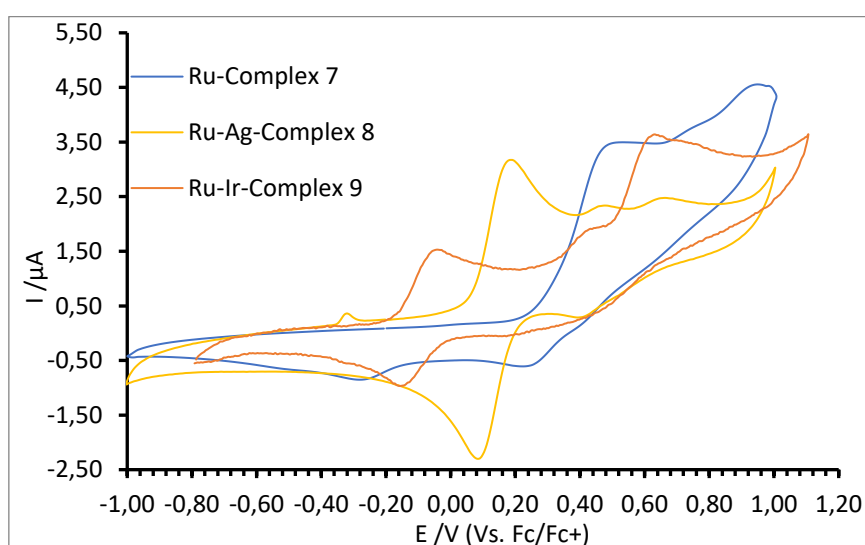
Figure 17: Cyclic voltammograms of complex **7** (blue), **8** (yellow) and **9** (orange). [L. Pardatscher, M. J. Bitzer, C. Jandl, J. W. Kück, R. M. Reich, F. E. Kühn and W. Baratta, *Dalton Trans.*, 2019, **48**, 79-89] – Reproduced by permission of the Royal Society of Chemistry.

The neutral complex **13** exhibits an irreversible and a reversible redox event at 0.41 V and 0.57 V respectively. Presumably, the Ru^{II}/Ru^{III} oxidation occurs at 0.62 V, as observed by DPV. The related cationic complex **14** shows an irreversible redox event at 0.42 V and a reversible one at 0.68 V, which is slightly higher than for **13**. The metal centered oxidation might occur at 0.67 V. The neutral metalated species **15** shows a reversible transition at 0.4 V (Ru^{II}/Ru^{III}) and a quasi-reversible process at 0.78 V (peak separation ΔE = 220 mV).[142] Presumably, the Ru centered redox process occurs at lower potential, when the NC*H*N proton is substituted by a AgBr moiety. The analogous **17** shows an irreversible oxidation at even lower potential (0.27 V), which might also be Ru centered.
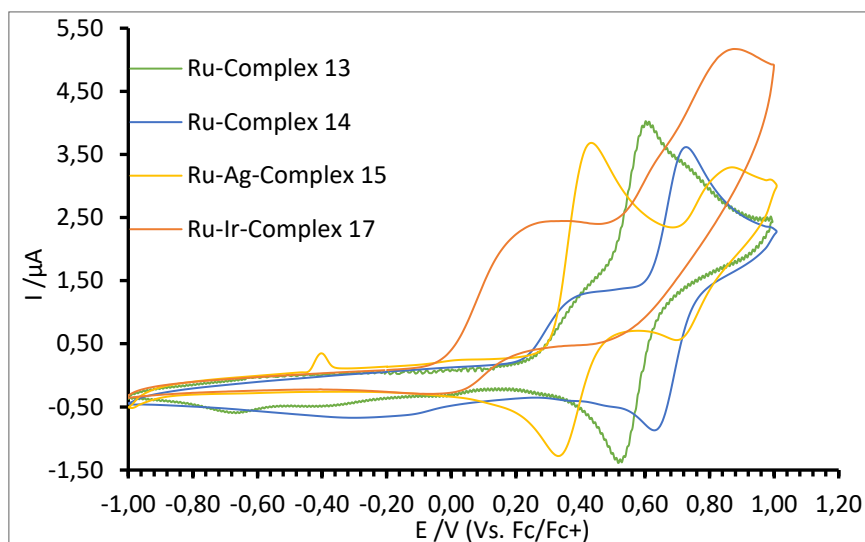
Figure 18: Cyclic voltammograms of complex **13** (green), **14** (blue), **15** (yellow) and **17** (orange). [L. Pardatscher, M. J. Bitzer, C. Jandl, J. W. Kück, R. M. Reich, F. E. Kühn and W. Baratta, *Dalton Trans*., 2019, **48**, 79-89] – Reproduced by permission of the Royal Society of Chemistry.

The first oxidation events in the DPVs of **9** and **17** are at −0.12 V and 0.10 V, respectively. The corresponding oxidations in **8** and **15** are observed at 0.14 V and 0.37 V, respectively. Thus, both substitutions of Ag^I with Ir^I result in a shift of the first metal centered oxidation by approx. 250 mV. The Ir^I/Ir^{III} transition of [IrCl(IMes)(cod)] is at 0.29 V. The complete absence of such an Ir centered 2-electron redox process, as found in [IrCl(IMes)(cod)], further indicates a strong influence of the Ru fragment on the electronic situation on the Ir center.
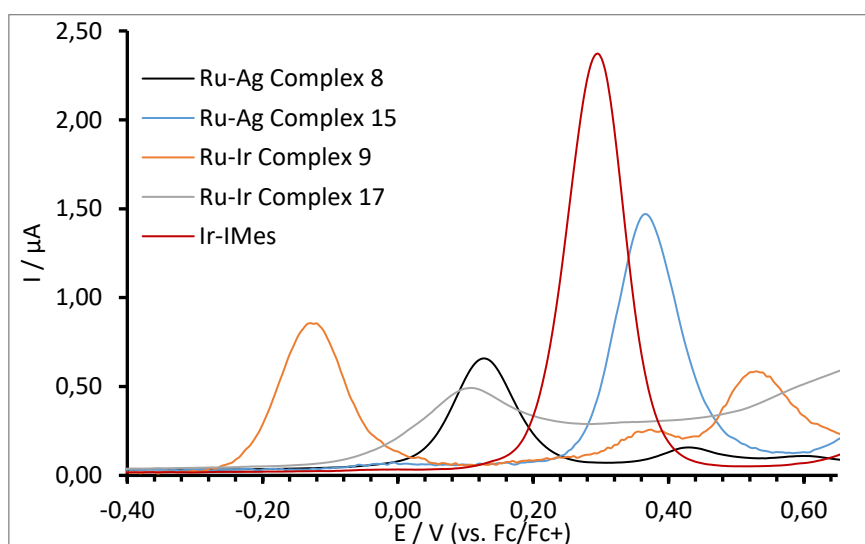
Figure 19: DP voltammograms of complex **8** (black), **15** (blue), **9** (orange), **17** (grey) and [IrCl(IMes)(cod)] (red). [L. Pardatscher, M. J. Bitzer, C. Jandl, J. W. Kück, R. M. Reich, F. E. Kühn and W. Baratta, *Dalton Trans*., 2019, **48**, 79-89] – Reproduced by permission of the Royal Society of Chemistry.

3.1.4 Investigation of the Influence of the Additional Metal Center on the Catalytic Activity of the aNHC Ru Complexes in TH of Acetophenone

The mononuclear Ru complexes **7** and **14**, and the heterobimetallic species **8**, **9**, **15** and **17** were tested as catalysts for the TH of acetophenone (0.1 M) in ^{i}PrOH with NaO^{i}Pr (2 mol%) as the promoter and at reflux conditions (100 °C oil bath temperature). The results are presented in Table 3.

Table 3: Results of TH experiments of acetophenone using Ru NHC and Ru NHDC complexes (0.1 mol%) as the catalysts with NaO^{i}Pr (2 mol%) in ^{i}PrOH at reflux conditions.

Entry	Catalyst	Time /min	Conversion /%[a]	TOF /h^{-1}[b]
1	**7**	5	97	26 000
2	**8**	120	50	250
3	**9**	120	98	6700
4	**13**[58]	120	97	38 000[c]
5	**14**	120	75	1500
6	**15**	120	64	360
7	**17**	120	97	1300
8	**7** + [IrCl(IMes)(cod)]	10	98	25 000
9	[IrCl(IMes)(cod)]	120	2	0

[a]Conversions were determined by GC analysis; [b]Turnover frequency (moles of ketone converted to alcohol, at 50% conversion, per moles of catalyst per hour). [c]Loading of **13** is 0.05 mol%.

The mononuclear mixed NHC/aNHC complex **7** shows a good activity in TH catalysis with a TOF of 26 000 h^{-1} and full conversion within 5 min. The metalation with Ag^I almost quenches the TH activity. **8** reaches only 50% conversion after 2 h and with a rate of 250 h^{-1}. This strong activity trop by two orders of magnitude might not solely be explained by the lower stability of the complex. In this case, the Ag atom could have an impact on the activity of the Ru fragment. Indeed, after transmetalation **9** reaches a TOF of 6700 h^{-1}, but still does not meet the activity of **7**. The stability of **9**, however, is not responsible for the lower activity, since full conversion is reached within 2 h. Therefore, electronic interactions

across the NHDC ring might affect the activity of the Ru fragment, unfortunately, in order to hinder the reaction and not to enhance the reaction rate. Alternatively, an involvement of a deprotonation step at the N*C*N position could potentially have an influence on the catalytic mechanism. After metalation, this position is protected and would not be accessible.

The previously published monometallic complex **13** is the most active complex under the applied conditions (the TOF was not determined again, the reported values stem from the corresponding publication).[46] **13** needs 2 h to complete the conversion of acetophenone to 1-phenyl ethanol. Although the initial rate of **13** is higher than for **7**, **7** is much more stable and does not undergo as fast deactivation. The related cationic species **14** with three P ligands in a *fac* arrangement reaches a TOF of 1500 h^{-1} an thus mostly loses its activity in TH. A reason for the low activity of **14** could be a steric hindrance for substrate coordination according to the presence of three bulky diphenylphosphane ligands. Upon metalation with Ag^{I} at the N*C*N position the activity of **15** drops further to a TOF of only 360 h^{-1}, which might be due to the low stability of Ag carbene bond and thus decomposition of the catalyst. The final conversion of only 64% after 2 h affirms its low stability. Upon transmetalation with Ir the activity again rises and reaches a TOF similar to that of **14**. Therefore, **17** reaches a TOF of 1300 h^{-1}. Interestingly, the Ru-Ir species **17** shows an enhanced stability compared to the initial complex **14** and completely converts the substrate. The Ir center itself does not catalyze the TH of acetophenone as shown by the use of [IrCl(IMes)(cod)] as the catalyst, which resembles the Ir moiety in **9** and **17**. The enhanced stability of **17** with respect to **13** and **14** could originate from the absence of the NC*H*N proton that under the basic catalysis conditions could potentially be abstracted. Possibly, an anionic unprotected aNHC ligand favors catalyst decomposition.

In summary, the Ir fragment does not positively affect the catalyst activities but can potentially enhance their stability. Cooperative effects of the two metal centers could not be established but might neither be excluded. Further studies shall clarify a potential bifunctional catalysis. A potential involvement of the ligands in catalysis will be discussed in chapter 3.2.3.

3.1.5 Conclusion

A potentially generally applicable synthesis route towards heterobimetallic NHDC complexes starting from Ru aNHC complexes was established. The NC*H*N protons of the cationic aNHC precursors **7** and **14** show ^{1}H NMR chemical shifts near 10 ppm, which can be compared with imidazolium salts that act as ligand precursors. In contrast to the neutral aNHC complex **13**, whose NC*H*N proton is at 7.89 ppm in the ^{1}H NMR spectrum, these complexes cleanly react with Ag_2O, leading to the heterobimetallic Ag-Ru NHDC species **15** and **8**. Transmetalation with [Ir(cod)Cl]$_2$ finally leads to the heterobimetallic Ru-Ir NHDC complexes **17** and **9**. Both Ru-Ir species show two different isomers in solution. The isomerism might originate from solvent dependent conformational changes of the 5- or 6-membered metallacycles, as inferred by NOESY NMR experiments. All novel complexes have been characterized in solution by ^{1}H NMR spectroscopy and in solid state by elemental analysis and SC-XRD. Electronic coupling between the metal centers were established through CV and DPV measurements. The complexes were furthermore tested as catalysts for the TH of acetophenone in ^{i}PrOH in order to evaluate the impact of the second metal center on the catalyst's activities. The monometallic species **7** and **13** exhibit the highest activities in catalytic TH of acetophenone. The heterobimetallic Ru-Ir NHDC complex **17**, however, shows enhanced stability under catalysis conditions compared to **13** and **14**. In this regard, **13** shows high initial rates but shows fast deactivation, completing the conversion of acetophenone only after 2 h, while **14** does not reach full conversion. The enhanced stability might be related to the formal protection of the NC*N* position from deprotonation. No cooperative effects could be established for catalytic TH.

3.2 Presentation of a di-Abnormal NHC Ru Complex as a Highly Active Catalyst for the Oppenauer-type Oxidation of Alcohols and Transfer Hydrogenation of Ketones

In this chapter, unpublished results are presented. The respective Manuscript is in preparation: L. Pardatscher, B.J. Hofmann, P. J. Fischer, S. M. Hölzl, R. M. Reich, F. E. Kühn and W. Baratta. [143]

In the following chapter a novel Ru di-aNHC complex will be presented that shows unprecedented activity in catalytic Oppenauer-type oxidation of alcohols. A reaction protocol has been developed where only stochiometric amounts of acetone are applied and no solvent is used. The catalyst, furthermore, is the most active NHC Ru catalyst in TH of ketones and among the most active catalysts for this reaction known to date. Based on deuteration experiments and DFT calculations a potential reaction mechanism has been proposed and a potential deactivation mechanism has been established according to the isolation of inactive hydride species.

3.2.1 Synthesis of the di-Abnormal NHC Ru complex **18**

When the synthesis of **13** is performed in the presence of NaOAc, as reported by Witt *et al.*, small amounts of a compound with a single peak in the $^{31}P\{^1H\}$ NMR spectrum are observed, hinting towards the formation of a symmetric Ru complex bearing two bidentate NHC ligands. This symmetric Ru aNHC complex **18** can be obtained selectively by reaction of **12** with **6** in presence of a high excess of NaOAc, or from **12** and **13** and stochiometric amounts of NaOAc (Scheme 23). As observed by Bitzer *et al.*, during the synthesis of **7** the first NHC ligand coordinates in its normal coordination mode to the Ru center.[44] Only the second NHC coordinates abnormally to the transition metal. Therefore, the 6-memebered metallacycle in **18** might force both NHC ligands into the abnormal binding fashion.
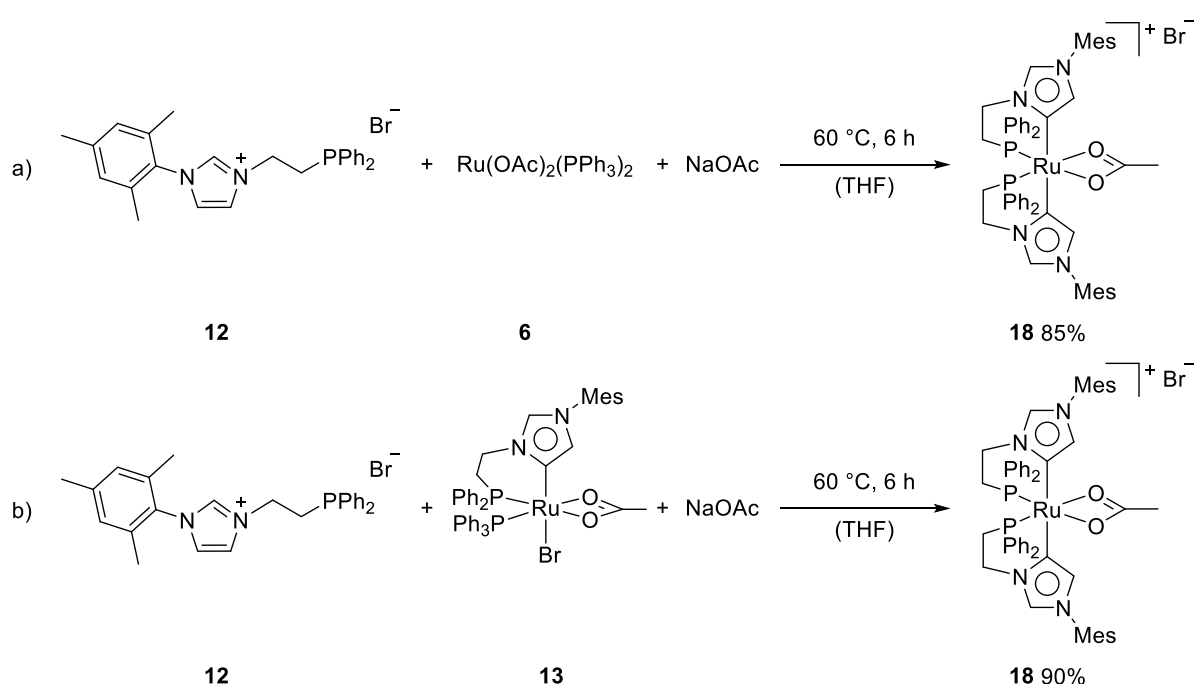
Scheme 23: Synthesis of **18** from **6** (a) and **13** (b).

As previously mentioned, in the $^{31}P\{^1H\}$ NMR spectrum in CD_2Cl_2 of **18** only a single peak at 56.6 ppm for the two phosphane moieties is observed. Three resonances at δ = 2.31, 2.10 and 1.80 ppm that account to six, six and nine protons, respectively, appear in the ^1H NMR spectrum. These resonances correspond to two mesityl methyl groups of **18** each overlapping with the acetate resonance at 1.80 ppm, as confirmed by HMBC NMR measurements that show a cross-peak with the carbonyl resonance at 184.2 ppm. This indicates a complex with a C_2-symmetry. The doublet at 8.72 ppm with a small coupling constant of $^4J_{HH}$ = 1.7 Hz corresponds to the NC*H*N protons of the NHCs and thus confirming the abnormal coordination mode. Compared to the neutral precursor complex **13**, the NC*H*N protons of the cationic **18** have undergone a significant down-field shift of $\Delta\delta$ = 0.83 ppm. However, the down-field shift is less pronounced than for the cationic **14** (9.93 ppm) and **7** (9.75 ppm) which display only one aNHC ligand. The *pseudo*-triplets at 7.75 ppm and 6.50 ppm can be assigned to the *ortho*-protons of the

phenyl groups. The NCCN protons of the aNHCs correspond to the doublet at 6.54 ppm ($^4J_{HH}$ = 1.7 Hz). In the ^{13}C NMR spectrum of **18**, a triplet at 165.3 ppm ($^2J_{CP}$ = 12.4 Hz) is observed for the abnormal carbene C. LIFDI MS shows a major peak with a m/z value of 957 which corresponds to **18** without the bromide counter ion. Furthermore, two peaks are observed at m/z = 977 for **18** without the acetate and at m/z = 898 for **18** without both, the bromide and the acetate. Single crystals suitable for SC-XRD were grown by layering a saturated solution of **18** in DCM with Et$_2$O (Figure 20).
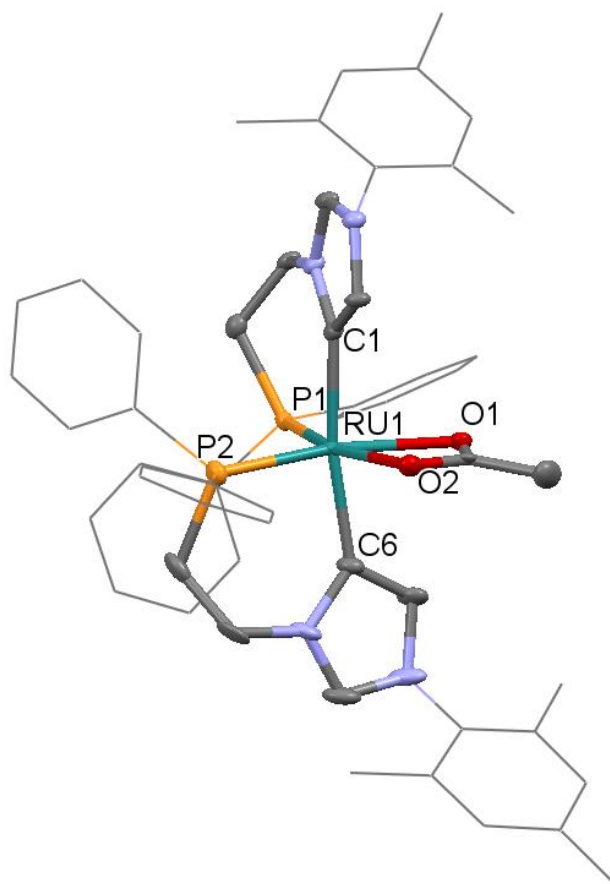
Figure 20: ORTEP-style presentation of the cationic fragment of **18**. Thermal ellipsoids are shown at a 50% probability level. H atoms and the bromide counter ion are omitted for clarity. Grey = C, blue = N, yellow = P, red = O, turquoise = Ru. Selected bond lengths (Å) and angles (°): C1-Ru1 2.098(5), C6-Ru1 2.096(5), O1-Ru1 2.240(4), O2-Ru1 2.210(4), P1-Ru1 2.2185(14), P2-Ru1 2.2181(15); C1-Ru1-C6 170.4(2), C1-Ru1-P1 90.39(15), C6-Ru1-P2 91.02(17), P1-Ru1-P2 92.00(5), O1-Ru1-O2 59.00(14).

18 displays an overall distorted octahedral geometry. The Ru center is coordinated by two P-C ligands and a chelating acetate with both NHCs in axial positions and coordinating in their abnormal mode. The C1-Ru1-C6 angle is 170.4(2) °. The C1-Ru1-P1 (90.39(15) °), C6-Ru1-P2 (91.02(17) °) and P1-Ru1-P2 (92.00(5) °) angles nearly match the ideal 90 °. The Ru carbene distances only slightly differ from each other being 2.098(5) Å and 2.096(5) Å. To the best of our knowledge, this is the first example of a Ru

complex bearing two imidazolylidene based aNHC ligands. Because of the abnormal coordination mode both wingtip substituents point away from the metal center.

When the reaction is performed with an under-stochiometric amount of base, a complex is obtained where the heterocycle is not coordinated to the metal (Scheme 24).
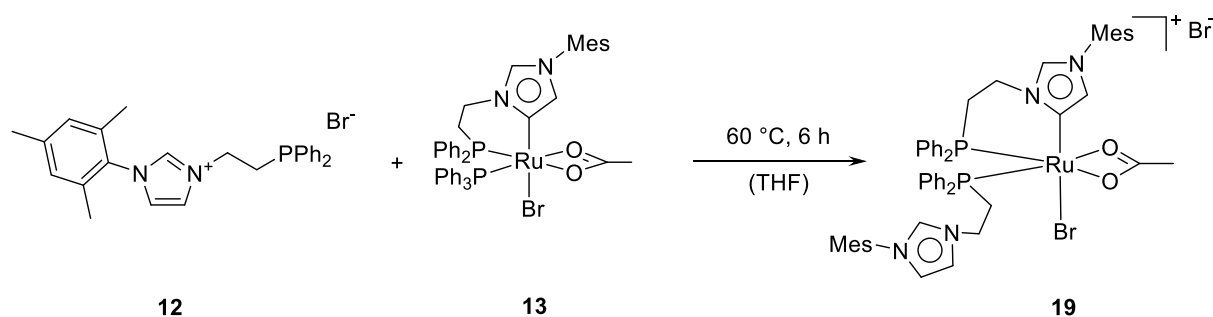
Scheme 24: Synthesis of **19**, i.e. synthesis of **18** without base addition.

19 shows two doublets at δ = 50.68 ppm and 50.11 ppm in the $^{31}P\{^1H\}$ NMR spectrum in CD_2Cl_2 with $^2J_{PP}$ coupling constants of 42.9 Hz. According to the pronounced roof effect, the signals resemble a doublet of doublets. When the $^{31}P\{^1H\}$ NMR spectrum is recorded in $CDCl_3$ the signals are even closer to each and roof effect is even more pronounced. The signals then resemble two singlets, because the outer resonances seem extinguished (Figure 21).
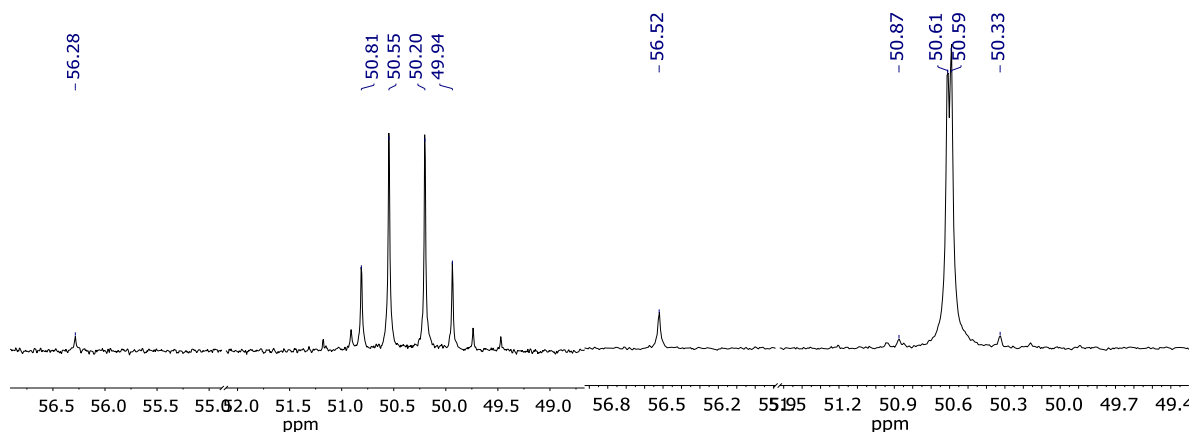
Figure 21: $^{31}P\{^1H\}$ NMR spectra of **19** in CD_2Cl_2 (left) and in $CDCl_3$ (right).

Single crystals suitable for SC-XRD of **19** were obtained by layering a solution of **19** in DCM with *n*-pentane. Strongly twinned single crystals did not allow for complete refinement of the molecular structure. The dangling imidazolium ring, however, is clearly visible in the obtained structure (Figure 22). The resulting Ru(II) species is cationic with a bromide counter ion and one bromide as ligand in the inner coordination sphere.
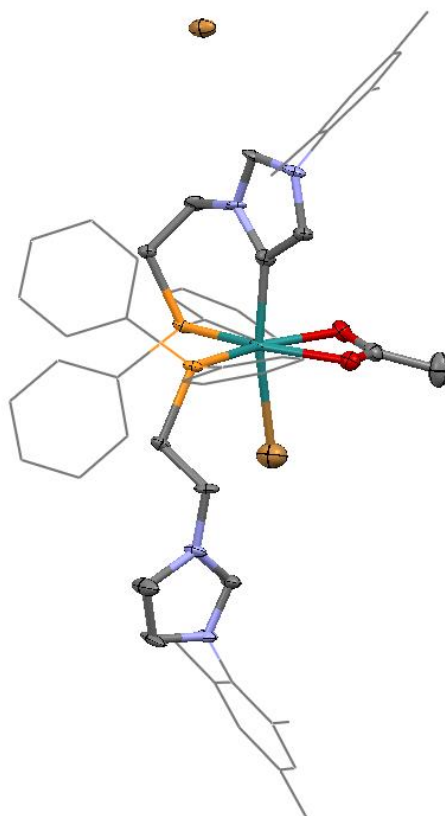
Figure 22: ORTEP-style presentation of the molecular structure of **19**. Thermal ellipsoids are shown at a 50% probability level. H atoms are omitted for clarity. Aromatic residues are shown in the wireframe-style for clarity. Grey = C, blue = N, yellow = P, red = O, turquoise = Ru, brown = Br. Bond lengths and angles cannot be discussed according to twinned crystals.

Therefore, the formation of **18** from **13** and **12** occurs *via* substitution of the PPh$_3$ with the phosphane functionality of the P-NHC ligand. Subsequently the imidazolium ring might be deprotonated and replaces the bromide.

The previously reported complex **13** shows very fast deactivation under catalytic conditions (^{i}PrOH/NaO^{i}Pr at elevated temperatures). In contrast, complex **7** which contains a second P-C ligand undergoes a slower deactivation and therefore might be considered the more efficient catalyst compared to **13**. Therefore, also **18**, displaying two NHC-P ligands might show promising catalytic properties in H transfer reactions.

3.2.2 Catalytic Investigations with Complex **18**

3.2.2.1 Catalytic TH of ketones

As described above, also **18** was tested as a catalyst for the TH of acetophenone in ^{i}PrOH. Therefore, the substrate (0.1 M) and the catalyst (0.1-0.005 mol%) were dissolved in ^{i}PrOH (9.7 mL). The mixture was heated to the desired temperature for 2 min and a solution of NaO^{i}Pr in ^{i}PrOH (0.1 M,, 200 µL, 2 mol%) was added to start the reaction. Blanc experiments were performed without the catalyst or without the base and no conversion of the ketone substrate to the corresponding alcohols was observed. The catalyst provides full conversion of acetophenone to 1-phenyl ethanol already after 1 min at loadings of higher than 0.05 mol%. Therefore, catalysis experiments were performed at a loading of 0.01 mol% if not otherwise specified. The results are summarized in Table 4.

At reflux conditions, **18** fully converts acetophenone to 1-phenylethanol in 1 min (Table 4, Entry 1). The TOF is therefore higher than 600 000 h^{-1}, which is in the range of the highest TOFs measured for TH catalysis. Attempts for a more precise determination of the initial rate will be discussed later. However, this value already exceeds the most active NHC and aNHC catalysts by an order of magnitude. Complex **18** is therefore the most active Ru NHC catalyst for TH of acetophenone in ^{i}PrOH known to date. When the temperature is lowered to 90 °C the TOF reaches 500 000 h^{-1} and acetophenone is fully converted within 5 min (Table 4, Entry 2). At 80 °C full conversion is obtained after 10 min with an initial rate of 300 000 h^{-1} (Table 4, Entry 3). At 70 °C, full conversion is reached after 20 min and with a rate 60 000 h^{-1} (Table 4, Entry 4). At 60 °C, only 42% conversion of acetophenone is observed after 40 min with a relatively slow rate of 5000 h^{-1} (Table 4, Entry 5). Thus, at temperatures beneath 70 °C, the activity drops significantly as the activation energy might not be overcome.

The following experiments were conducted at 80 °C, for an easier TOF determination and an easier handling of the catalytic reactions. When temperatures beneath the boiling point of the solvent are applied, the temperature does not temporarily drop upon overpressure loss.

p-Bromoacetophenone is converted to the corresponding alcohol within 5 min and a TOF of 200 000 h^{-1} (Table 4, Entry 6). The same activity was observed for *p*-phenylacetophenone which is also fully converted in 5 min and with a rate of 200 000 h^{-1} (Table 4, Entry 7). Benzophenone is converted to 80% in 10 min and a TOF of 100 000 h^{-1}, which might be due to the two sterically demanding phenyl groups (Table 4, Entry 8). The cyclic aliphatic cyclohexanone is fully converted in 10 min and with a rate of 120 000 h^{-1} (Table 4, Entry 9). Cyclopentanone is converted with a rate of 300 000 h^{-1} (Table 4, Entry 10). The open-chained aliphatic ketone 2-pentanone is reduced to 2-pentanol in 10 min and with a rate of 120 000 h^{-1} (Table 4, Entry 11). The analogous internal ketone 3-pentanone is hydrogenated to 3-pentanol to 91% within 20 min and a rate of 70 000 h^{-1} (Table 4, Entry 12).

Table 4: Catalytic TH of ketones (0.1 M) with **18** (0.01 mol%) as the catalyst and NaO^{i}Pr (2 mol%) as the promoter and reaction starter.
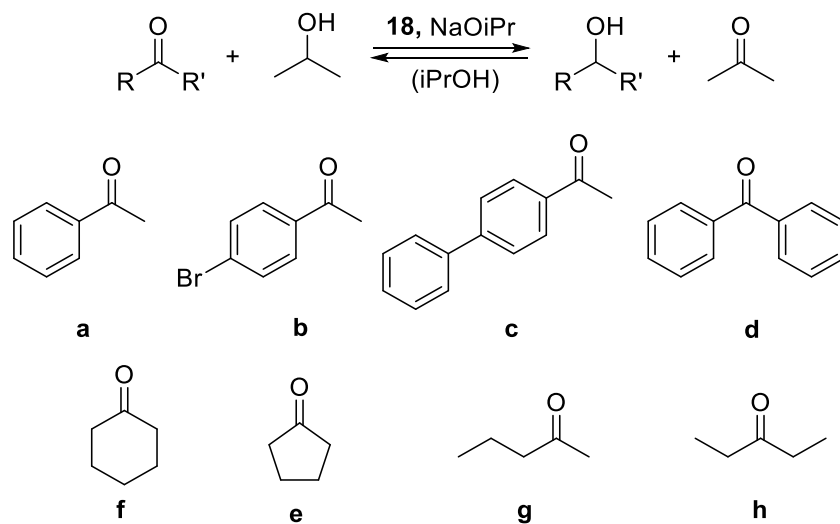
Entry	Substrate	Temperature /°C	TOF[b] /h^{-1}	Conversion[a] /%	Time /min
1	a	reflux	600 000	99	1
2	a	90	500 000	98	5
3	a	80	300 000	99	10
4	a	70	60 000	97	20
5	a	60	5000	42	30
6	b	80	200 000	99	5
7	c	80	200 000	97	5
8	d	80	100 000	80	10
9	e	80	120 000	98	20
10	f	80	300 000	99	3
11	g	80	120 000	98	10
12	h	80	70 000	91	20

[a]Conversions were determined by GC analysis; [b]Turnover frequency (moles of ketone converted to alcohol, at 50% conversion, per moles of catalyst per hour).

To investigate the course of the catalytic TH of acetophenone during the first minutes, samples were taken every 10 sec at 100 °C and every 20 sec at 80 °C oil bath temperature, respectively (Figure 23). The sampling was performed with a 30 cm long teflon cannula with a diameter of 0.5 mm that was shortly dipped into the reaction mixture at an Ar overpressure of 0.2 mbar. To ensure an immediate stop of the reaction, the samples of about 0.3 mL were directly quenched by addition to ice-cold diethylether. The cannula was not removed from the reaction vessel, having an open system with a continuous Ar counterflow.
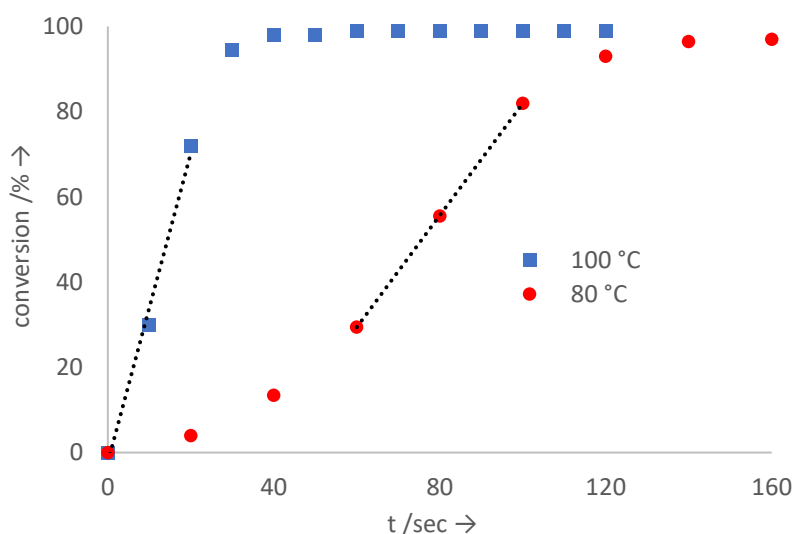
Figure 23: Investigation of the initial phases of the TH of acetophenone at 80 °C (spheres) and 100 °C (squares).

At 80 °C an induction period of about 1 min is observed, which corresponds to the formation of active species by addition of NaO^{i}Pr. Between sec 60 and 100 **18** reaches a TOF of 470 000 h^{-1} and the conversion flattens thereafter to a total conversion of 98% after 3 min. At 100 °C (reflux) the formation of the active species occurs faster and is not observed, even immediately after base-addition. The catalyst reaches its maximal TOF of 1 300 000 h^{-1}. After 20 sec the reaction decelerates and reaches 99% after 1 min.

These reaction rates are among the highest ever measured for catalytic TH of acetophenone. Usually, only complexes bearing primary or secondary amines and therefore following the outer sphere mechanism reach such activities. Therefore, an involvement of the ligand in the catalytic mechanism and thus bifunctional catalysis should be taken into account. Investigations concerning the reaction mechanism will be presented in the paragraph 3.2.3.

3.2.2.2 Oppenauer-type Oxidation of Alcohols

Oppenauer-type oxidation of alcohols has mostly been carried out in acetone as the solvent to take advantage of the large excess of the oxidative reagent and to have one component less in the reaction mixture. However, the performances of the catalysts do not meet those of the catalytic TH of ketones. One major difference between the two reaction protocols, therefore, is the chemical environment in which the catalysts are dissolved, namely alcohol vs. ketone. The performance of the reaction in acetone furthermore dictates the use of weak bases like carbonates to prevent acetone to undergo aldol condensation reactions. Although it is desirable to use weak bases, the strength of the applied base has a significant influence on the performance of the TM catalysts.[82] Therefore, **18** was tested in Oppenauer-type oxidation of alcohols in ^{t}BuOH as an innocent alcohol solvent and with KO^{t}Bu as a relatively strong base. Under these conditions **18** catalyzes the fast oxidation of several secondary alcohols. In order to suppress undesired condensation reactions, only 6 eq of acetone are applied. Furthermore, full conversion is mostly reached after very short reaction times. The results are summarized in Table 5.

i is cleanly oxidized to α-tetralone at 40 °C within 5 min and at a catalyst loading of 0.1 mol% reaching a TOF of 38 000 h^{-1} (Table 5, Entry 1). At a catalyst concentration of 0.05 mol%, and at a temperature of 30 °C the oxidation proceeds with a TOF of 12 000 h^{-1}. Full conversion is obtained in 20 min (Table 5, Entry 2). At 40 °C (0.05 mol%), the TOF reaches 40 000 h^{-1}, which is similar to the determined TOF at 0.1 mol% (Table 5, Entry 3). Therefore, the catalyst loading might be in the optimal range, as the reaction is not overloaded with the catalyst and on the other hand the reaction does not proceed at lower loadings than 0.05 mol%. At 50 °C, full conversion is obtained in 2 min and the TOF is 100 000 h^{-1} (Table 5, Entry 4). At 40 °C and a catalyst loading of 0.05 mol%, the dehydrogenation of **j** proceeds with a TOF of 80 000 h^{-1}. Full conversion towards 1-indanone is accomplished in 5 min (Table 5, Entry 7). However, **j** shows traces of a side-product formation, probably due to aldol condensations involving the five-membered cyclic ketone. The bulkier **k** requires 60 °C for a proper conversion to fluorenone. 95% conversion are observed after 60 min. The TOF reaches 4000 h^{-1} (Table 5, Entry 8). At a loading of 0.1 mol% **l** is converted by 92% within 10 min (Table 5, Entry 9). At lower loading (0.05 mol%) the conversion reaches 78% (Table 5, Entry 10). **m** is converted to 80% within 15 min at 60°C and at 0.05 mol% loading (Table 5, Entry 11). **n** is oxidized by 87% to the 4-heptanone within 30 min (Table 5, Entry 12). **o** is fully oxidized to camphor within 30 min and with a TOF of 24 000 h^{-1} (Table 5, Entry 13). At 40 °C, **p**, which is a stereoisomer of **o**, is only converted by 45% and with a TOF of 2000 h^{-1} (Table 5, Entry 14). Camphor is obtained faster (TOF = 12 000 h^{-1}) and in higher yield (70%) at 60 °C (Table 5, Entry 15). At 60 °C full conversion of **p** is obtained in 10 min and the TOF reaches 60 000 h^{-1} (Table 5, Entry 16). The sterically demanding **q** is only converted at 80 °C and a loading of 0.1 mol% (Table 5, Entry 17).

Table 5: Catalytic Oppenauer-type oxidation of alcohols (i-q) by application of **18** as the catalyst.

Entry	Substrate	Loading	Temperature /°C	TOF[b] /h^{-1}	Conversion[a] /%	Time /min
1	i	0.1 mol%	40	38 000	99	5
2	i	0.05 mol%	30	12 000	97	20
3	i	0.05 mol%	40	40 000	99	10
4	i	0.05 mol%	50	100 000	100	3
5[c]	i	0.05 mol%	40	100 000	98[d]	5
6[c]	i	0.01 mol%	50	550 000	98	2
7	j	0.05 mol%	40	80 000	99	5
8	k	0.05 mol%	60	4000	95	60
9	l	0.1 mol%	60	15 000	92	10
10	l	0.05 mol%	60	18 000	78	30
11	m	0.05 mol%	60	25 000	80	15
12	n	0.1 mol%	60	10 000	87	30

13	o	0.05 mol%	40	24 000	97	20
14	p	0.05 mol%	40	2000	45	60
15	p	0.05 mol%	50	12 000	67	45
16	p	0.05 mol%	60	60 000	99	10
17	q	0.1 mol%	80	3400	90	60

[a]Conversions were determined by GC analysis; [b]Turnover frequency (moles of ketone converted to alcohol, at 50% conversion, per moles of catalyst per hour). [c] reaction carried out without solvent. [d] isolated yield after column chromatography.

Furthermore, the same reaction was carried out without addition of ^{t}BuOH. With 0.05 mol% **18**, a temperature of 40 °C and by addition of only 2 eq of acetone, **i** is fully converted with a TOF of 100 000 h^{-1} within 3 min (Table 5, Entry 5). Obviously, the reaction rate is drastically enhanced if no solvent is used. Following this reaction protocol α-tetralone was isolated in 98% yield after column chromatography. Therefore, it could be highly promising for a potential larger scale application, because the workup is relatively simple: the catalyst is removed by a filtration over a silica-pad and the small amounts of volatiles are removed under reduced pressure. As the absolute catalyst concentration is higher following this reaction protocol without a solvent, the amount of catalyst applied can be reduced to 0.01 mol%. At 50 °C full conversion is obtained within 1 min (Table 5, Entry 6). The TOF for this transformation reaches unprecedented 550 000 h^{-1}.

3.2.3 Mechanistic Investigations on the Catalytic Hydrogen Transfer Reaction with 18

3.2.3.1 The Role of Abnormal Coordination for the Catalytic Activity in TH and a Potential Deactivation Mechanism

To investigate the catalyst species that might possibly be present after a catalytic reaction, **18** was reacted with NaO^{i}Pr (10eq) in ^{i}PrOH at 80 °C (approx. catalysis conditions). After 2 h the symmetric dihydride dicarbene complex **20** is selectively obtained (Scheme 25).
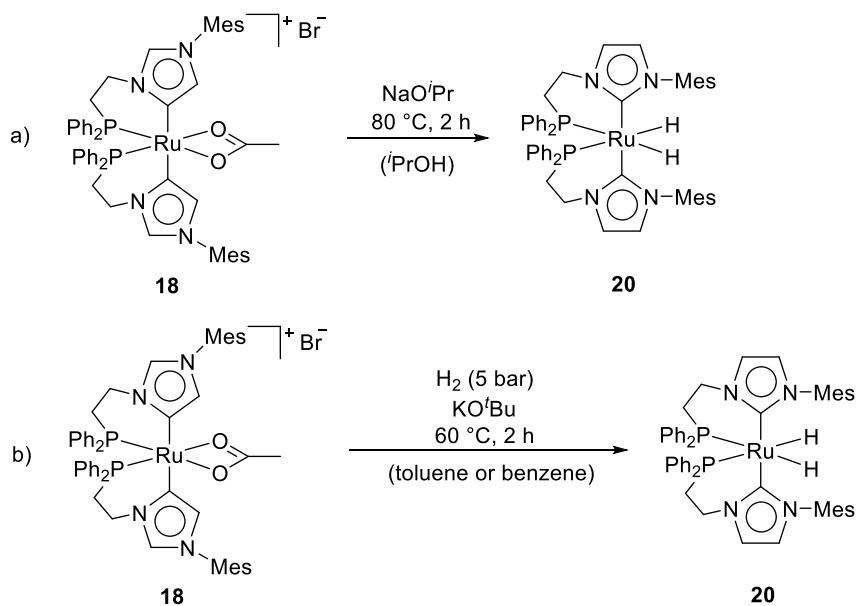
Scheme 25: Synthesis of **19** by a) hydrogen transfer or b) activation of dihydrogen.

20 is also achieved by reaction of **18** with dihydrogen (5 bar) in toluene or benzene with KO^{t}Bu (5 eq) at 60 °C after 2 h. In the ^{1}H NMR spectrum in C$_6$D$_6$, **20** displays a doublet of doublets at $\delta = -6.81$ ppm for two hydride atoms with of $^2J_{HPtrans} = 87.0$ Hz and $^2J_{HPcis} = 19.6$ Hz (Figure 24, left). No strongly down-field resonance corresponding to a NC*H*N proton is observed. However, two signals as doublets at $\delta = 6.11$ ppm and 5.93 ppm with a coupling constant of $^3J_{HH} = 1.9$ Hz are obtained, which correspond to the backbone protons of the NHCs. This indicates NHC ligands coordinated in their normal mode. The ^{31}P{^{1}H} NMR spectrum displays a singlet at $\delta = 39.0$ ppm for the two P atoms, confirming the presence of a symmetric compound (Figure 24, right).
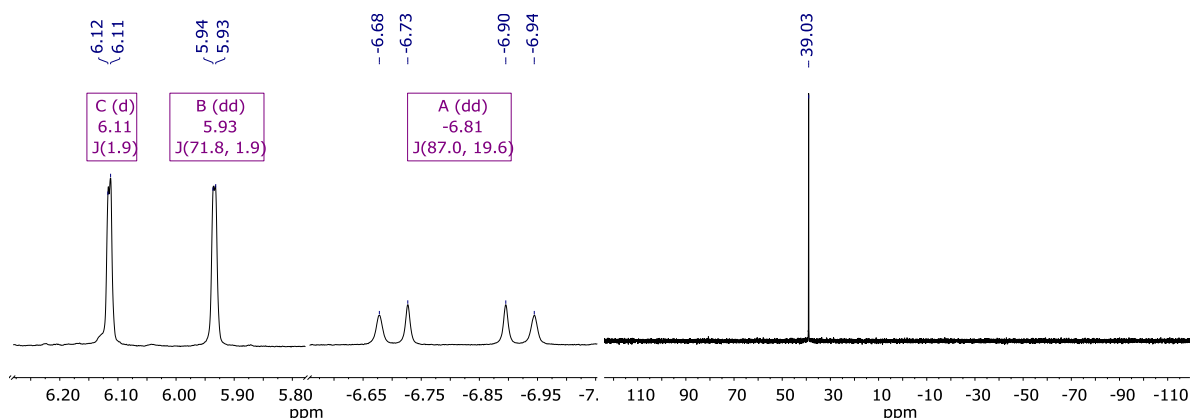
Figure 24: ^1H NMR spectrum in C_6D_6 of **20** (left) and $^{31}P\{^1H\}$ NMR spectrum in C_6D_6 of **20** (right).

The $^{13}C\{^1H\}$ NMR spectrum of **20** shows a triplet at δ = 196.6 ppm, a typical shift for a normal NHC, which further confirms their normal coordination mode. Although the dihydride species could not be isolated as pure complex due to its high sensitivity against air and moisture and probably also due to intramolecular decomposition by reductive elimination of the NHCs[41], single crystals were obtained by cooling a saturated solution of the raw product in *n*-hexane to −31 °C (Figure 25). It is noteworthy, that **20** is only soluble in *n*-hexane if traces of toluene or benzene are present.

Figure 25: ORTEP-style presentation of the molecular structure of **20**. Thermal ellipsoids are shown at a 50% probability level. H atoms (except for the hydrides) are omitted for clarity. Only one of the independent molecules of the asymmetric unit is depicted. Grey = C, blue = N, yellow = P, turquoise = Ru. Selected bond lengths (Å) and angles (°): Ru1-C8 2.071(2), Ru1-C2 2.075(2), Ru1-P1 2.2933(6), Ru1-P2 2.3015(6), Ru1-H1R 1.74(2), Ru1-H2R 1.74(3), C8-Ru1-C2 167.86(9), C2-Ru1-P1 88.15(6), C8-Ru1-P2 90.15(7), P1-Ru1-P2 108.86(2), H1R-Ru1-H2R 56.2(11).

The molecular structure of **20** confirms the formation of a dihydride complex bearing two normal NHC ligands. The Ru-carbene distances (2.071(2) Å and 2.075(2) Å) are slightly shorter than in complex **18**, while the Ru-P distances (2.2933(6) Å and 2.3015(6) Å) are longer with a large P1-Ru1-P2 angle

(108.86(2) °). This is in accordance with a strong *trans* influence of the hydrides on the phosphanes. The large P1-Ru1-P2 angle could in turn indicate a small H1R-Ru1-H2R angle. Therefore, the H atoms that might be very close to each other in order that the dihydride could rather resemble a Ru dihydrogen complex.

It is likely that **20** is obtained by substitution of the acetate with ^{i}PrO$^-$ affording an alkoxide species which is converted to the hydride by β-H-elimination and concomitant carbene isomerization from the abnormal to the normal coordination mode. However, to form a dihydride species by two subsequent β-H-elimination reactions, a further coordination site would be necessary. A hemilabile behavior of the NHC-P ligands should therefore be considered. Alternatively, intramolecular C-H activation could potentially be a hydride source.[81] Attempts to isolate hydride species that occur during the formation **20** were not successful.

Notably, the dihydride **20**, obtained *in-situ* by reaction of **18** with NaO^{i}Pr (10 eq), does not react with acetophenone. Obviously, the formation of **20** represents a deactivation pathway of **18**. It furthermore shows that the abnormal coordination mode of the NHC ligands is crucial for its catalytic activity. Indeed, the Mes substituents point away from the metal center if the NHCs coordinate in their abnormal fashion, resulting in a large pocket for potential catalytic transformations. When the coordination mode of the NHCs changes, the Mes substituents shield the dihydride from a potential substrate attack, rendering **20** completely inactive in catalysis.

The analogous experiments were also conducted with complex **7** to compare its reactivity with **18**. After 2 h the reaction with NaO^{i}Pr (10 eq) in ^{i}PrOH affords an analogous symmetric dihydride complex (**21**) (Scheme 26).
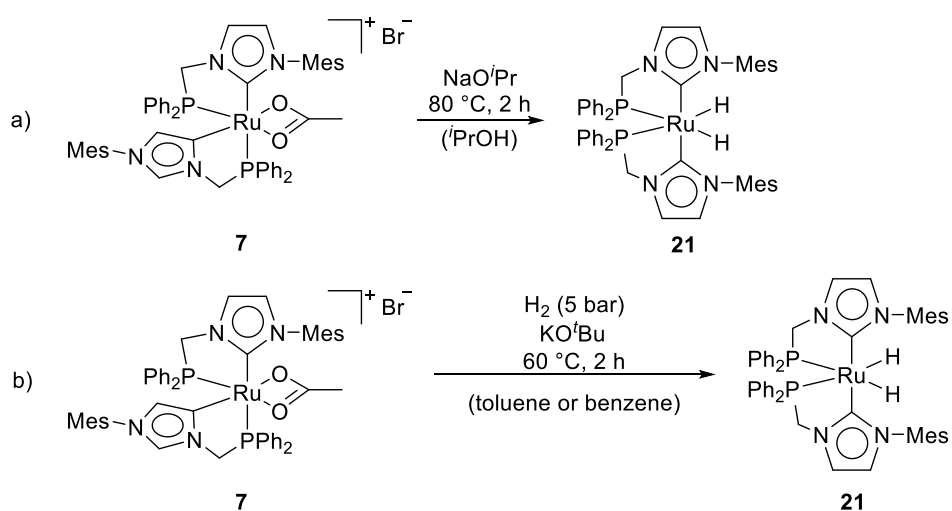
Scheme 26: Synthesis of **21** by a) hydrogen transfer or b) activation of dihydrogen.

In the ^{1}H NMR spectrum in toluene-d$_8$, **21** shows a doublet of doublets at $\delta = -6.68$ ppm and with coupling constants of $^2J_{HPtrans} = 98.4$ Hz and $^2J_{HPcis} = 16.9$ Hz for the two Ru hydrides. The ^{31}P NMR spectrum (not pulse decoupled) shows a signal as a doublet at 66.3 ppm with the corresponding P-H coupling constant $^2J_{PHtrans}$ of 97.6 Hz; in the ^{31}P{^{1}H} NMR spectrum the signal appears as a singlet (Figure 26).
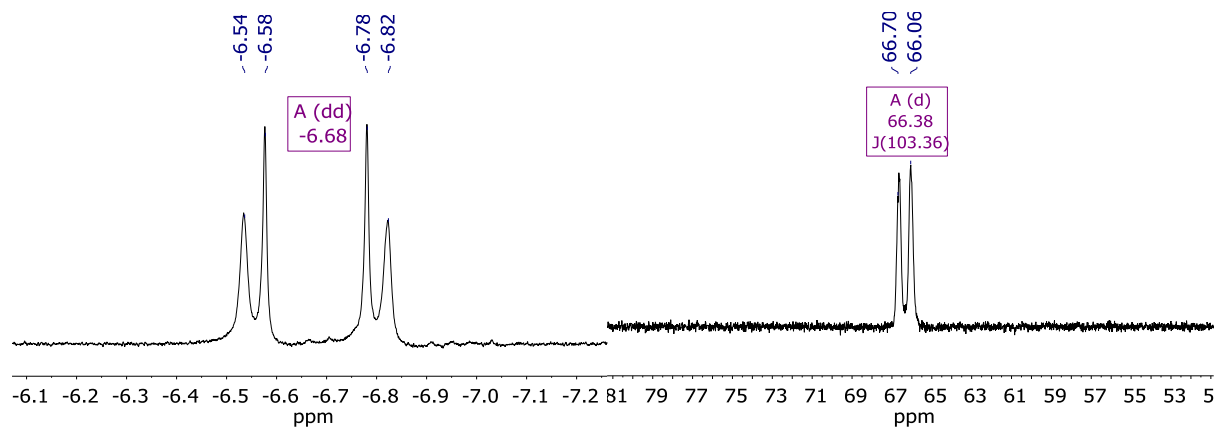
Figure 26: Hydridic signal in the ^{1}H NMR (left) and P signal in the ^{31}P NMR spectrum (right) of **21** in toluene-d$_8$.

LIFDI mass spectrometry confirms the formation of the symmetric dihydride giving a *m/z* of 872 which corresponds to the molecular mass of **21**. The reaction of **7** with KO^{t}Bu and pressurized dihydrogen (5 bar) in benzene or toluene cleanly yields the same dihydride complex. When the benzene or toluene is evaporated, and hexane is added, **21** initially dissolves due to the presence of residual benzene or toluene. After stirring for a few minutes, **21** purely precipitates as a bright yellow powder from the *n*-hexane solution. The resonance at $\delta = 208$ ppm in the ^{13}C{^{1}H} NMR spectrum of **21** in toluene-d$_8$ indicates the normal coordination mode of the NHC ligands. Single crystals have grown from a saturated solution of **21** in *n*-hexane at -31 °C (Figure 27).
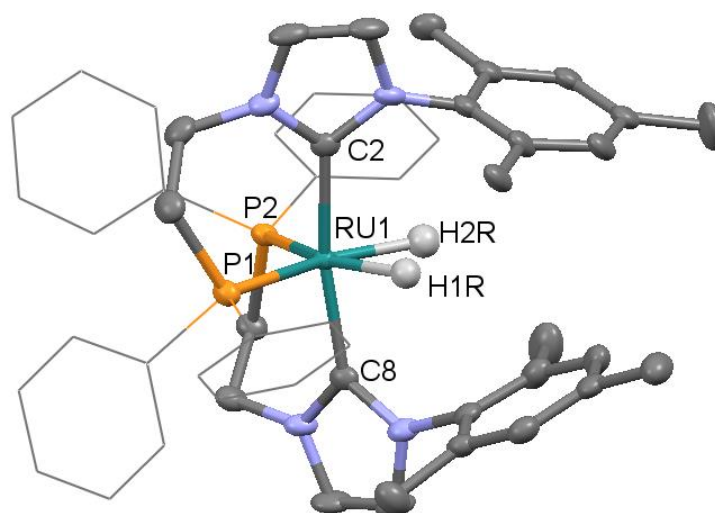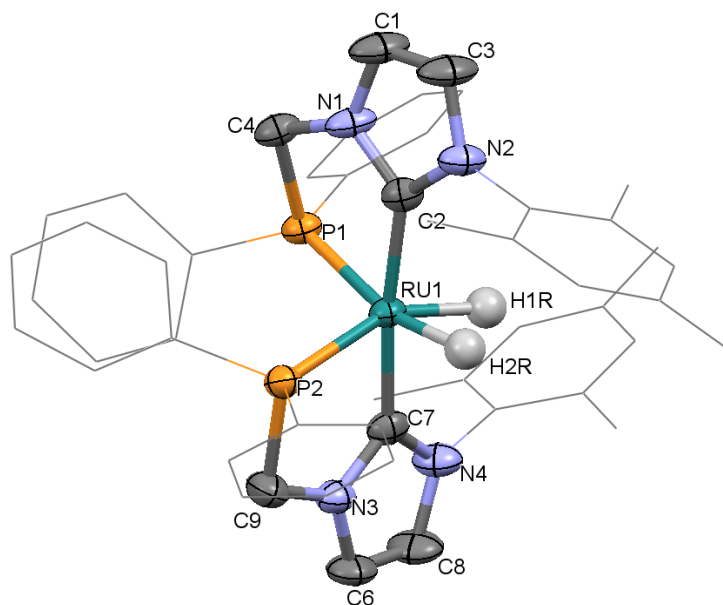
Figure 27: ORTEP-style presentation of the molecular structure of **21**. Thermal ellipsoids are shown at a 50% probability level. H atoms (except for the Ru-hydrides) are omitted for clarity. Aromatic substituents are shown in the wireframe-style. Grey = C, blue = N, yellow = P, turquoise = Ru. Selected bond lengths (Å) and angles (°): Ru1-P1 2.2732(15), Ru1-P2 2.2755(16), C7-Ru1-C2 173.04(15), C2-Ru1-P1 80.59(10), C7-Ru1-P2 82.00(12), P1-Ru1-P2 99.73(6).

The crystal structure of **21** confirms the formation of a symmetric dihydride complex with two NHCs in axial positions coordinating in their normal mode. Therefore, the structure is an analogue of **20**. The C2-Ru1 and C7-Ru1 distances are 2.048(4) Å and 2.034(4) Å, respectively, and are shorter than the corresponding distances in **20**. The P1-Ru1 and P2-Ru1 distances only slightly differ from each other (2.2732(15) and 2.2755(16) Å, respectively) and are both shorter than in **20** as well. The C2-Ru1-C7 angle is 173.04 ° and slightly deviates from the ideal 180 °expected for a regular octahedral coordination geometry. The P1-Ru1-P2 angle is 99.73 °, which is significantly smaller than observed for **20**. In turn, the H1R-Ru1-H2R angle might presumably be comparably large and the H1R-H2R distance might be too long for covalent H-H interactions. The differences in the bond angles and distances could explain the huge difference between the chemical shifts of the P atoms in the ^{31}P NMR spectra of **20** vs. **21**. For instance, **20** shows a resonance for the two P atoms at 39.0 ppm, whereas the corresponding signal of **21** is at 66.4 ppm. The structural motif with two normally coordinated NHCs and two hydrides seems thermodynamically stable, as it is obtained from both complexes **18** and **7**, which originally have different coordination environments around the Ru center. Namely, starting from **18** hydride formation and NHC isomerization from abnormal to normal are sufficient to obtain **20**. In order to obtain **21** from **7**, the P-aNHC ligand has to undergo a more complex rearrangement.

Furthermore, a second independent molecule is included in the same single crystal of **21**, which shows an intramolecular C-H activated benzylic Me group. This C-H activated compound is present in a ratio of

about 15% within the single crystal. Presumably, the dihydride complex can activate the C-H bond at RT, yielding a six-membered Ru-C-N-C-C-C metallacycle. Additionally, one hydride is coordinated to the Ru center. Figure 28 shows an overlay of both molecular structures that were obtained by SC-XRD. In Figure 29, only the C-H activated species is depicted for clarity. The respective Mes substituents are shown in blue (**21**) and yellow (C-H activated) for clarity.
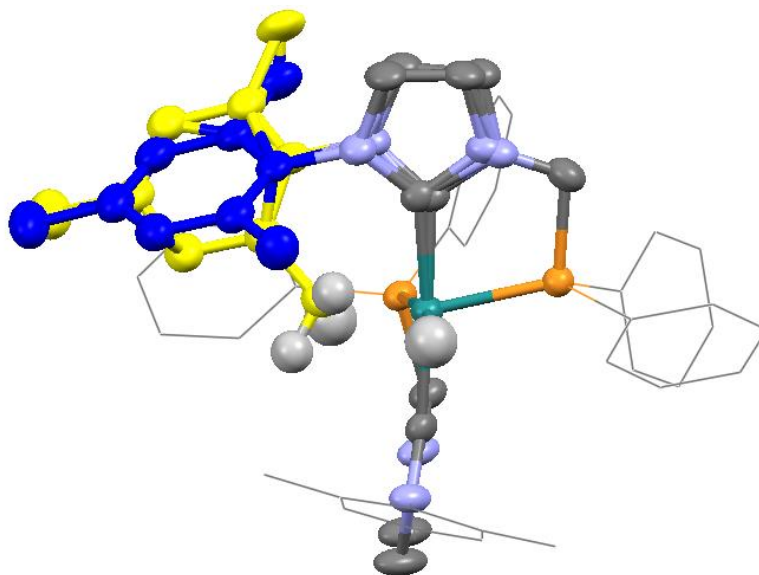
Figure 28: ORTEP-style presentation of the molecular structure of **21** including the second, C-H activated structure.
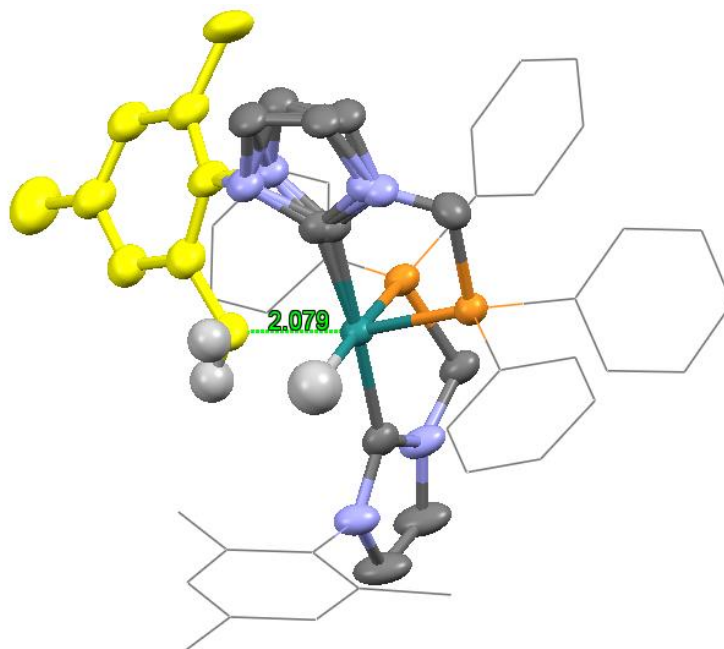
Figure 29: ORTEP-style presentation of the molecular structure of the C-H activated compound.

This species present in the solid state is also observed in solution in the ^{1}H NMR spectrum of **21** in toluene-d$_8$: a doublet of doublets at δ = -7.56 ppm ($^2J_{HPcis}$ = 32.7 Hz and $^2J_{HPtrans}$ = 111.3 Hz) indicates a hydride species and five distinct Me groups indicate the absence of the C_2-symmetry. The resonance for the hydride accounts for one H atom and the five resonances for the methyl groups account for three protons each. The respective signals are shown in Figure 30, where the integrated peak areas are given relative to the dihydride resonance of **21**. One proton of the cyclometalated species, therefore, accounts to 0.18 integration units.
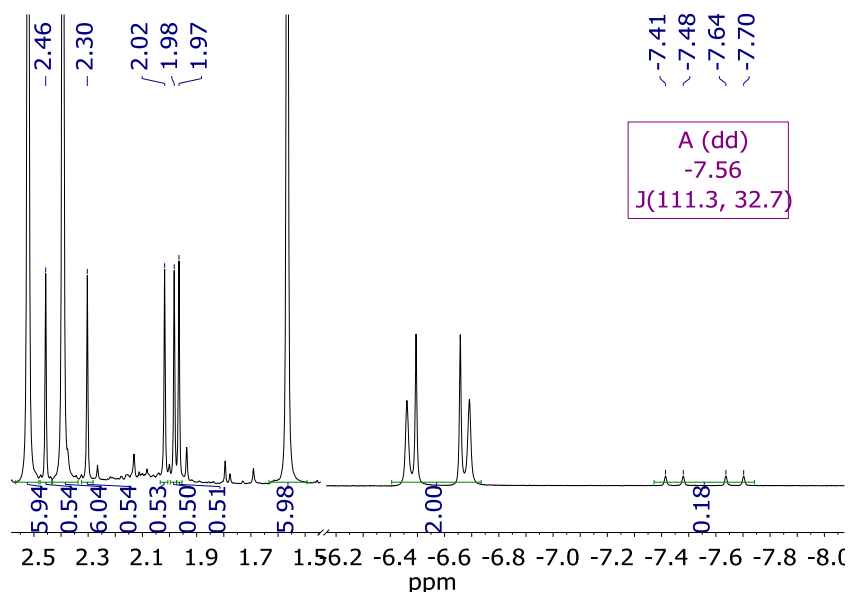
Figure 30: ^{1}H NMR spectrum in toluene-d$_8$ of **21** including the cyclometalated species.

As observed for **20**, **21** shows no catalytic activity in TH acetophenone under the usually applied reaction conditions. The Mes substituents in **21** also completely shield the hydrides from a potential substrate attack. Therefore, the rearrangement of the NHCs towards their normal coordination mode could generally represent a deactivation pathway for aNHC complexes.

7 shows a significantly lower activity in TH of acetophenone (TOF of 26 000 h^{-1}) with respect to **18** (TOF > 600 000 h^{-1}). This further indicates the importance of abnormal coordination, since **7** displays one aNHC and one normal NHC ligand. Thus, it is likely that the Mes substituent of the normal carbene partly impedes the substrate approach to the metal center, resulting in lower activity.

To quantitatively evaluate the influence of the different coordination modes on the steric accessibility of the reactive metal center, the buried volumes of compounds **18**, **20**, **7** and **21** for sphere radii of 3.5 Å and 5.0 Å, respectively, were determined by means of DFT calculations. The results are shown in Table 6 for **18** *versus* **20** and Table 7 for **7** *versus* **21**. The applied internal coordinates for the calculation are given. The steric maps demonstrate the steric shielding of the Ru center for both sphere radii. At a sphere radius of 3.5 Å, the buried volume of **18** is 79.9%, whereas for **20** it is 90.8%. At a sphere radius of 5.0 Å, the buried volume of **18** is only 70.6%, whereas for **20** it still is 88.6%. Compound **18**, therefore, is significantly more accessible than **20**, which is strongly pronounced for a sphere radius of 5 Å. The same trend was found for the complexes **7** and **21**. At a sphere radius of 3.5 Å, the buried volume of **7** is 79.7%, whereas for **21** it is 88.4%. At a sphere radius of 5.0 Å, the buried volume of **7** is 74.5%, whereas for **21** it is 85.2%. Compound **7**, showing good activity in TH, therefore, is significantly more accessible than **21**, which again is more strongly pronounced for a sphere radius of 5 Å. The buried volumes of **18** and **7** are similar at sphere radii of 3.5 Å. However, at sphere radii of 5.0 Å the buried volume of **7** is higher than for **18** and therefore the Ru center is slightly more shielded by the Mes and phenyl substituents. This might be one possible explanation for the higher activity in catalytic TH of **18** with respect to **7**.

Steric maps were calculated to visualize the surface of the interaction between the Ru center and the substrate, which is determined by the ligand environment. The different colors represent the distances along the *z*-axis at which the ligands start to occupy the coordination sphere of the Ru center. Thus, the steric maps clearly show that the ligands in **20** and **21** start to bury space already at a distance of 5 Å to the metal center, not allowing for substrate coordination. In contrast, complex **18** shows that the metal center is freely accessible. The steric maps further suggest that the cavity of **18** resembles a symmetric conus, while the cavity of **7** resembles an asymmetric cave that seems more difficult to get through. Therefore, also the asymmetry of the reaction cavity might contribute to an overall lower activity in catalytic TH of **7** with respect to **18**.

Table 6: Steric maps and buried volumes of **18** and **20** for sphere radii of 3.5 Å and 5.0 Å.
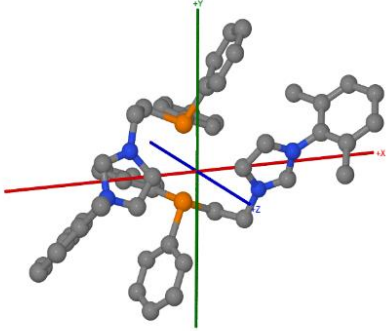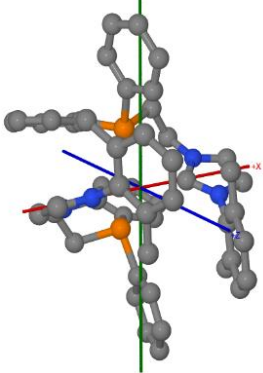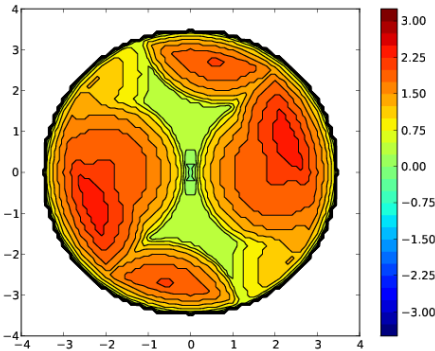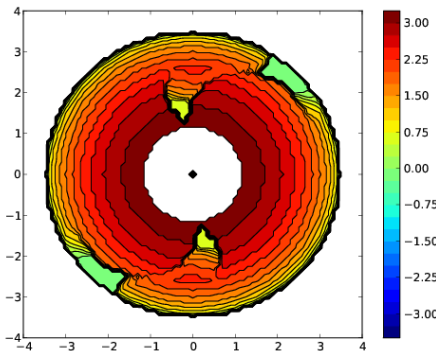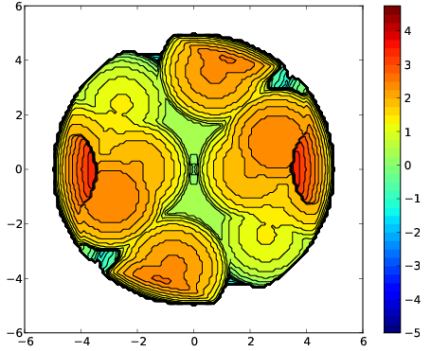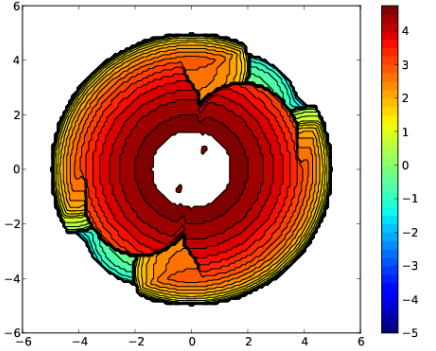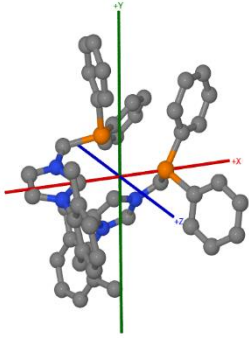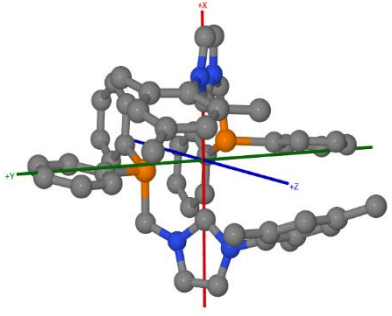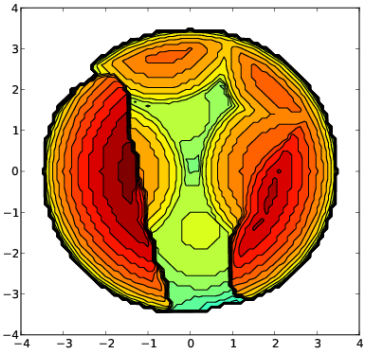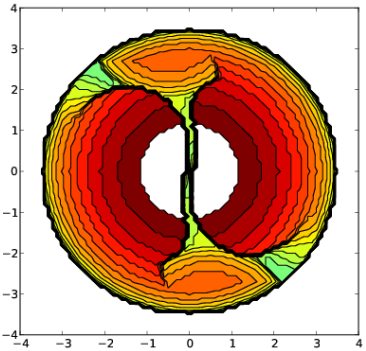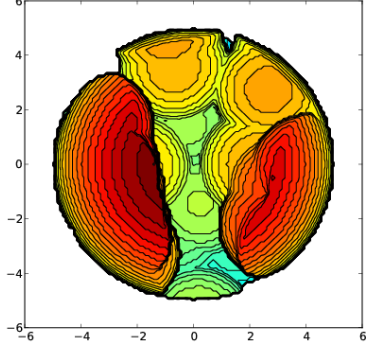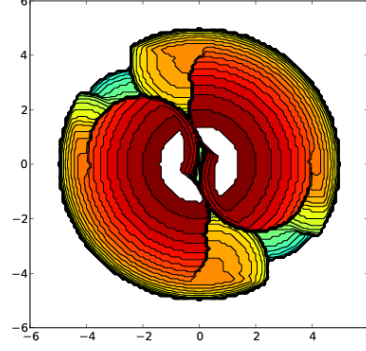
Compound	18	20
Internal Coorinate		
Steric Map r = 3.5 Å [Axis in Å]		
Buried Volume /%	79.9	90.8
Steric Map r = 5 Å [Axis in Å]		
Buried Volume /%	70.6	88.6

Table 7: Steric maps and buried volumes of **18** and **20** for sphere radii of 3.5 Å and 5.0 Å.

Compound	7	21
Internal Coorinate		
Steric Map r = 3.5 Å [Axis in Å]		
Buried Volume /%	79.7	88.4
Steric Map r = 5 Å [Axis in Å]		
Buried Volume /%	74.5	85.2

Although the dihydrides are both completely shielded by the Mes substituents on the NHCs, a longer reaction time (3 d) of **15** in ^{i}PrOH/NaO^{i}Pr *in-situ* leads to another symmetric species bearing two normal NHC ligands and with an acetate in place of the hydrides (Scheme 27). In ^{i}PrOH-d$_8$, **22** gives one singlet for two P-atoms in ^{31}P{^{1}H} NMR spectrum at δ = 71.8 ppm. However, **21** is not completely converted to **22** within weeks.
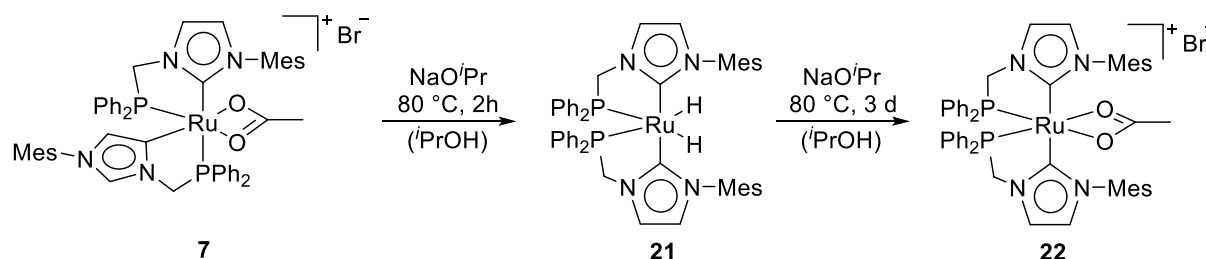
Scheme 27: Formation of **22** from **21** by extending the reaction time.

The formation of **22** could potentially be a consequence of two subsequent intramolecular C-H activations followed by the slow protonation of the benzylic positions by ^{i}PrOH. A reductive elimination of dihydrogen might not occur, since the oxidation state of the Ru(II) center does not change. **22** is a cationic complex with a bromide counter ion. Single crystals were obtained directly from the reaction mixture (Figure 31).
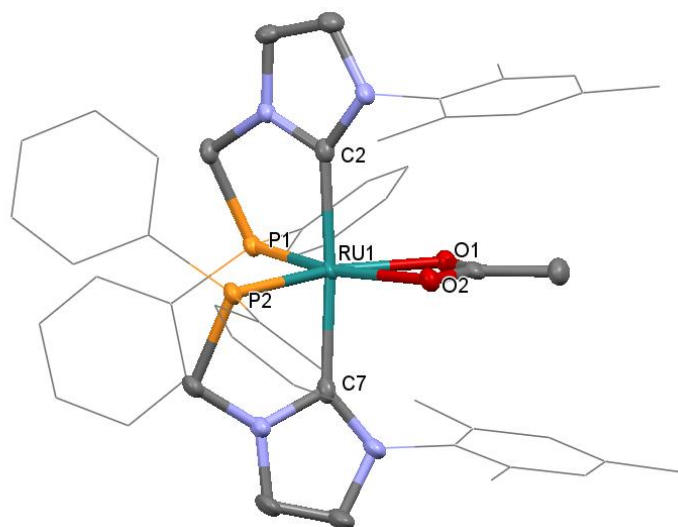
Figure 31: ORTEP-style presentation of the molecular structure of **22**. Thermal ellipsoids are shown at a 50% probability level. H atoms are omitted for clarity. Aromatic substituents are shown in the wireframe-style. Grey = C, blue = N, yellow = P, red = O, turquoise = Ru. Selected bond lengths (Å) and angles (°): Ru1-C7 2.094(4), Ru1-C2

2.089(4), Ru1-P1 2.2282(12), Ru1-P2 2.2237(12), C7-Ru1-C2 175.54(16), C2-Ru1-P1 79.29(12), C7-Ru1-P2 79.55(12), P1-Ru1-P2 92.35(4), O1-Ru1-O2 59.80(11).

The molecular structure of **22** confirms the formation of a di-NHC Ru complex with an acetate in equatorial position. The C2-Ru1-C7 angle (175.54(16) °) is close to the ideal 180 °. Both Ru-carbene distances (2.089(4) and 2.094(4) Å) are longer than in the hydride analogue **21**. The P1-Ru1-P2 angle (92.35(4) °) is smaller than in **21**. The Mes substituents are partially pushed away from the metal center by the steric strain of the equatorial acetate. They exhibit a nearly in-plane orientation with the equatorial ligands. The rotation of the Mes substituents might be completely blocked. In Figure 32 planes were calculated through the the Mes groups. The plane in the center is calculated for the five P, Ru and O atoms.
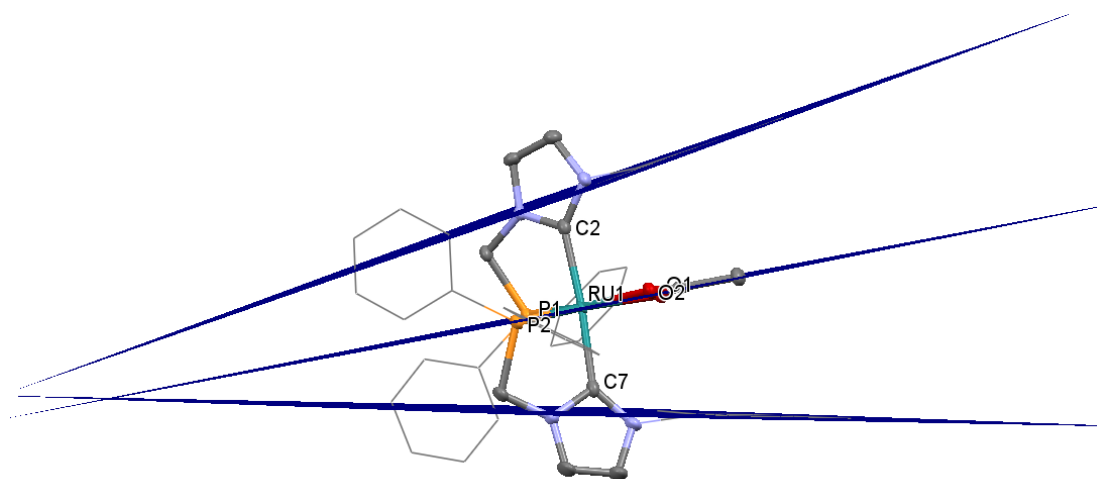
Figure 32: Visualization of the in-plane orientation of the Mes groups with respect to the equatorial plane of the distorted octahedron.

3.2.3.2 Potential Involvement of the Ligands – Bifunctional Mechanism

In catalytic TH, activities of 10^5 turnovers per hour or higher are usually only observed for catalysts bearing amine ligands and therefore following an outer-sphere mechanism.[82] A potential involvement of the ligands in catalytic TH according to bifunctional catalysis with **18** as the catalyst will be discussed in the following paragraph.

According to the molecular structure of **18**, the backbone protons of the aNHC ligands directly point towards the reactive center. Therefore, one could assume that they would potentially be involved in the reaction mechanism and act as intramolecular proton reservoir. If that was true, the respective protons should undergo deprotonation/protonation processes under catalytic conditions. Therefore, they should be exchanged with deuterium if reacted with a high excess of ^{i}PrOH-d$_8$/NaO^{i}Pr-d$_7$ at elevated temperatures. The corresponding signal in the ^{1}H NMR should therefore disappear. However, the signal for the backbone protons is untouched, and the integrated peak area does not change. Thus, a direct involvement of the backbone protons is very unlikely. ^{1}H and ^{31}P{^{1}H} NMR experiments in ^{i}PrOH-d$_8$ reveal that **18** is stable at elevated temperatures. After addition of NaO^{i}Pr (2 eq) the NC*H*N protons of the NHCs are immediately in exchange with deuterium and the NC*H*N signal in the ^{1}H NMR spectrum disappears. The ^{31}P{^{1}H} NMR spectrum, however, remains unchanged which confirms the stability of **18** also under basic conditions. When the complex is heated to 80 °C for 20 min, the ^{31}P{^{1}H} NMR spectrum still shows one singlet peak, however, up-field shifted by $\Delta\delta$ = 0.55 ppm. In the ^{1}H NMR spectrum, the signals for the alkylic protons and the alkyl bridges remain unchanged. In the aromatic region, however, the signals corresponding to the *ortho*-protons of the phenyl substituents of the phosphane ligands disappear, while the integrated peak areas of *meta*-, *para*-protons and the Mes protons are not affected. The multiplicity of the signals corresponding to the *meta*-protons in the ^{1}H NMR spectrum changes from a triplet to a doublet. This hints towards a selective deuteration of all *ortho*-positions of the phenyls. Thus, the slight up-field shift in the ^{31}P{^{1}H} NMR spectrum might also result from deuteration at the relatively near *ortho*-positions.

VT-NMR experiments reveal that with 5 eq of NaO^{i}Pr in ^{i}PrOH-d$_8$ the deuteration of **18** at the phenyl groups slowly starts at 50 °C and proceeds fast at higher temperatures (Figure 33). When the deuterated solvent is evaporated, and the residue is stirred in non-deuterated ^{i}PrOH at 80 °C, the signals of the *ortho*-protons again re-appear, confirming a simple deuteration/protonation process at these positions, while the overall complex is still stable. The Mes substituents might start to rotate, as the aromatic signals and the *ortho*-methyl signals are broadened at elevated temperatures and appear as sharp signals when cooled to RT again. Since the *ortho*-protons of the phenyl groups are exchangeable under catalysis conditions, the *ortho*-protons of the phenyl groups could potentially be involved in the catalytic mechanism, while the overall structure of the complex remains unchanged.

25 °C after stirring in iPrOH at 80 °C

25 °C (r.t.) after VT-NMR studies

80 °C

70 °C

60 °C

50 °C

40 °C

30 °C
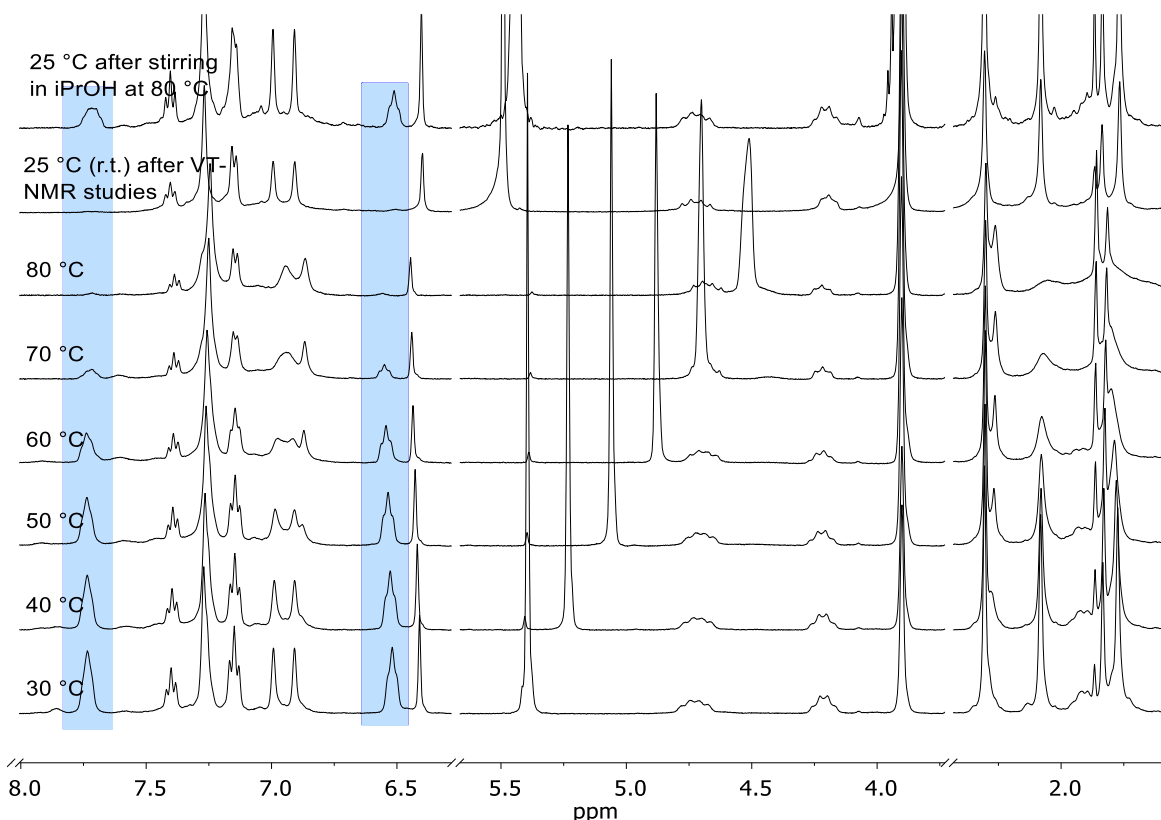
Figure 33: ^{1}H VT-NMR study of **18** in *i*PrOH with 5 eq NaO*i*Pr.

The acetate is the weakest ligand in **18** and should therefore readily be replaced by an alkoxide. However, the signal for the acetate moiety does not change during the VT experiments. At least temporary alkoxide coordination and hydride formation are necessary though for catalytic transformations. Thus, the alkoxide/hydride species might be highly reactive and in a formal equilibrium with **18**. A metal-hydride itself might not deprotonate the *ortho*-position of the phenyl substituents as there is no peak observed for dihydrogen, which would be generated upon formal hydride-proton combination.

Possibly, an alkoxide coordinated to metal center might deprotonate the phenyl substituent and leave the active center as an alcohol (Scheme 28). In a next step, the proton would be abstracted by the *i*PrO⁻ over a transition state were the respective proton is partly bound to both, the *i*PrO⁻ and the phenyl. When the proton is bound to the O, *i*PrOH can easily leave the inner coordination sphere. DFT calculations confirm that the resulting *ortho*-deprotonated phenyl is stabilized by donation of electron density to the metal center forming cyclometalated species. The acetate is used as a dummy ligand that occupies the free coordination site. Therefore, the presented species might be stable enough to occur during the catalytic reaction mechanism. The optimized molecular structure of the cyclometalated species is depicted in Figure 34. The *para*-Me groups of the Mes substituent are removed to facilitate

convergence. Further DFT calculations will focus on the pathway for the deprotonation of the *ortho*-positions of the phenyl groups.
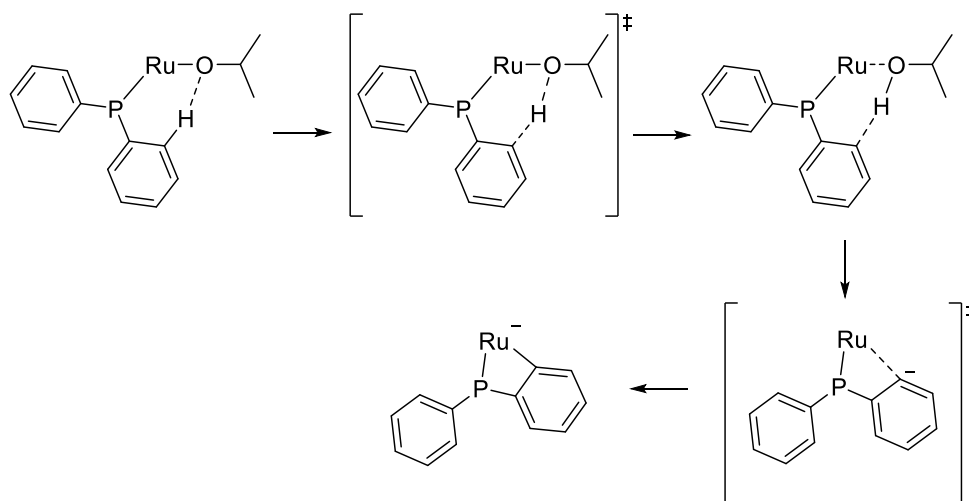
Scheme 28: Potential deprotonation mechanism at the *ortho*-positions of the phenyl substituents.
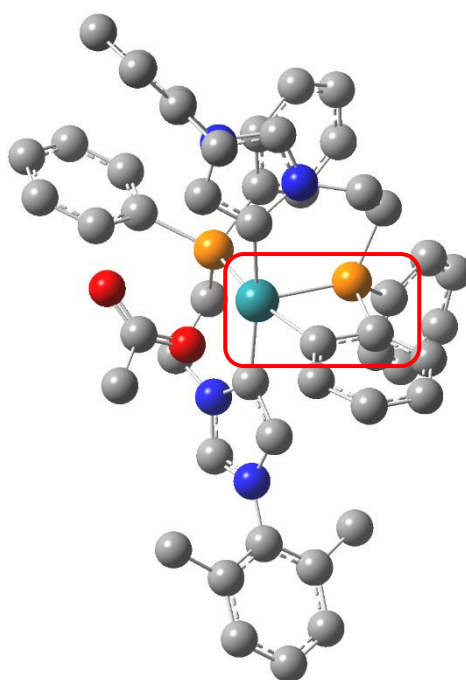
Figure 34: DFT optimized molecular structure of the cyclometalated species (highlighted in red) that stabilizes the complex after deprotonation at the *ortho* position of the phenyl substituents.

If this mechanism applies for the deprotonation of **18** at the *ortho*-positions of the phenyls, now the complex would be activated to perform a bifunctional catalysis (Scheme 29). Upon coordination of the alcohol substrate, the negatively charged *ortho*-position could deprotonate the hydroxy group. According to a β-H-elimination, a metal hydride could be formed, and the ketone could leave the coordination sphere. The other ketone substrate could than coordinate to the metal, the hydride could

be transferred and the upon leaving the coordination sphere it could again deprotonate the *ortho*-position. This mechanism will also be investigated by means of DFT calculations.
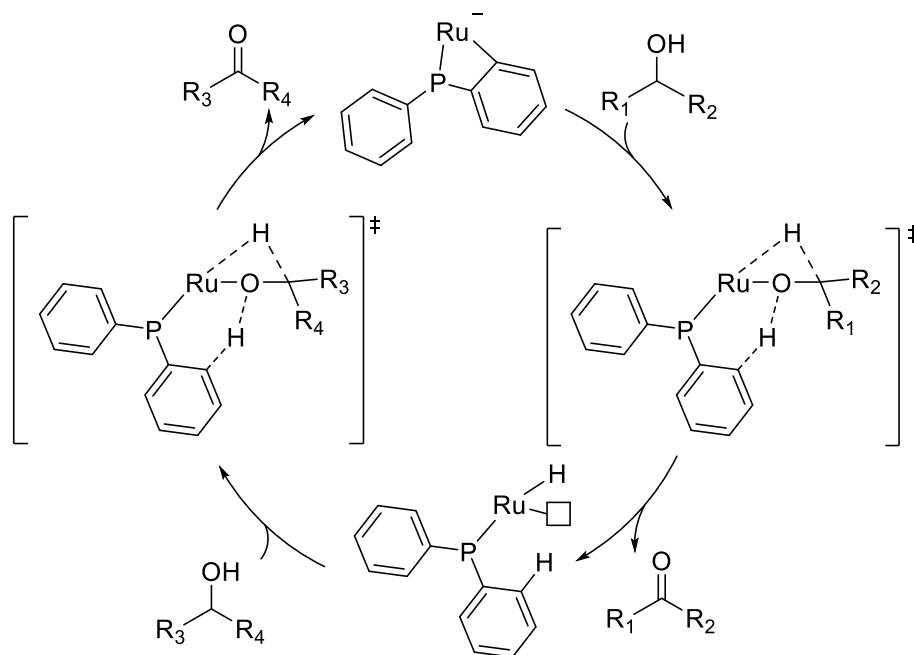
Scheme 29: Possible bifunctional reaction mechanism for catalytic TH and Oppenauer-type oxidation.

Since only four out of eight *ortho*-protons of **18** are potentially close to the metal center, proton transfer from one phenyl to the other is assumed. According to the rotation of the phenyls, the *ortho* carbons might get close enough to directly transfer a proton from the *ortho* C-H to the *ortho* carbanion. Otherwise, the phosphane groups would have to dissociate, rotate and re-coordinate, which would not be in line with the high stability of **18**. A direct deprotonation by a base might not take place, since the pK$_A$-values of *ortho-* vs. *para*-protons might be comparable. DFT calculations focusing on the scrambling pathway are ongoing.

The analogous deuteration experiment was performed with complex **7** to investigate, if the same mechanism could apply as well. Therefore, **7** was reacted with NaO^{i}Pr (5 eq) in ^{i}PrOH-d$_8$ at 80 °C for 20 min (Figure 35).
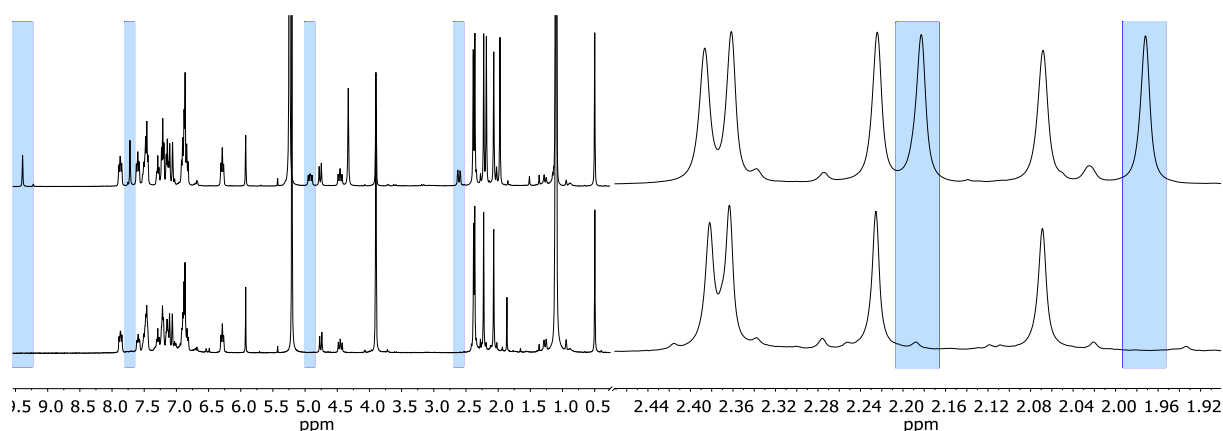
Figure 35: Whole ^{1}H NMR spectrum (left) and alkylic region (right) of **7** in ^{i}PrOH-d$_8$ before base addition (top) and after base addition and heating to 80 °C (bottom). Disappearing signals are highlighted with blue rectangles.

The integrated peak area of the signal of the NC*H*N proton of **7** in ^{i}PrOH-d$_8$ corresponds to less than one proton. Thus, the NC*H*N proton of **7** is already in a slow exchange with deuterium before base addition. After base addition, the resonance for the NC*H*N proton completely disappears. Also, the resonance at 7.72 ppm, which is assigned to the backbone proton of the aNHC, is not observed in the presence of NaO^{i}Pr. Therefore, the protons of the aNHC of **7** might exhibit overall lower pK$_A$ values than in **18**. Furthermore, two signals for two diastereotopic C$_1$-backbone protons vanish under basic conditions. In this regard, Sortais *et al.* applied this type of ligands for the hydrogenation of ketones on Mn, in which the non-innocent ligand is deprotonated at the C located between the P and N, leading to an NHC-phosphanomethanide complex, as reservoir for an unconventional 16-e NHC phosphonium.[144] This could represent a potential pathway to towards the deuteration of the C$_1$-backbone. In contrast to **18**, the deuteration at **7** does not occur at the phenyl substituents but at the *ortho*-Me groups of one Mes substituent. The alkylic region of the ^{1}H NMR is depicted in Figure 35. The benzylic C-H activation might be involved in this deuteration process. In summary, the suggested mechanism for **18** might not apply for **7**, since the aromatic protons are not accessible under these conditions, which is in line with the significantly different activities in TH of acetophenone.

3.2.4 Conclusion

The di-aNHC-phosphane Ru complex **18** is a highly efficient catalyst for TH and Oppenauer-type oxidation reactions with several substrates. Best results in Oppenauer-type oxidation were obtained when the reactions were performed neat with only small amounts of acetone as oxidizing agent. The TOF of **18** with α-tetralol as the substrate is 550 000 h^{-1} and therefore the highest measured rate so far for this reaction. Furthermore, this reaction protocol is highly interesting for synthetic chemistry, as no solvent and only small amounts of oxidant are used. Also, in catalytic TH, **18** is among the most active systems known to date and the most active NHC Ru catalyst reported. By conversion of **18** with ^{i}PrOH/NaO^{i}Pr the formation of dihydride species under catalytic conditions was observed. The stable dihydride Ru complexes **20** and **21**, both bearing NHC ligands in their normal coordination mode, were isolated. DFT calculations of the buried volume of **7**, **18**, **20** and **21** reveal that the Mes substituents shield the reactive metal center if the NHCs coordinate in their normal mode. **20** and **21** are therefore not active in TH catalysis and the formation of the species **20** and **21** could represent catalyst deactivation mechanism. NMR experiments suggest an involvement of the *ortho*-protons of the phenyl substituents in the catalytic mechanism, because they are selectively exchanged with deuterium under catalysis conditions. The proposed bifunctional reaction mechanism could potentially explain the extraordinarily high activities of **18**. This bifunctional mechanism involving the *ortho*-protons of the phenyl substituents might not apply for **7**, because the aromatic protons are not exchanged with deuterium in this case, which is in line with a lower activity in TH catalysis.

3.3 Synthesis of aNHC-Amine Ru Complexes

In this chapter, unpublished and preliminary results will be presented.

Analogous to the phosphane functionalized imidazolium ligand precursors, amine functionalized ligand precursors could be suitable for the synthesis bidentate aNHC Ru complexes. The amine functionality herein could induce a bifunctional mechanism according to the previously mentioned NH-effect. Such ligand precursors are available for example by reaction of **1** with 2-Bromoethylamine hydrobromide salt (Scheme 30).
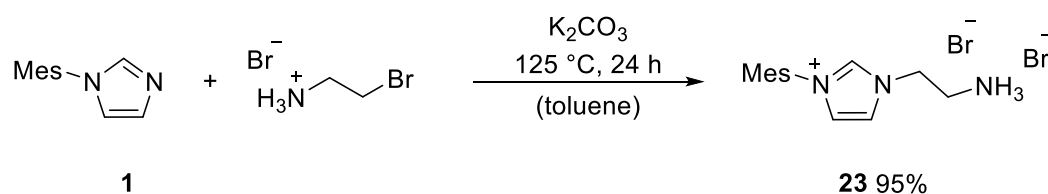
Scheme 30: Synthesis of **23**.

A similar reaction is reported in literature[145], however, significantly higher yields (95% vs. 60% in lit.) are obtained, when the reaction is performed in toluene and the product is purified by precipitation from DMF with Et_2O. Although the reaction is performed in the presence of a base, the product is dicationic, as inferred from elemental analysis. Therefore, a base will be necessary to obtain bidentate coordination of **23** to the Ru center. Like the synthesis of **6**, **23** was reacted with **5** in presence of soft bases (Scheme 31).
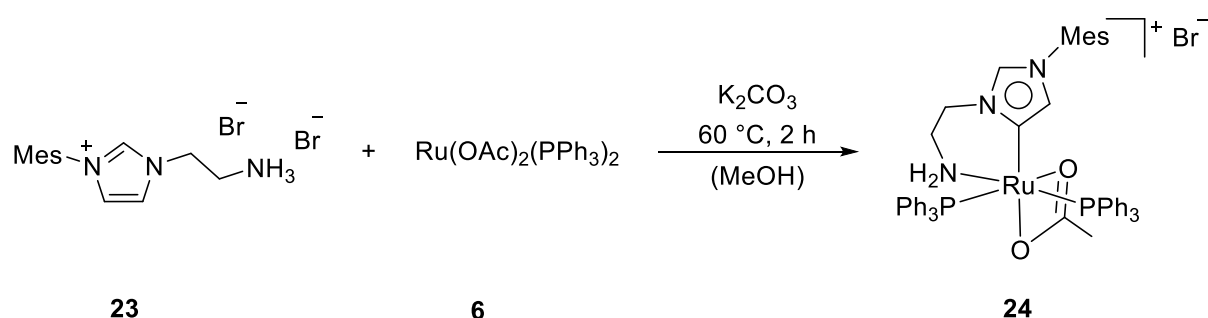
Scheme 31: Synthesis of **24**.

According ^{1}H NMR spectroscopy, **24** bears one chelating aNHC-amine, a bidentate acetate and two PPh_3 ligands. The resonance at $\delta = 9.05$ ppm is assigned to the NC*H*N proton of the aNHC and the strong down-field shift is in accordance with the presence of a cationic complex. The integrated peak area in the aromatic region accounts to 32 protons, which is in accordance with two PPh_3 groups and one Mes

substituent. The backbone proton of the aNHC is at 5.28 ppm, which is in comparably high field. In $^{31}P\{^{1}H\}$ NMR spectrum, two signals as doublets at 56.1 ppm and 52.6 ppm for the for two P atoms adjacent to the Ru center are observed. The coupling constant of $^{2}J_{PP}$ = 32.8 Hz indicates their *cis* coordination.

Therefore, in contrast to **13**, no PPh$_3$ was replaced upon introduction of **23**. This reaction was carried out various combinations of solvents and bases. In THF and DCM for example, only decomposition products were obtained. Also, when MeOH is used as the solvent, only K$_2$CO$_3$ leads to the formation of **24**, whereas the application of NaOAc or KO^{t}Bu only leads to decomposition. However, **24** can also be obtained in ^{t}BuOH as the solvent with NaOAc as the base. Single crystals suitable for SC-XRD spectroscopy were obtained by layering a solution in DCM with *n*-pentane (Figure 36).
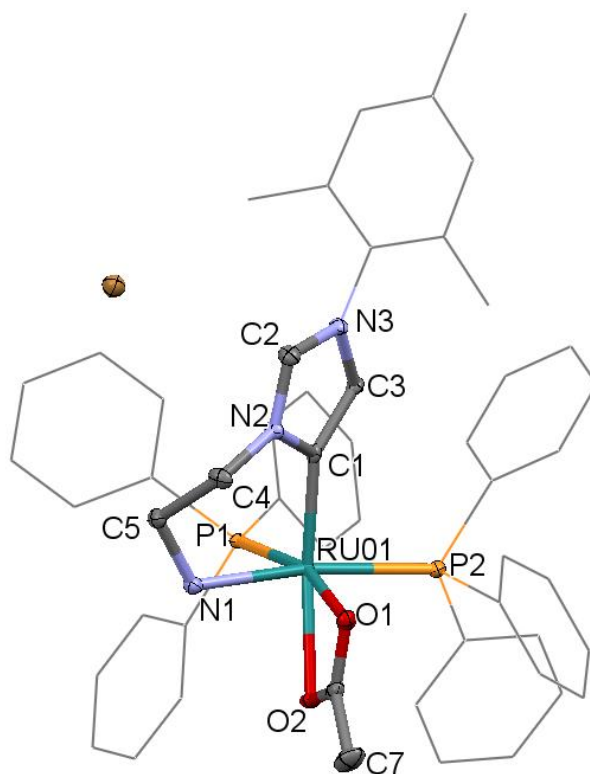
Figure 36: ORTEP-style presentation of the molecular structure of **23**. Thermal ellipsoids are shown at a 50% probability level. H atoms and solvent molecules are omitted for clarity. Aromatic substituents are shown in the wireframe-style for clarity. Grey = C, blue = N, yellow = P, red = O, brown = Br, turquoise = Ru.

The molecular structure of **24** confirms the coordination of one bidentate aNHC-amine, an acetate and two PPh$_3$ ligands to the Ru center in a distorted octahedral coordination geometry. The Ru1-C1 distance is 2.0318(19) Å and the Ru1-P1 and Ru1-P2 distances are 2.2638(5) Å and 2.3124(6) Å, respectively. The C1-Ru1-O2 is 156.12(7) ° which highlights the distortion of the octahedral coordination sphere, being far from the ideal 180 °.

Thus, **24** exhibits two PPh$_3$ moieties that allow for further modification of the complex. In order to render it more stable, a bidentate phosphane was applied to replace the PPh$_3$ groups. For this purpose, a Ru precursor was used that displays two acetate and a bidentate 1,4-bis(diphenylphosphano) butane ligand (Scheme 32).
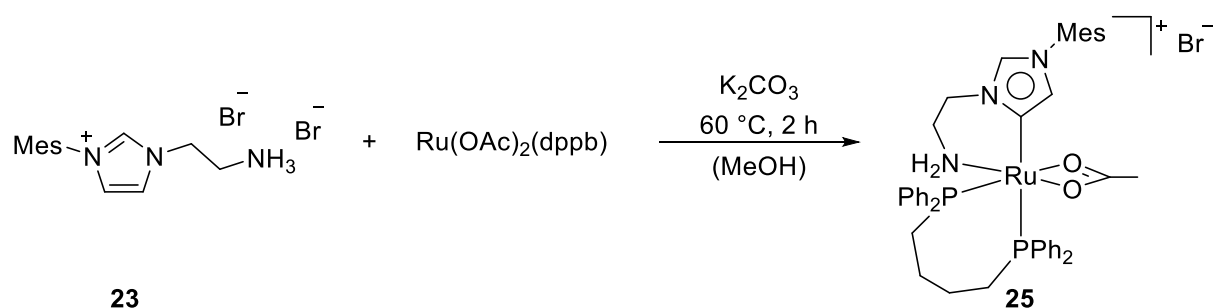
Scheme 32: Synthesis of **25**.

25 exhibits two resonances at 58.2 ppm and 54.1 ppm in the ^{31}P{^{1}H} NMR spectrum with coupling constants of $^2J_{PP}$ = 37.6 Hz. The resonance at 9.16 ppm in the ^{1}H NMR spectrum is assigned to the NC*H*N proton of the aNHC and therefore at slightly lower field than in **24**.

The relatively easy introduction of chelating diphosphane ligands as shown for **25** vs. **24** might allow for the introduction of chiral diphosphane ligands like BINAP. This could be a pathway towards asymmetric TH reactions and/or the kinetic resolution of alcohols by stereoselective oxidation of a racemic alcohol.

4. Conclusion and Outlook

In the course of this work, a general route towards heterobimetallic NHDC complexes was elaborated. The transformation of the neutral aNHC Ru complex **13** towards a cationic aNHC Ru complex **7** induced the desired reactivity towards Ag_2O to form a heterobimetallic Ag-Ru NHDC complex. The reactivity of the aNHC precursor complexes is directly related to the chemical shift of the NC*H*N proton of the aNHC ligands. Namely, a strong down-field chemical shift in the ^{1}H NMR spectra of around δ = 10 ppm, which is close to the NC*H*N chemical shift of imidazolium salts, indicates the favored reactivity towards metalation reagents. All complexes were characterized by SC-XRD, in addition to NMR spectroscopic and mass spectrometric methods and elemental analysis. The redox properties of the heterobimetallic complexes were investigated by voltammetry experiments and electronic interactions between the metal centers could be found. The combination of two transition metals with similar catalytic properties like Ir and Ru, however, did not lead to an overall higher catalytic activity of the Ru-Ir complexes **17** and **9** with respect to the monometallic aNHC complexes **14** and **7** and therefore, no indications for cooperative effects of the metals were found.

In the course of this work, the first di-aNHC Ru complex **18** was synthesized. **18** is the most active NHC Ru catalyst in TH of ketones reaching TOFs up to $1.3 \cdot 10^6$ h^{-1}. Furthermore, **18** is the most active Ru catalyst in the Oppenauer-type oxidation of alcohols reaching unprecedented TOFs up to $5.5 \cdot 10^5$ h^{-1}. A potential deactivation mechanism for **18** and **7** involving an NHC isomerization step towards their normal coordination mode was identified. Namely, two catalytically inactive dihydride species were isolated displaying two normally coordinated NHCs. The steric bulk of the Mes groups shield the reactive center from substrate approach, as confirmed by DFT calculations of the buried volumes. These mechanistic investigations on complex **18** could further explain the higher stability of the heterobimetallic species **17** compared to the mononuclear precursor complex **14**. For instance, an isomerization of the NHCs towards their normal coordination mode is not possible due the protection of the NCN position. Therefore, the proposed deactivation mechanism cannot be applied.

According to NMR spectroscopy and DFT calculational studies, the *ortho*-protons of the phenyl substituents are accessible under catalytic reaction conditions. In this regard, a bifunctional reaction mechanism was proposed, where the substrates undergo a simultaneous hydride and proton transfer in the inner coordination sphere. The proposed reaction mechanism might not apply for **7**, as the corresponding aromatic protons are not accessible under catalytic conditions. To get experimental data to confirm the proposed reaction mechanism a series of similar complexes should be synthesized that either shows substituents that enhance or decrease the reaction rates. For this purpose, a complex with CF_3 groups in the *para*-position of the phenyl groups could be synthesized. The electron withdrawing

substituent should lead to a more acidic *ortho*-proton and therefore enhance the reaction rate. On the other hand, a methoxy group would decelerate the reaction (Figure 37).
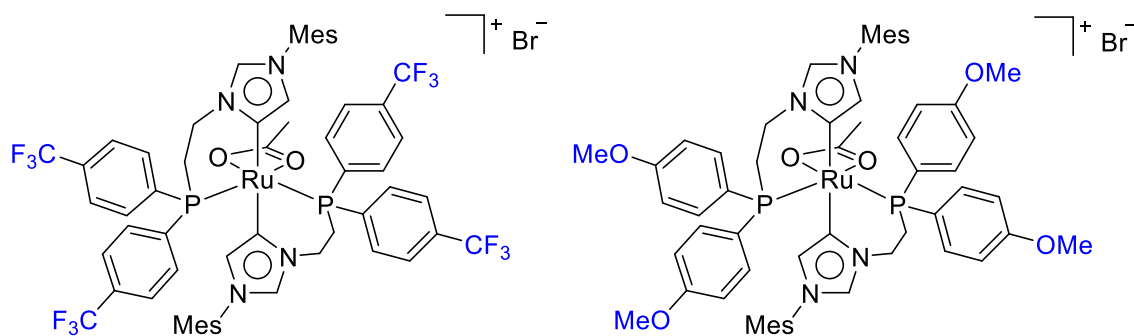
Figure 37: Introduction of potentially activating CF₃ (left) and deactivating OMe (right) groups.

To prevent the catalyst deactivation by normal coordination of the NHC ligands, the N*C*N position could be protected with a methyl group (Figure 38, red). Alternatively, the bulky Mes substituents, which are responsible for the abnormal coordination of NHCs, could be replaced by slightly more sterically demanding 2,6-diisopropylphenyl (DIPP) groups (Figure 38, blue). These substituents might sterically prevent *trans*-standing aNHC ligands to change into their normal coordination mode according to their steric repulsion even without the acetate ligand standing in between. Application of bulkier DIPP substituents could also allow for the synthesis of di-aNHC Ru complexes with a C_1 backbone (Figure 38, green) between the N and P atoms. In consequence, the steric bulkiness in front of the Ru center due to the normal NHC in complex **7** would be eliminated. This would allow further insight into the influence of the length of the alkyl bridge on the catalytic activity of the complexes.
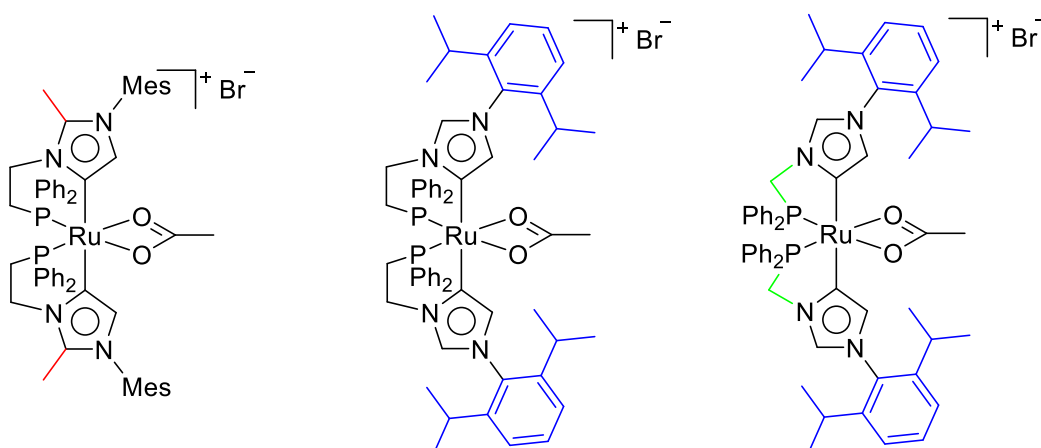
Figure 38: Protection of the catalyst from deactivation by NHC isomerization and a novel envisioned di-aNHC complex.

To compare the influence of abnormal coordination *versus* normal coordination, a small wingtip substituent like a methyl group (Figure 39, blue) could be used instead of the Mes and the DIPP. Abnormal coordination could then be obtained by protection of the N*C*N position with a methyl group

(Figure 39, red), while the unprotected NHC would presumably coordinate in its normal mode to the metal center.
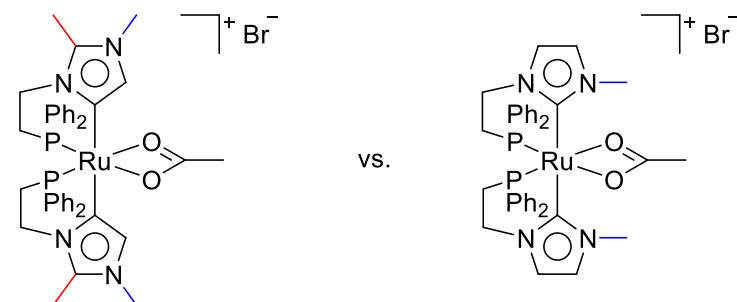
Figure 39: Abnormal vs. normal coordination mode of NHCs.

Finally, an aNHC-amine Ru complex **23** was isolated that exhibits two phosphane ligands. This complex is highly sensitive against oxygen and steadily decomposes in halogenated solvents. By introduction of bidentate phosphanes, more stable derivatives could be obtained. For this purpose, even chiral bis-phosphane ligands could be applied to obtain chiral aNHC complexes with an amine functionality for bifunctional asymmetric TH catalysis (Scheme 33).
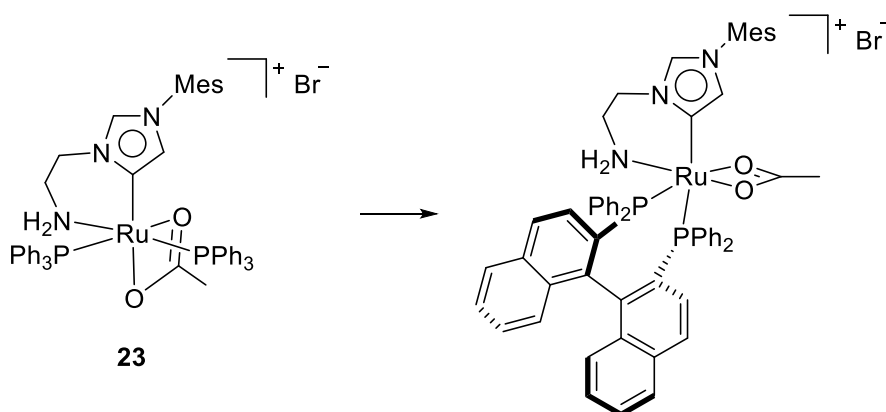
Scheme 33: Introduction of chiral diphosphane ligands into aNHC-amine Ru complexes.

5. Experimental Section

5.1 General Aspects

Unless otherwise specified, all reactions were performed under dry, O_2 free conditions in an argon atmosphere using standard *Schlenk* and glovebox techniques. The solvents were purified, degassed (freeze-pump-thaw) and dried according to standard purification techniques[146] or obtained from a M. Braun SPS purification system. Unless otherwise specified, all other chemicals were purchased from commercial sources and used without further purification. NMR spectra were recorded on a Bruker Avance Ultrashield 400 MHz and a Bruker DPX 400 MHz spectrometer. All ^1H and $^{13}C\{^1H\}$ chemical shifts are reported in parts per million (ppm) relative to TMS, with the residual solvent peak serving as internal reference. $^{31}P\{^1H\}$ NMR spectra are referenced to 85% H_3PO_4. Single crystals were measured in the SC-XRD laboratory of the Catalysis Research Center at the Technical University of Munich. FAB mass spectrometry was carried out using a Finnigan MAT 90 and ESI mass spectra were acquired on a Thermo Scientific LCG Fleet. LIFDI mass spectrometry was detected with a Waters LCT. The special ionization cell was obtained from Linden CMS GmbH, Leeste, Germany. GC analysis was done with an Agilent Technologies 7890B GC system using an Agilent VF-200ms column (30 m × 250 μm × 0.25μm). Elemental CHN analyses were carried out in the microanalytical laboratory of the Catalysis Research Center at the Technical University of Munich. Cyclic voltammograms and differential pulse voltammograms were recorded using a Metrohm Autolab potentiostat employing three-electrode cell under an argon atmosphere. A glassy carbon electrode was used as the working electrode and polished before each measurement. A graphite electrode was used as the counter electrode. The potential was measured against Ag/AgCl (3.4 M KCl, 0.200 V vs. NHE) with a scan rate of 100 mV/s. (nBu$_4$N)PF$_6$ (0.1 M) in DCM) was used as electrolyte.

5.2 Synthetic Procedures

5.2.1 Synthesis of 1
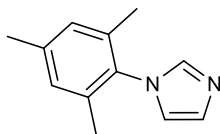
Chemical Formula: $C_{12}H_{14}N_2$
Molecular Weight: 186,26 g mol^{-1}

Aqueous formaldehyde (13.8 mL, 37%, 185 mmol, 1.00 eq) and aqueous oxalaldehyde solution (21.3 mL, 40%, 185 mmol, 1.00 eq) are mixed with saturated HOAc (45 mL) and heated up to 60 °C. 2,4,6-trimethylaniline (26.0 mL, 185 mmol, 1.00 eq) and ammonium acetate (14.3 g, 185 mmol, 1.00 eq) are dissolved in saturated HOAc (45 mL) and H_2O (10 mL) in a separate flask. This latter solution is added dropwise to the formaldehyde solution at 60 °C and is stirred over night at 60 °C. After cooling to RT, the reaction mixture is added to a saturated solution of $NaHCO_3$ in H_2O (1.5 L). The precipitated brown solid is isolated *via* filtration, dried in vacuo and purified by re-sublimation at 200 °C and 10^{-3} mbar. **1** is obtained as a colorless, crystalline solid in 85% (29.3 g) yield.

^{1}H-NMR: (400 MHz, DMSO-d$_6$, 297 K): δ (ppm) = 7.67 (s, 1H, NC*H*N), 7.19 (s, 1H, NCC*H*N), 7.13 (s, 1H, NC*H*CN), 7.04 (s, 2H, Ar-H), 2.29 (s, 3H, *p*-Me$_{Mes}$), 1.92 (s, 6H, *o*-Me$_{Mes}$).

5.2.2 Synthesis of **2**
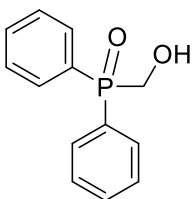
Chemical Formula: $C_{13}H_{13}O_2P$
Molecular Weight: 232,22 g mol^{-1}

Chlorodiphenylphosphane (13.0 mL, 70.7 mmol, 1.00 eq) and formaldehyde (43.0 mL, 580 mmol, 8.15 eq) are dissolved in concentrated hydrochloric acid (160 mL). The reaction mixture is stirred at 100 °C over night. Removal of the solvent under reduced pressure yields a yellow oil which is neutralized to pH = 7 using saturated Solution of $NaHCO_3$ in H_2O. The aqueous solution is extracted with chloroform (2 · 500 mL) and, subsequently, the solvent is removed under reduced pressure. The residue is dissolved in benzene and precipitated by addition of *n*-hexane. The precipitant is isolated *via* centrifugation and dried under reduced pressure. **2** is obtained as a colorless solid in 51% (29.3 g) yield.

^{1}H NMR (400 MHz, CDCl$_3$, 297 K): δ (ppm) = 7.80 (m, 4H, Ar-H), 7.54 (m, 6H, Ar-H), 3.81 (s, ^3J = 5.73 Hz, 2H, PC*H$_2$*O).

^{31}P{^{1}H} NMR (162 MHz, CDCl$_3$, RT): δ (ppm) = 27.1 (s, 1P).

5.2.3 Synthesis of **3**
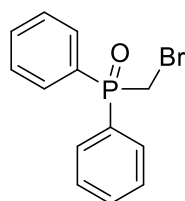
Chemical Formula: $C_{13}H_{12}BrOP$
Molecular Weight: 295,12 g mol^{-1}

2 (8.37 g, 36.0 mmol, 1.00 eq) are dissolved in DCM (67.0 mL) and cooled to 0 °C. Thionylbromide (6.99 mL, 90.1 mmol, 2.50 eq) is added dropwise to the mixture. Subsequently the reaction mixture is heated up to RT and stirred at RT overnight. The solvent is removed under reduced pressure and water (40 mL) is added to the mixture at 0 °C. The resulting aqueous solution is extracted with DCM (2 · 100 mL) and the combined organic phases are washed with a saturated NaHCO$_3$ solution (1 · 70.0 mL). The solvent is removed under reduced pressure. The crude product is recrystallized from EtOAc. The obtained solid are purified by column chromatography (EtOAc), the solvent is removed under reduced pressure. **3** is obtained as a off-white solid in 31.9% (3.39 g) yield.

^{1}H NMR (400 MHz, CDCl$_3$, 297 K): δ (ppm) = 7.79 (m, 4H, Ar-H), 7.53 (m, 6H, Ar-H), 3.81 (d, ^3J = 5.77, 2H, C*H*$_2$Br).

^{31}P{^{1}H} NMR (162 MHz, CDCl$_3$, RT): δ (ppm) = 27.3 (s, 1P).

5.2.4 Synthesis of **4**
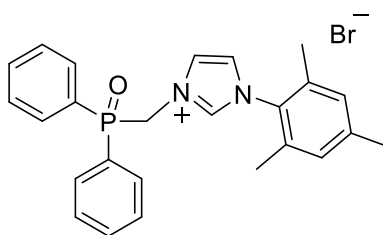
Chemical Formula: $C_{25}H_{26}BrN_2OP$
Molecular Weight: 481,37 g mol^{-1}

3 (3.39 g, 11.5 mmol, 1.00 eq) and **1** (3.21 g, 17.2 mmol, 1.50 eq) are mixed in a thick-walled glass reactor without additional solvent. The mixture is stirred at 140 °C for 6 d. After the mixture cooled down to RT, DCM (20 mL) is added. Et$_2$O is added under vigorous stirring until a yellow solid precipitated from the mixture. The precipitant is isolated, dried under reduced pressure, dissolved in acetonitrile (10 mL) and reprecipitated by adding Et$_2$O. The precipitant is isolated and dried under reduced pressure. **4** is obtained as a colorless solid in 80% (4.42 g) yield.

^{1}H NMR (400 MHz, CDCl$_3$, 297 K): δ (ppm) = 10.20 (t, ^4J = 1.8 Hz, 1H, NC*H*N), 8.24 (m, 4H, Ar-H), 8.11 (*pseudo*-t, $^3J = {}^4J$ = 1.8 Hz, 1H, NC*H*C*H*N), 7.54 (m, 6H, Ar-H), 6.97 (*pseudo*-t, $^3J = {}^4J$ = 1.8 Hz, 1H, NC*H*C*H*N), 6.92 (s, 2H, Ar-H$_{Mes}$), 6.18 (d, $^2J_{HP}$ = 6.4 Hz, 2H, NC*H$_2$*P), 2.31 (s, 3H, *p*-Me$_{Mes}$), 1.69 (s, 6H, *o*-Me$_{Mes}$).

^{31}P{^{1}H} NMR (162 MHz, CDCl$_3$, RT): δ (ppm) = 27.5 (s, 1P).

5.2.5 Synthesis of **5**
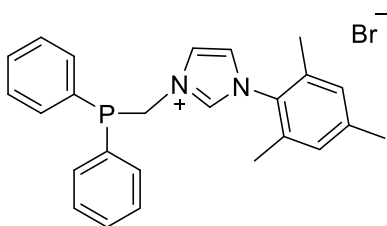
Chemical Formula: $C_{25}H_{26}BrN_2P$
Molecular Weight: 465,37 g mol^{-1}

4 (300 mg, 623 µmol, 1.00 eq) is dissolved in chlorobenzene (5 mL). Trichlorosilane (375 µL, 3.74 mmol, 6.00 eq) are added and the reaction mixture is stirred at 120 °C for 2 h. After cooling down to RT, DCM (4.00 mL) are added before dropwise addition of NaOH (7 mL, 10%). The aqueous phase is removed and extracted with DCM (2 · 12 mL) under argon. The combined organic phases are dried over MgSO$_4$, filtered and the solvent is removed under reduced pressure. The residue is dissolved in DCM (4 mL) and Et$_2$O (12 mL) are added for precipitation. The supernatant solution is removed, and the residue dried under reduced pressure. **5** is obtained as a colorless powder in 75% (226 mg) yield.

^{1}H-NMR (400 MHz, CDCl$_3$, 297 K): δ (ppm) = 10.40 (s, 1H, NC*H*N), 7.72 (m, 4H), 7.45 (*pseudo*-t, 1H, NC*H*C*H*N), 7.40 (m, 6H), 6.96 (*pseudo*-t, 1H, NC*H*C*H*N), 6.92 (s, 2H, Ar-H$_{Mes}$), 5.70 (d, 2H, NC*H*$_2$P), 2.30 (s, 3H, *p*-Me$_{Mes}$), 1.83 (s, 6H, *o*-Me$_{Mes}$).

^{13}C-NMR (101 MHz, CDCl$_3$, RT): δ (ppm) = 141.1 (s, N*C*N), 139.0 (s, Ar-C$_{Mes}$), 134.3 (s, Ar-C$_{Mes}$), 133.8 (d, $^{1}J_{CP}$ = 20.4 Hz, Ar-C), 132.7 (d, $^{2}J_{CP}$ = 11.5 Hz, Ar-C), 130.7 (s, Ar-C$_{Mes}$), 130.5 (s, Ar-C$_{Mes}$), 129.9 (s, N*CC*N), 129.4 (d, $^{3}J_{CP}$ = 7.7 Hz, Ar-C), 122.7 (s, N*CC*N), 122.5 (d, $^{4}J_{CP}$ = 5.2 Hz, Ar-C), 47.0 (t, N*C*P), 21.2 (s, *o*-Me$_{Mes}$), 17.5 (s, *p*-Me$_{Mes}$).

^{31}P{^{1}H} NMR (162 MHz, CDCl$_3$, RT): δ (ppm) = -11.2 (s, 1P).

5.2.6 Synthesis of **6**
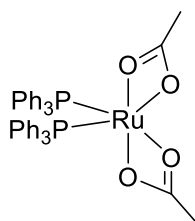
Chemical Formula: $C_{40}H_{36}O_4P_2Ru$
Molecular Weight: 743,74 g mol^{-1}

Tris(triphenylphosphano)Ru(II) dichloride (3.40 g, 3.55 mmol, 1.00 eq) and NaOAc · 3H$_2$O (4.83 g, 35.5 mmol, 10.0 eq) are suspended in degassed *tert*-butyl alcohol (110 mL) and stirred under reflux (83 °C) for 12 h. The work-up is performed under atmospheric conditions. The precipitate is filtered off and washed with water (3 · 30 mL), methanol (3 · 30 mL) and *n*-pentane (1 · 20 mL). **6** is obtained as orange solid in 86% (2.27 g) yield.

¹H NMR (400 MHz, CD$_2$Cl$_2$, 297 K): δ [ppm] = 7.33-7.28 (m, 3H,), 7.18-7.12 (m, 24H), 1.48 (s, 6H).

¹³C{¹H} NMR (101 MHz, DMSO, 297 K): δ [ppm] = 188.9 (C$_{Ac}$), 134.7 (*m*-Ar-C), 129.8 (*p*-Ar-C), 128.1 (*o*-Ar-C), 23.7 (Me$_{Ac}$).

³¹P{¹H} NMR (162 MHz, CD$_2$Cl$_2$, 297 K): δ [ppm] = 63.6 (s, 2P).

5.2.7 Synthesis of **7**
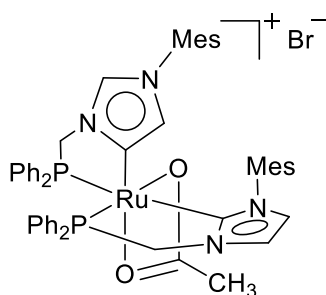
Chemical Formula: $C_{52}H_{53}N_4BrO_2P_2Ru$

Molecular Weight: 1008,94 g mol^{-1}

6 (50.0 mg, 66.9 mmol, 1.00 eq) and **5** (64.1 mg, 138 mmol, 2.05 eq) are dissolved in THF (2 mL) and stirred at 60 °C and for 3 h. After cooling back down to RT, the suspension is filtered and the and the residue is washed with THF (2 · 15 mL). The residue is dissolved in DCM and filtered to remove inorganic salts. The solvent is removed under reduced pressure and **7** is obtained as a yellow solid in 70% (47.5 mg) yield.

¹H-NMR (400 MHz, CDCl₃, 297 K): δ (ppm) = 10.28 (s, 1H, NC*H*N), 7.85 (m, 2H, Ar-H), 7.51 (m, 5H, Ar-H), 7.31 (m. 8 H, Ar-H), 7.05 (s, 1H, Ar-H), 7.02 (s, 1H, Ar-H), 6.91 (m, 6H, Ar-H), 6.74 (s, 1H, NC*H*C*H*N), 6.22 (m, 2H, Ar-H), 5.86 (s, 1H, NC*H*C*H*N), 5.41 (dd, $^2J_{PH}$ = 15.0 Hz, ^2J = 9.5 Hz, 1H, NC*H*₂P), 4.67 (*pseudo*-d, 1H, CH₂P, ^2J = ^2J = 12.6 Hz), 4.18 (m, 1H, NC*H*₂P), 2.81 (dd, $^2J_{PH}$ = 15.0 Hz, ^2J = 3.1 Hz, 1H, C*H*₂P), 2.40 (s, 3H, Me_Mes), 2.37 (s, 3H, Me_Mes), 2.26 (s, 3H, Me_Mes), 2.17 (s, 3H, Me_Mes), 2.08 (s, 3H, Me_Mes), 2.02 (s, 3H, Me_Mes), 0.53 (s, 3H, Me_Ac).

¹³C{¹H} NMR (101 MHz, CD₂Cl₂, 297 K): δ [ppm] = 191.6 (dd, $^2J_{CPcis}$ = 11.4 Hz, $^2J_{CPtrans}$ = 102.5 Hz, N*C*N), 185.3 (s, OAc), 163.0 (dd, $^2J_{CPcis}$ = 8.5 Hz, $^2J_{CPcis}$ = 18.4 Hz, N*C*CHN), 140.8, 139.1, 137.1,136.3, 136.1, 135.7, 135.5, 135.3, 134.8, 134.7, 134.2, 133.7, 133.4, 133.3, 132.9, 131.4, 131.0,130.6, 130.2, 129.8, 129.5, 129.1 - 128.6, 125.1, 124.8, 121.1 (all Ar-C), 53.0 (d, $^1J_{CP}$ = 36.0 Hz, N*C*P), 48.2 (d, $^1J_{CP}$ = 36.0 Hz, N*C*P), 23.5, 21.4, 21.1, 19.3, 18.3, 17.7, 17.5 (Me groups).

³¹P{¹H} NMR (162 MHz, CDCl₃, RT): δ (ppm) = 79.4 (d, $^2J_{PP}$ = 23.7 Hz), 63.2 (d, $^2J_{PP}$ = 23.7 Hz).

MS (FAB) *m/z* (%) = 928.5 (100) [**7** − Br⁻]⁺.

Elemental analysis calcd (%) for $C_{52}H_{53}BrN_4O_2P_2Ru$: C, 61.90; H, 5.30 N, 5.55. Found: C, 62.15; H, 5.67; N, 5.43.

5.2.8 Synthesis of 8
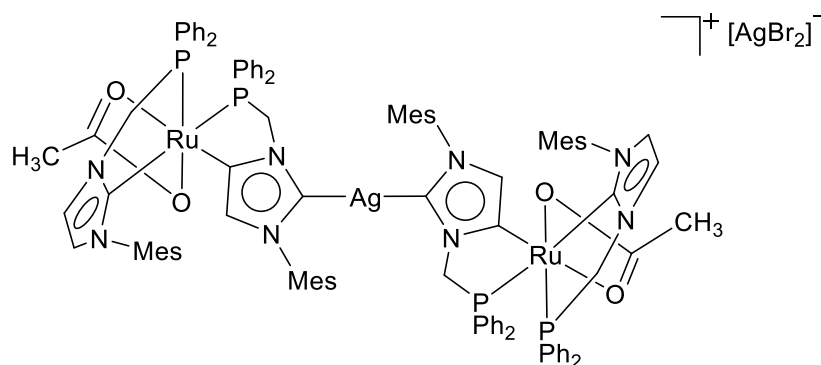
Chemical Formula: $C_{104}H_{104}Br_2N_8O_4P_4Ag_2Ru_2$

Molecular Weight: 2231,61 g mol^{-1}

7 (200 mg, 200 µmol, 1.00 eq) and Ag$_2$O (46.3 mg, 200 µmol, 1.00 eq) are suspended in DCM and stirred at RT for 7 d under protection from light. The mixture is filtered, and the solvent is removed under reduced pressure. The resulting residue is washed with *n*-pentane (3 · 4 mL) and dried under reduced pressure. **8** is obtained as yellow powder in 92% (202 mg) yield.

¹H NMR (400 MHz, CD$_2$Cl$_2$): δ [ppm] = 7.89 (t, $^3J_{HH}$ = 8.7 Hz, 4H, Ar-H), 7.55 - 7.35 (m, 12H, Ar-H), 7.30 - 7.18 (m, 14H, Ar-H), 7.04 (s, 2H, Ar-H), 7.00 (s, 2H, Ar-H), 6.92 - 6.87 (m, 12H, Ar-H), 6.71 (s, 2H, Ar-H), 6.29 (t, $^3J_{HH}$ = 8.7 Hz, 4H, Ar-H), 5.72 (s, 2H, Ar-H), 4.75 - 4.69 (m, 4H, CH2P), 4.13 (*pseudo*-t, $^2J_{HP}$ = 11.6 Hz, 2H, C*H*$_2$P), 2.49 (dd, $^2J_{HP}$ = 13.7 Hz, $^4J_{HH}$ = 1.6 Hz, 2H, C*H*$_2$P), 2.36 (s, 6H, Me$_{Mes}$), 2.35 (s, 6H, Me$_{Mes}$), 2.23 (s, 6H, Me$_{Mes}$), 2.15 (s, 6H, Me$_{Mes}$), 1.99 (s, 6H, Me$_{Mes}$), 1.97 (s, 6H, Me$_{Mes}$), 0.58 (s, 6H, Me$_{Ac}$).

¹³C {¹H} NMR (101 MHz, CD$_2$Cl$_2$): δ [ppm] = 193.2 (dd, $^2J_{CPcis}$ = 11.2 Hz, $^2J_{CPtrans}$ = 101.7 Hz, N*C*N), 184.4 (s, OAc), 154.7 (dd, $^2J_{CPcis}$ = 9.2 Hz, $^2J_{CPcis}$ = 18.9 Hz, N*CC*N), 138.9, 138.0, 137.4, 137.2, 136.6, 136.5, 136.4, 136.0, 135.0 - 134.7, 134.3, 134.0, 133.5, 131.3, 131.0, 130.8, 130.4, 129.7, 129.3, 128.9, 128.8 - 128.4, 125.1, 124.2, 120.6, 53.2, 51.7 (d, $^1J_{CP}$ = 37.0 Hz, N*C*P), 23.4, 21.4, 21.1, 19.3, 18.6, 17.8, 17.5 (Me groups).

³¹P{¹H} NMR (162 MHz, CD$_2$Cl$_2$): δ [ppm] = 81.0 (d, $^2J_{PP}$ = 24.6 Hz), 56.3 (d, $^2J_{PP}$ = 24.2 Hz).

Elemental analysis calcd (%) for $C_{104}H_{104}Br_2N_8O_4P_4Ag_2Ru_2$ · CH$_2$Cl$_2$: C, 54.44; H, 4.61 N, 4.84. Found: C, 54.20; H, 4.93; N, 4.67.

5.2.9 Synthesis of **9**
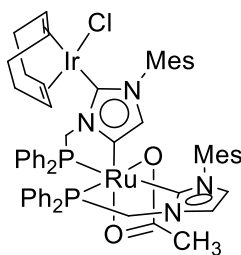
Chemical Formula: $C_{60}H_{64}ClN_4O_2P_2IrRu$

Molecular Weight: 1263,88 g mol^{-1}

8 (50.0 mg, 22.4 μmol, 1.00 eq), [IrCl(cod)]$_2$ (17.4 mg, 25.9 μmol, 1.20 eq) and Ag$_2$O (7.65 mg, 33.1 mmol, 1.50 eq) are suspended in DCM (3 mL) and stirred at RT for 3 h under protetion from light. The suspension is filtered off with a cannula and a mixture of Et$_2$O (15 mL) and *n*-pentane (20 mL) is added to the resulting brownish solution. After stirring the solution at 0 °C for 3 h excess [IrCl(cod)]$_2$ precipitates. The supernatant solution is filtered off and the solvent is removed under reduced pressure. Washing with *n*-pentane (3 · 3 mL) affords **9** as yellow powder in 83% (46.0 mg) yield.

^{1}H NMR (400 MHz, CD$_2$Cl$_2$, RT, major isomer): δ 7.91 - 7.82 (m, 2H, Ar-H), 7.61 - 7.53 (m, 2H, Ar-H), 7.44 - 7.30 (m, 5H, Ar-H), 7.25 - 6.84 (m, 14H, Ar-H), 6.63 (s, 1H, Ar-H), 6.38 - 6.32 (m, 2H, Ar-H), 5.58 (s, 1H, Ar-H), 5.38 (dd, ^2J = 14.5 Hz, ^2J = 10.0 Hz, 1H, C*H*HP), 4.76 (dd, ^2J = ^2J = 11.0 Hz 1H, C*H*HP), 4.32 - 4.28 (m, 1H, CH$_{cod}$), 4.10 (dd, ^2J = ^2J = 11.6 Hz 1H, CH*H*P), 4.05 - 3.97 (m, 1H, CH$_{cod}$), 3.38 (*pseudo*-d, ^2J = 14.7 Hz, ^2J = 14.7 Hz, 1H, CH*H*P), 3.02 - 2.94 (m, 2H, CH$_{cod}$), 2.45 (s, 3H, Me), 2.35 (s, 3H, Me), 2.22 (s, 3H, Me), 2.18 (s, 3H, Me), 2.00 (s, 3H, Me), 1.99 - 1.94 (m, 1H, CH$_{cod}$), 1.92 (s, 3H, Me), 1.78 - 1.72 (m, 1H, CH$_{cod}$), 1.55 - 1.42 (m, 4H, CH$_{cod}$), 1.27 - 1.16 (m, 2H, CH$_{cod}$), 0.53 (s, 3H, Me).

^{1}H NMR (400 MHz, CD$_2$Cl$_2$, RT, minor isomer): δ 7.91 - 7.82 (m, 2H, Ar-H), 7.61 - 7.53 (m, 2H, Ar-H), 7.44 - 7.30 (m, 5H, Ar-H), 7.25 - 6.84 (m, 14H, Ar-H), 6.67 (s, 1H, Ar-H), 6.42 - 6.36 (m, 2H, Ar-H), 5.69 (dd, ^2J = 14.0 Hz, ^2J = 10.2 Hz, 1H, C*H*HP), 5.49 (s, 1H, Ar-H), 4.76 (dd, ^2J = ^2J = 11.0 Hz 1H, C*H*HP), 4.21 - 4.17 (m, 1H, CH$_{cod}$), 4.11 (dd, ^2J = ^2J = 11.9 Hz 1H, CH*H*P), 4.05 - 3.96 (m, 1H, CH$_{cod}$), 3.02 - 2.94 (m, 3H, CH$_{cod}$ and CH*H*P), 2.38 (s, 3H, Me), 2.35 (s, 3H, Me), 2.21 (s, 3H, Me), 2.20 (s, 3H, Me), 2.08 (s, 3H, ME), 1.99 - 1.94 (m, 1H, CH$_{cod}$), 1.97 (s, 3H, ME), 1.78 - 1.72 (m, 1H, CH$_{cod}$), 1.55 - 1.42 (m, 4H, CH$_{cod}$), 1.27 - 1.16 (m, 2H, CH$_{cod}$), 0.50 (s, 3H, Me).

^{13}C{^{1}H} NMR (101 MHz, CD$_2$Cl$_2$, RT, both isomers) δ 194.0 (dd, $^2J_{CPcis}$ = 35.1 Hz, $^2J_{CPtrans}$ = 111.2 Hz, N*C*N), 183.9 (s, OAc), 175.9 (d, $^3J_{CP}$ = 11.8 Hz, N*C'*N, major isomer), 177.7 (d, $^3J_{CP}$ = 12.0 Hz, N*C'*N, minor isomer), 152.0 (dd, $^2J_{CPcis}$ = 11.0 Hz, $^2J_{CPcis}$ = 20.5 Hz, N*C*CHN), 138.7, 138.6, 138.1, 138.0, 137.9, 137.7, 137.6, 137.5, 137.1, 137.0, 136.8, 136.6, 136.2, 135.6, 135.5, 135.2, 135.1, 135.0, 134.9, 134.6, 134.5, 134.4, 134.3, 134.2, 134.0, 133.5, 132.2, 131.3 - 131.0, 130.7, 130.5, 129.8 - 129.6, 129.2, 129.1, 128.6

- 127.9, 125.7, 125.2, 124.1, 123.7, 120.7, 120.4 (all Ar-C), 81.8, 81.0, 80.0, 79.8 (olefinic cod C atoms), 53.2, 51.4, 51.2, 51.0, 50.0, 49.3, 49.0 (NCP and cod C atoms), 34.8, 34.2, 34.0, 33.2, 32.4, 30.2, 29.6, 23.3, 21.3, 21.1, 19.9, 19.7, 19.4, 19.3, 18.8, 18.6, 17.5 (cod and Me).

^{31}P{^{1}H} NMR (162 MHz, CD$_2$Cl$_2$, RT, major isomer): δ 80.3 (d, $^2J_{PPcis}$ = 24.3 Hz), 57.2 (d, $^2J_{PPcis}$ = 23.4 Hz).

^{31}P{^{1}H} NMR (162 MHz, CD$_2$Cl$_2$, RT, minor isomer): δ 80.8 (d, $^2J_{PP}$ = 24.9 Hz), 58.6 (d, $^2J_{PP}$ = 24.4 Hz).

MS (FAB) *m/z* (%) = 1262.1 (18) [**9** − H], 927.9 (9) [**9** − [IrCl(cod)].

Elemental analysis calcd (%) for C$_{60}$H$_{64}$ClN$_4$O$_2$P$_2$IrRu: C, 57.02; H, 5.33 N, 4.27. Found: C, 56.64; H 5.29; N, 4.20.

5.2.10 Synthesis of **10**
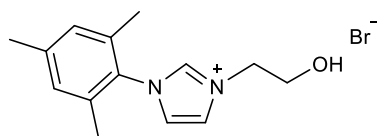
Chemical Formula: $C_{14}H_{19}BrN_2O$
Molecular Weight: 311,22 g mol^{-1}

1 (1.50 g, 8.05 mmol, 1.00 eq) is dissolved in dry toluene (20 mL) and 2-Bromoethanol (1.11 g, 8.86 mmol, 1.10 eq) is added slowly to the stirred solution. The reaction mixture is heated to 120 °C and stirred for 16 h. The work-up is performed under atmospheric conditions. The precipitate is isolated and washed with toluene (3 · 10 mL) and diethyl ether (2 · 10 mL). **10** is obtained as a colorless solid in 84% yield (2.10 g).

^{1}H NMR (400 MHz, DMSO-d$_6$, 297 K): δ [ppm] = 9.40 (t, ^4J = 1.5 Hz, 1H, NCHN), 8.05 (t, ^3J = 1.7 Hz, 1H, NCCHN), 7.91 (t, ^3J = 1.7 Hz, 1H, NCHCN), 7.14 (s, 2H, Ar-H$_{Mes}$), 5.24 (t, ^3J = 5.1 Hz, 1H, OH), 4.33 (t, ^3J = 5.1 Hz, 2H, NCH_2CP), 3.80 (m, 2H, NCCH_2P), 2.33 (s, 3H, p-Me$_{Mes}$), 2.02 (s, 6H, o-Me$_{Mes}$).

^{13}C{^{1}H} NMR (101 MHz, DMSO-d$_6$, 297 K): δ [ppm] = 140.2 (p-Ar-C$_{Mes}$), 137.7 (NCN), 134.3 (o-Ar-C$_{Mes}$), 131.2 (Ar-C$_{Mes}$), 129.2 (m-Ar-C$_{Mes}$), 123.7 (NCCN), 123.4 (NCCN), 59.1 (NCCO), 52.0 (NCCO), 20.6 (p-Me$_{Mes}$), 16.9 (o-Me$_{Mes}$).

ESI-MS m/z (%) = 231 [**10** $-$ Br$^-$]$^+$, 187 [**10** $-$ Br$^-$ $-$ C$_2$H$_4$OH]$^+$.

Elemental Analysis calcd (%) for $C_{14}H_{20}BrN_2O$: C, 54.03; H, 6.15; N, 9.00. Found: C, 53.74; H 6.17; N, 8.92.

5.2.11 Synthesis of **11**
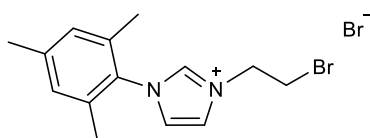
Chemical Formula: $C_{14}H_{18}Br_2N_2$
Molecular Weight: 374,12 g mol^{-1}

10 (2.10 g, 6.75 mmol, 1.00 eq) is dissolved in DCM (11 mL) and cooled to 0 °C. PBr$_3$ (1.92 g, 7.08 mmol, 1.10 eq) is separately mixed with DCM (8 mL) and then slowly added to the cooled solution of **2**. The colorless solution is heated to 40 °C and stirred for 2 h. The work-up is performed under atmospheric conditions. After dilution of the reaction mixture with DCM (30 mL) it is transferred to a separatory funnel and neutralized by slow addition of a saturated. NaHCO$_3$ solution (10 mL). The organic phase is isolated, the aqueous phase is extracted with DCM (3 · 40 mL) and the unified organic phases are dried over MgSO$_4$. Solvent removal under reduced pressure gives **11** as a colorless powder in 81% (2.04 g) yield.

^{1}H NMR (400 MHz, DMSO-d$_6$, 297 K): δ [ppm] = 9.53 (t, ^4J = 1.5 Hz, 1H, NC*H*N), 8.13 (t, ^3J = 1.7 Hz, 1H, NCC*H*N), 7.99 (t, ^3J = 1.7 Hz, 1H, NC*H*CN), 7.16 (s, 2H, Ar-H$_{Mes}$), 4.71 (t, ^3J = 5.5 Hz, 2H, NC*H$_2$*CBr), 4.06 (t, ^3J = 5.5 Hz, 2H, NCC*H$_2$*Br), 2.34 (s, 3H, *p*-Me$_{Mes}$), 2.03 (s, 6H, *o*-Me$_{Mes}$).

^{13}C{^{1}H} NMR (101 MHz, DMSO-d$_6$, 297 K): δ [ppm] = 140.4 (*p*-Ar-C$_{Mes}$), 137.9 (N*C*N), 134.3 (*o*-Ar-C$_{Mes}$), 131.0 (Ar-C$_{Mes}$), 129.3 (*m*-Ar-C$_{Mes}$), 124.1 (N*C*CN), 123.1 (NC*C*N), 59.1 (N*C*CBr), 52.0 (NC*C*Br), 20.6 (*p*-Me$_{Mes}$), 16.9 (*o*-Me$_{Mes}$).

ESI-MS *m/z* (%) = 295 [**11** − Br$^-$]$^+$.

Elemental Analysis calcd (%) for C$_{14}$H20BrN$_2$O: C, 44.83; H, 5.11; N, 7.47. Found: C, 44.47; H 5.14; N, 7.36.

5.2.12 Synthesis of **12**
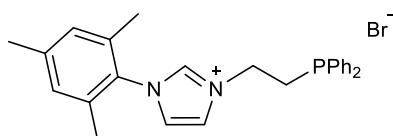
Chemical Formula: $C_{26}H_{28}BrN_2P$
Molecular Weight: 479,40 g mol^{-1}

Potassium *tert*-butoxide (157 mg, 1.40 mmol, 1.05 eq) is dissolved in dry and degassed DMSO (2 mL) and slowly mixed with diphenylphosphane (274 mg, 1.47 mmol, 1.10 eq). The red potassium diphenylphosphide solution is slowly added to a solution of **11** (500 mg, 1.34 mmol, 1.00 eq) in DMSO (1 mL) and is stirred for 2 h at rt The solvent is removed under reduced pressure at 70 °C and degassed methanol (3 mL) is added to the oily residue, which is again removed under reduced pressure. The crude product is dissolved in degassed DCM (6 mL), filtered, concentrated to 2 mL and precipitated with Et$_2$O (15 mL). After filtering, **12** is obtained as a colorless solid in 75% (481 mg) yield.

^{1}H NMR (400 MHz, CD$_2$Cl$_2$, 297 K): δ [ppm] = 10.56 (s, 1H, NC*H*N), 7.75 (t, $^3J_{HH}$ = 1.6 Hz, 1H, NCHC*H*N), 7.53-7.49 (m, 4H, Ar-H$_{Ph}$), 7.40-7.35 (m, 6H, Ar-H$_{Ph}$), 7.18 (t, $^3J_{HH}$ = 1.7 Hz, 1H, NC*H*CHN), 7.03 (s, 2H, Ar-H$_{Mes}$), 4.73-4-67 (m, 2H, NC*H$_2$*CH$_2$N), 2.91 (t, ^3J = 7.5 Hz, 2H, NCH$_2$C*H$_2$*N), 2.34 (s, 3H, *p*-Me$_{Mes}$), 2.06 (s, 6H, *o*-Me$_{Mes}$).

^{13}C{^{1}H} NMR (101 MHz, DMSO, 297 K): δ [ppm] = 140.4 (*p*-Ar-C$_{Mes}$), 137.9 (N*C*N), 134.3 (*o*-Ar-C$_{Mes}$), 131.0 (q-Ar-C$_{Mes}$), 129.3 (*m*-Ar-C$_{Mes}$), 124.1 (N*C*CN), 123.1 (NC*C*N), 59.1 (N*C*CP), 52.0 (NC*C*P), 20.6 (*p*-Me$_{Mes}$), 16.9 (*o*-Me$_{Mes}$).

^{31}P{^{1}H} NMR (162 MHz, CD$_2$Cl$_2$, 297 K): δ [ppm] = −23.3 (s, 1P).

ESI-MS *m/z* (%) = 399 [**12** − Br$^-$]$^+$.

5.2.13 Synthesis of **13**
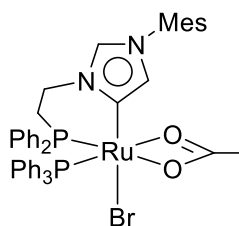
Chemical Formula: $C_{46}H_{45}BrN_2O_2P_2Ru$
Molecular Weight: 900,80 g mol^{-1}

6 (580 mg, 780 μmol, 1.00 eq) and **3** (623 mg, 1.17 mmol, 1.50 eq) are suspended in dry and degassed THF (30 mL) and stirred under reflux for 12 h. The resulting yellow suspension is filtered, the precipitate is dissolved in dry and degassed DCM and again filtered. The solvent is removed under reduced pressure and the resulting solid is washed with dry and degassed EtOH (2 · 5 mL) and *n*-pentane (1 · 5 mL). **13** is obtained as an orange yellow powder in 85% (597 mg) yield.

^{1}H NMR (400 MHz, CD$_2$Cl$_2$, 297 K): δ [ppm] = 8.24-8.19 (m, 2H, Ar-H), 7.90 (d, *J* = 1.8 Hz, 1H, NC*H*N), 7.42-7.36 (m, 3H, Ar-H), 7.28-7.19 (m, 4H, Ar-H), 7.16-6.89 (m, 18H, Ar-H), 5.82 (d, *J* = 1.8 Hz, 1H, CC*H*N), 4.32 (dddd, ^{2}*J* = 1.5 Hz, ^{3}*J* = 13.8 Hz, *J* = 29.5 Hz, 1H, NC*H*$_2$CH$_2$N), 4.03 (q, ^{3}*J* = 13.3 Hz, 1H, NC*H*$_2$CH$_2$P), 2.35 (dd, ^{2}*J* = 5.0 Hz, ^{3}*J* = 14.0 Hz, 1H, NCH$_2$C*H*$_2$P), 2.31 (s, 3H, *p*-H$_{Mes}$), 2.13 (s, 3H, *o*-H$_{Mes}$), 1.86 (s, 3H, *o*-H$_{Mes}$), 1.72 (s, 1H, Me$_{Ac}$), 1.62-1.53 (m, 1H, NCH$_2$C*H*$_2$P).

^{13}C{^{1}H} NMR 184.8, 161.4, 140.6, 137.0, 136.5, 135.5, 135.4, 135.2, 135.1, 134.3, 132.9, 132.8, 132.7, 132.2, 130.0, 129.8, 129.3, 128.2, 128.1, 128.0, 127.9, 127.6, 127.5, 126.7, 46.4, 34.7, 25.5, 23.5, 23.3, 23.2, 22.9, 17.9, 17.4.

^{31}P{^{1}H} NMR (162 MHz, CD$_2$Cl$_2$, 297 K): δ [ppm] = 61.8 (d, ^{2}*J*$_{PPcis}$ = 43.1 Hz, 1P), 53.1 (d, ^{2}*J*$_{PPcis}$ = 43.1 Hz, 1P).

FAB-MS *m/z* (%) = 819.8 (100%) [**13** − Br$^-$]$^+$.

Elemental Analysis calcd (%) for C$_{46}$H$_{45}$BrN$_2$O$_2$P$_2$Ru: C, 61.34; H, 5.04; N, 3.11. Found: C, 61.02; H 5.16; N, 3.25.

5.2.14 Synthesis of **14**

Chemical Formula: $C_{54}H_{54}BrN_2O_2P_3Ru$

Molecular Weight: 1036,93 g mol^{-1}

13 (97.5 mg, 108 µmol, 1.00 eq) and 1,2-bis(diphenylphosphano)ethane (47.4 mg, 119 µmol, 1.10 eq) are dissolved in DCM (4 mL) and stirred at RT. After 30 min, the solvent is removed under reduced pressure, the resulting pale-yellow residue is dissolved in THF (5 mL) and stirred at 60 °C for 60 min. The resulting suspension is then cooled to -20 °C to complete the precipitation, the solvent is filtered off and the yellow residue is washed with diethyl ether (3 · 4 mL) and with *n*-pentane (2 mL). **14** is obtained as a bright yellow powder in 76% (92.0 mg) yield.

^{1}H NMR (400 MHz, CD$_2$Cl$_2$, RT): δ 9.93 (s, 1H, NC*H*N), 7.67 - 7.56 (m, 6H, Ar-H), 7.49 - 7.42 (m, 2H, Ar-H), 7.38 - 7.24 (m, 10H, Ar-H), 7.18 (*pseudo*-dt, ^4J = 1.5 Hz, ^3J = 7.8 Hz, 2H, Ar-H), 7.05 - 7.00 (m, 5H, Ar-H), 6.95 - 6.91 (m, 3H, Ar-H), 6.79 (*pseudo*-t, ^3J = 9.1 Hz, 2H, Ar-H), 6.76 (*pseudo*-d, J = 1.2 Hz, 1H, Ar-H), 5.98 (*pseudo*-t, ^3J = 8.8 Hz, 2H, Ar-H), 5.22 (ddt, ^2J = 3.8 Hz, ^2J = 14.4 Hz, J = 30.7 Hz, 1H, NC*H*$_2$CH$_2$P), 4.14 (*pseudo*-q, ^2J = ^3J = 13.1 Hz, 1H, NC*H*$_2$CH$_2$P), 2.87 - 2.69 (m, 1H, PC*H*$_2$CH$_2$P), 2.58 - 2.39 (m, 1H, PC*H*$_2$CH$_2$P), 2.32 (s, 3H, Me), 2.12 (s, 3H, Me), 2.08 - 2.04 (m, 1H, PC*H*$_2$CH$_2$P), 2.01 (s, 3H, Me), 1.96 - 1.89 (m, 1H, NCH$_2$C*H*$_2$P), 1.81 - 1.73 (m, 1H, NCH$_2$C*H*$_2$P), 1.30 (s, 3H, Me), 1.11 - 1.00 (m, 1H, PC*H*$_2$CH$_2$P).

^{13}C{^{1}H} NMR (101 MHz, CD$_2$Cl$_2$, RT): δ 185.8 (s, OAc), 155.8 (ddd, $^2J_{CPcis}$ = 11.5 Hz, $^2J_{CPcis}$ = 14.7 Hz, $^2J_{CPtrans}$ = 89.5 Hz, NC*C*HN), 140.3 (s, N*C*N), 137.5, 137.4, 136.9, 136.5, 136.2, 135.9, 135.8, 135.6, 135.5, 135.1, 134.5, 134.2, 134.1, 133.4, 133.3, 133.0, 132.9, 132.8, 132.5, 132.4, 132.2, 132.1, 132.0, 130.8, 130.6, 130.5, 130.3, 129.8, 129.1, 129.0, 128.9, 128.8, 128.7, 128.6, 128.5, 128.3, 128.2, 126.7 (aromatic C atoms), 45.0 (s, N*C*H$_2$CH$_2$P), 29.3 (dd, $^1J_{CP}$ = 19.1 Hz, $^2J_{CP}$ = 34.7 Hz, P*C*H$_2$CH$_2$P), 27.8 (d, $^2J_{CP}$ = 32.6 Hz, NCH$_2$*C*H$_2$P), 25.0 (Me), 21.3 (Me), 20.4 (dd, $^1J_{CP}$ = 9.1 Hz, $^2J_{CP}$ = 26.2 Hz, PCH$_2$*C*H$_2$P), 18.0 (2 · Me).

^{31}P{^{1}H} NMR (162 MHz, CD$_2$Cl$_2$, RT): δ 72.0 (dd, $^2J_{PPtrans}$ = 8.8 Hz, $^2J_{PPcis}$ = 23.2 Hz, P$_{eq}$), 56.9 (dd, $^2J_{PPtrans}$ = 8.8 Hz, $^2J_{PPcis}$ = 38.8 Hz, P$_{eq}$), 42.4 (dd, $^2J_{PPcis}$ = 23.2 Hz, $^2J_{PPcis}$ = 38.8 Hz, P$_{ax}$).

MS (ESI) *m/z* (%) = 957.3 (100) [**14** – Br$^-$]$^+$.

Elemental analysis calcd (%) for C$_{54}$H$_{54}$BrN$_2$O$_2$P$_3$Ru: C, 62.55; H, 5.25; N, 2.70. Found: C, 61.90; H 5.27; N, 2.74.

5.2.15 Synthesis of **15**

Chemical Formula: $C_{54}H_{53}BrN_2O_2P_3AgRu$

Molecular Weight: 1143,79 g mol^{-1}

14 (100 mg, 96.4 µmol, 1.00 eq) and Ag$_2$O (56.0 mg, 242 µmol, 2.51 eq) are suspended in THF (3 mL) and stirred at 40 °C. After 3 d, the mixture is filtered, and the solvent is removed under reduced pressure. After washing with *n*-pentane (2 × 2 mL) **15** is obtained as a bright yellow powder in 90% (103 mg) yield.

^{1}H NMR (400 MHz, CD$_2$Cl$_2$, RT): δ 7.69 - 7.59 (m, 6H, Ar-H), 7.48 - 7.34 (m, 5H, Ar-H), 7.31 - 7.21 (m, 8H, Ar-H), 7.14 (*pseudo*-dt, J = 1.5 Hz, ^3J = 7.9 Hz, 2H, Ar-H), 7.06 - 7.03 (*pseudo*-dt, J = 1.8 Hz, ^3J = 8.3 Hz, 2H, Ar-H), 7.01 - 6.97 (m, 3H, Ar-H), 6.94 - 6.91 (m, 3H, Ar-H), 6.85 (*pseudo*-t, ^3J = 9.2 Hz, 2H, Ar-H), 6.61 (s, br, 1H, Ar-H), 5.99 (*pseudo*-t, ^3J = 8.8 Hz, 2H, Ar-H), 4.79 (*pseudo*-dd, ^2J = 13.6 Hz, ^2J = 30.8 Hz, 1H, NC*H*$_2$CH$_2$P), 4.08 (*pseudo*-q, ^2J = ^3J = 12.9 Hz, 1H, NC*H*$_2$CH$_2$P), 2.81 - 2.64 (m, 1H, PC*H*$_2$CH$_2$P), 2.57 - 2.39 (m, 1H, PC*H*$_2$CH$_2$P), 2.32 (s, 3H, Me), 2.06 (s, 3H, Me), 2.03 - 1.96 (m, 1H, PCH$_2$CH$_2$P), 2.00 (s, 3H, Me), 1.93 - 1.87 (m, 1H, NCH$_2$C*H*$_2$P), 1.73 - 1.65 (m, 1H, NCH$_2$C*H*$_2$P), 1.30 (s, 3H, Me), 0.98 - 0.92 (m, 1H, PCH$_2$CH$_2$P).

^{13}C{^{1}H} NMR (101 MHz, CD$_2$Cl$_2$, RT): δ 185.1 (s, OAc), 151.4 (ddd, $^2J_{CPcis}$ = 13.0 Hz, $^2J_{CPcis}$ = 16.5 Hz , $^2J_{CPtrans}$ = 89.2 Hz, NC*C*HN), 138.5, 138.0, 137.7, 137.3, 137.2, 136.9, 136.8, 136.7, 136.5, 136.1, 136.0, 135.1, 134.3, 134.2, 133.5, 133.4, 133.1, 133.0, 132.6, 132.1, 132.0, 130.6, 130.3, 130.2, 130.1, 129.4, 129.3, 128.8, 128.7, 128.5, 128.4, 128.3, 128.1, 126.7 (aromatic C atoms), 48.1 (s, N*C*H$_2$CH$_2$P), 29.4 (d, $^1J_{CP}$ = 32.5 Hz, NCH$_2$*C*H$_2$P), 29.0 (dd, $^1J_{CP}$ = 14.9 Hz, $^2J_{CP}$ = 20.2 Hz, P*C*H$_2$CH$_2$P), 25.1 (Me), 21.4 (Me), 20.6 (dd, $^1J_{CP}$ = 9.0 Hz, $^2J_{CP}$ = 25.5 Hz, PCH$_2$*C*H$_2$P), 18.3 (Me), 18.2 (Me).

^{31}P{^{1}H} NMR (162 MHz, CD$_2$Cl$_2$, RT): δ 72.6 (dd, $^2J_{PPtrans}$ = 7.3 Hz, $^2J_{PPcis}$ = 40.2 Hz, P$_{eq}$), 57.0 (dd, $^2J_{PPtrans}$ = 5.5 Hz, $^2J_{PPcis}$ = 21.7 Hz, P$_{eq}$), 46.1 (dd, $^2J_{PPcis}$ = 22.3 Hz, $^2J_{PPcis}$ = 40.2 Hz, P$_{ax}$).

MS (FAB) *m/z* (%) = 1061.0 (100%) [**15** − Br$^-$]$^+$.

Elemental analysis calcd (%) for C$_{54}$H$_{53}$BrN$_2$O$_2$P$_3$AgRu: C, 56.71; H, 4.67; N, 2.45. Found: C, 56.96; H 4.80; N, 2.55.

5.2.16 Synthesis of **17**
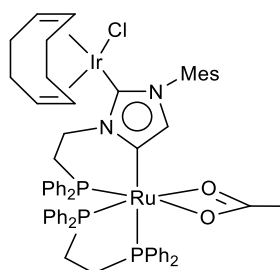
Chemical Formula: $C_{62}H_{65}ClN_2O_2P_3IrRu$

Molecular Weight: 1291,87g mol^{-1}

[Ir(cod)Cl]$_2$ (80.6 mg, 120 µmol, 1.2 eq) and Ag$_2$O (55.9 mg, 241 µmol, 2.42 eq) are suspended in THF (3 mL). In a separate flask **15** (110 mg, 9.61 µmol, 1.00 eq) is dissolved in THF (2 mL) and is added dropwise to the other suspension. The mixture is stirred at 40 °C for 2 h and then filtered off. The solvent is removed under reduced pressure and the resulting orange solid is washed with cold THF (1 mL). After washing with *n*-pentane **17** is obtained as a yellow powder in 65% (81 mg) yield.

^{1}H NMR (400 MHz, CD$_2$Cl$_2$, RT, major isomer): δ 7.71-7.56 (m, 5H, Ar-H), 7.49-7.35 (m, 7H, Ar-H), 7.29-7.13 (m, 9H, Ar-H), 7.06-6.86 (m, 7H, Ar-H), 6.81-6.76 (m, 2H, Ar-H), 6.10 (s, br, 1H, CC*H*N), 6.00-5.86 (m, 1H, NC*H*$_2$CH$_2$P), 5.82 (t, ^3J = 8.8 Hz, 2H, Ar-H), 4.01-3.95 (m, 2H, CH$_{cod}$), 3.94-3.85 (m, 1H, NC*H*$_2$CH$_2$P), 3.27-3.24 (dt, ^3J = 2.2 Hz, ^3J = 7.0 Hz, 1H, CH$_{cod}$), 2.95-2.68 (m, 1H, NCH$_2$C*H*$_2$P, 1H, CH$_{cod}$), 2.47-2.41 (m, 1H, NCH$_2$C*H*$_2$P), 2.30 (s, br, 3H, Me$_{Mes}$), 2.28 (s, br, 3H, Me$_{Mes}$), 2.17-1.98 (m, 2H, PCH$_2$CH$_2$P, 1H, CH$_{cod}$), 1.95 (s, br, 3H, Me$_{Mes}$), 1.92-1.85 (m, 1H, CH$_{cod}$), 1.79-1.66 (m, 1H, PCH$_2$CH$_2$P, 1H, CH$_{cod}$), 1.50-1.44 (m, 2H, CH$_{cod}$), 1.38-1.32 (m, 1H, CH$_{cod}$), 1.32-1.27 (m, 1H, CH$_{cod}$), 1.31 (s, br, 3H, Me$_{OAc}$), 1.23-1.14 (m, 1H, PCH$_2$CH$_2$P), 1.11-1.00 (m, 1H, CH$_{cod}$).

^{1}H NMR (400 MHz, CD$_2$Cl$_2$, RT, minor isomer): δ 7.71-7.56 (m, 5H, Ar-H), 7.49-7.35 (m, 7H, Ar-H), 7.29-7.13 (m, 9H, Ar-H), 7.06-6.86 (m, 7H, Ar-H), 6.81-6.76 (m, 2H, Ar-H), 6.35 (s, br, 1H, CC*H*N), 5.93 (t, ^3J = 8.8 Hz, 2H, Ar-H), 5.75-5.63 (m, 1H, NC*H*$_2$CH$_2$P), 4.01-3.95 (m, 2H, CH$_{cod}$), 3.94-3.85 (m, 1H, NC*H*$_2$CH$_2$P), 3.33-3.29 (dt, ^3J = 2.2 Hz, ^3J = 7.0 Hz, 1H, CH$_{cod}$), 2.95-2.68 (m, 1H, NCH$_2$C*H*$_2$P, 1H, CH$_{cod}$), 2.47-2.41 (m, 1H, NCH$_2$C*H*$_2$P), 2.31 (s, br, 3H, Me$_{Mes}$), 2.25 (s, br, 3H, Me$_{Mes}$), 2.17-1.98 (m, 2H, PCH$_2$CH$_2$P, 1H, CH$_{cod}$), 1.92-1.85 (m, 1H, CH$_{cod}$), 1.79-1.66 (m, 1H, PCH$_2$CH$_2$P, 1H, CH$_{cod}$), 1.73 (s, br, 3H, Me$_{Mes}$), 1.50-1.44 (m, 2H, CH$_{cod}$), 1.38-1.32 (m, 1H, CH$_{cod}$), 1.32-1.27 (m, 1H, CH$_{cod}$), 1.25 (s, br, 3H, Me$_{OAc}$), 1.23-1.14 (m, 1H, PCH$_2$CH$_2$P), 1.11-1.00 (m, 1H, CH$_{cod}$).

^{13}C{^{1}H} NMR (101 MHz, CD$_2$Cl$_2$, RT, both isomers): δ 184.8 (s, OAc), 176.5 (s, N*C*N), 138.2, 138.1, 138.0, 137.8, 137.7, 137.6, 137.2, 136.9, 136.5, 135.5, 134.6, 134.4, 134.3, 133.4, 133.3, 133.2, 133.1, 133.0, 132.9, 132.8, 132.7, 132.6 132.5, 132.2, 132.1, 132.0, 131.9, 130.4, 130.2, 130.1, 130.0, 129.9, 129.8, 129.7, 129.5, 129.3, 129.2, 128.8, 128.7, 128.6, 128.5, 128.4, 128.3, 128.2, 128.1 (aromatic C atoms),

80.5, 80.5, 80.2, 79.5 (olefinic cod C), 51.7, 51.7, 50.2, 49.9, 46.4 (aliphatic cod C), 35.6, 35.3, 33.1, 32.7, 30.6, 30.4, 29.4, 29.1, 25.3, 25.2, 21.3, 19.9, 18.4, 18.3 (aliphatic C).

^{31}P{^{1}H} NMR (162 MHz, CD$_2$Cl$_2$, RT, major isomer): δ 72.1 (dd, $^2J_{PPtrans}$ = 7.6 Hz, $^2J_{PPcis}$ = 40.4 Hz), 51.8 (dd, $^2J_{PPtrans}$ = 7.9 Hz, $^2J_{PPcis}$ = 22.0 Hz), 46.7 (dd, $^2J_{PPcis}$ = 22.0 Hz, $^2J_{PPcis}$ = 40.4 Hz).

^{31}P{^{1}H} NMR (162 MHz, CD$_2$Cl$_2$, RT, minor isomer): δ 72.7 (dd, $^2J_{PPtrans}$ = 7.6 Hz, $^2J_{PPcis}$ = 40.4 Hz), 55.2 (dd, $^2J_{PPtrans}$ = 7.9 Hz, $^2J_{PPcis}$ = 22.0 Hz), 45.2 (dd, $^2J_{PPcis}$ = 22.0 Hz, $^2J_{PPcis}$ = 40.4 Hz).

MS (LIFDI) m/z (%) = 1292 (100) [17]$^+$.

Elemental analysis calcd (%) for C$_{62}$H$_{65}$ClN$_2$O$_2$P$_3$IrRu: C, 57.64; H, 5.07; N, 2.17. Found: C, 57.30; H, 5.47; N, 2.03.

5.2.17 Synthesis of **18**
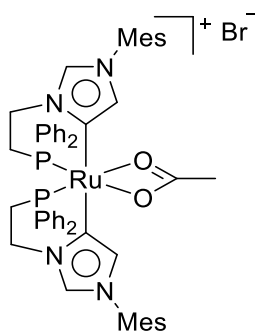
Chemical Formula: $C_{54}H_{57}BrN_4O_2P_2Ru$

Molecular Weight: 1037,00 g mol^{-1}

a) Method from **6**

6 (221 mg, 297 µmol, 1.00 eq), **12** (300 mg, 626 µmol, 2.1 eq) and anhydrous NaOAc (244 mg, 2.98 mmol, 10.0 eq) are dissolved in dry and degassed THF (10 mL) and stirred for 6 h at 60 °C. The resulting precipitate is isolated *via* filtration, washed with THF (2 mL) and dissolved in DCM (5 mL). The yellow solution is filtered off, the solvent is removed under reduced pressure and the resulting solid is washed with *n*-hexane. **18** is obtained as a yellow powder in 85% (260 mg) yield.

b) Method from **13**

13 (270 mg, 300 µmol, 1.00 eq), **12** (158 mg, 330 mmol, 1.10 eq) and anhydrous NaOAc (123 mg, 1.50 mmol, 5.00 eq) are dissolved in dry and degassed THF (10 mL) and stirred for 3 h at 60 °C. The resulting precipitate is isolated *via* filtration, washed with THF (2 mL) and dissolved in DCM (5 mL). The yellow solution is filtered off, the solvent is removed under reduced pressure and the resulting solid is washed with *n*-hexane. **18** is obtained as a yellow powder in 90% (280 mg) yield.

^{1}H NMR (500 MHz, CD$_2$Cl$_2$, RT): δ 8.72 (d, ^4J = 1.7 Hz, 2H, NCHN), 7.75 (m, 4H, *o*-Ar-H), 7.38 (t, ^3J = 7.5 Hz, 2H, *p*-Ar-H), 7.30-7.21 (m, 6H, *m*-Ar-H, *p*-Ar-H), 7.15 (t, ^3J = 7.5 Hz, 4H, *m*-Ar-H), 7.00 (s, 2H, Ar-H$_{Mes}$), 6.92 (s, 2H, Ar-H$_{Mes}$), 6.54 (d, ^4J = 1.7 Hz, 2H, NCCHN), 6.50 (m, 4H, *o*-Ar-H), 4.71-4.57 (m, 2H, CH_2CH$_2$P), 4.21-4.11 (m, 2H, CH_2CH$_2$P), 2.31 (s, 6H, *p*-Me$_{Mes}$), 2.10 (s, 6H, *o*-Me$_{Mes}$), 1.98-1.88 (m, 2H, CH$_2$CH_2P) 1.80 (s, 9H, Me$_{Ac}$, *o*-Me$_{Mes}$), 1.69-1.59 (m, 2H, CH$_2$CH_2P).

^{13}C {^{1}H} NMR (125 MHz, CD$_2$Cl$_2$, RT): δ 184.2 (s, OAc), 162.3 (t, J_{CP} = 12.4 Hz, NCCHN), 140.3 (s, *p*-Ar-C$_{Mes}$), 138.5 (dd, J_{CP} = 17.5 Hz, J_{CP} = 20.1 Hz, q-Ar-C$_{Ph}$), 137.9 (dd, J_{CP} = 22.2 Hz, J_{CP} = 25.3 Hz, q-Ar-C$_{Ph}$), 135.1 (s, NCN), 134.6 (s, *o*-Ar-C$_{Mes}$), 134.3 (s, *o*-Ar-C$_{Mes}$), 133.9 (t, $^2J_{CP}$ = 4.7 Hz, *o*-Ar-C$_{Ph}$), 132.9 (s, q-Ar-C$_{Mes}$), 132.2 (s, br, *o*-Ar-C$_{Ph}$), 130.1 (s, *p*-Ar-C$_{Ph}$), 129.9 (s, *p*-Ar-C$_{Ph}$), 129.8 (s, *m*-Ar-C$_{Mes}$), 129.8 (s, *m*-Ar-C$_{Mes}$), 128.4 (t, $^3J_{CP}$ = 4.3 Hz, *m*-Ar-C$_{Ph}$), 128.3 (t, $^3J_{CP}$ = 4.5 Hz, m-Ar-C$_{Ph}$), 127.4 (s, NCCHN), 45.8 (s, NCH_2CH$_2$P), 26.1

(dd, $^1J_{CP}$ = 13.7 Hz, $^1J_{CP}$ = 16.0 Hz, NCH$_2$CH$_2$P), 25.3 (s, Me$_{Ac}$), 21.3 (s, p-Me$_{Mes}$), 17.8 (s, o-Me$_{Mes}$), 17.6 (s, o-Me$_{Mes}$).

^{31}P{^{1}H} NMR (162 MHz, CD$_2$Cl$_2$, RT): δ 56.6 (s).

Elemental analysis calcd (%) for C$_{54}$H$_{57}$BrN$_4$O$_2$P$_2$Ru: C, 62.55; H, 5.54; N, 5.40. Found: C, 62.11; H, 5.68; N, 5.33.

MS (LIFDI) m/z (%): 957.1 (100) [**18** − Br$^−$]$^+$, 978.0 (60) [**18**–OAc$^−$]$^+$.

5.2.18 Synthesis of **20**
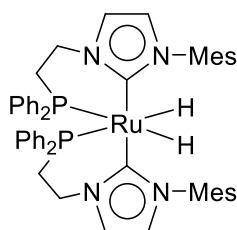
Chemical Formula: $C_{52}H_{56}N_4P_2Ru$

Molecular Weight: 900,07 g mol^{-1}

18 (50.0 mg, 48.2 μmol, 1.00 eq) and KO^{t}Bu (27.0 mg, 241 μmol, 5.00 eq) are suspended in dry and degassed toluene (15 mL) in a Fisher-Porter-bottle. The reaction vessel is pressurized with 5 bar dihydrogen and stirred at 70 °C for 3 h. The resulting suspension is filtered, and the solvent is removed under reduced pressure. The residue is washed with *n*-hexane (3 · 5 mL). The product is not obtained purely according to the presence of decomposition products. A yield could not be determined. Single crystals are ontained by cooling the *n*-hexane washing solutions to –31°C.

^{1}H NMR (400 MHz, C$_6$D$_6$, RT, selected signals): δ 8.05 - 7.91 (m, 4H), 6.86 (s, 2H), 6.11 (d, *J* = 1.9 Hz, 2H, NC*HCH*N), 5.92 (d, *J* =1.9 Hz, 2H, NC*HCH*N), 2.91 (dt, *J* = 21.3 Hz, *J* = 5.5 Hz, 4H), 2.50 (s, 6H), 2.19 (s, 6H), 1.72 (s, 3H), 1.48 (s, 6H), -6.78 (dd, $^2J_{HPtrans}$ = 87.1 Hz, $^2J_{HPcis}$ =19.6 Hz, 2H, RuH).

^{31}P{^{1}H} NMR (162 MHz, C$_6$D$_6$, RT): δ 39.0 (s).

MS (LIFDI) *m/z* (%): 900 (100) [**20**]$^+$.

5.2.19 Synthesis of **21**
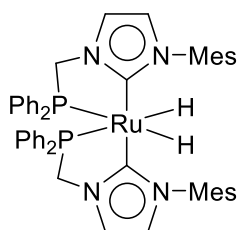
Chemical Formula: $C_{50}H_{52}N_4P_2Ru$

Molecular Weight: 872,01 g mol^{-1}

7 (50.0 mg, 49.6 µmol, 1.00 eq) and KO^{t}Bu (27.8 mg, 248 mmol, 5.00 eq) are suspended in 15 mL of dry and degassed benzene in a Fisher-Porter-bottle. The reaction vessel is pressurized with 5 bar dihydrogen and stirred at 70 °C for 3 h. The resulting suspension is filtered, and the solvent is removed under reduced pressure. The oily residue is dissolved in 10 mL of dry and degassed *n*-hexane and stirred for 20 min. **21** precipitates as a yellow powder in 75% (32 mg) yield.

¹H NMR (500 MHz, C$_6$D$_6$, RT): δ 7.82 (m, 4H), 7.18 (s, 2H, Ar-H$_{Mes}$), 7.10-6.91 (m, 18H, Ar-H), 6.73 (d, $^4J_{HH}$ = 2.0 Hz, 2H, Ar-H$_{Mes}$), 6.32 (d, $^4J_{HH}$ = 1.9 Hz, 2H, NC*H*C*H*N), 6.19 (t, $^4J_{HH}$ = 1.7 Hz, 2H, NC*H*C*H*N), 3.91 (d, $^2J_{HH}$ = 12.0 Hz, 2H, PC*H$_2$*N), 3.63 (dd, $^2J_{HH}$ = 12.0 Hz, $^2J_{HP}$ = 7.5 Hz, 2H, PC*H$_2$*N), 2.53 (s, 6H, Me$_{Mes}$), 2.39 (s, 6H, Me$_{Mes}$), 1.57 (s, 6H, Me$_{Mes}$), -6.57 (dd, $^2J_{HPtrans}$ = 98.3 Hz, $^2J_{HPcis}$ = 16.8 Hz, 2H, RuH).

¹³C NMR (125 MHz, C$_6$D$_6$, RT): δ 208.0 (t, $^2J_{CP}$ = 7.3 Hz, N*C*N), 143.9 (d, $^1J_{CP}$ = 24.0 Hz, q-Ar-C$_{Ph}$), 143.3 (d, $^1J_{CP}$ = 18.2 Hz, q-Ar-C$_{Ph}$), 140.8 (s, q-Ar-C$_{Mes}$), 138.4 (s, *o*-Ar-C$_{Mes}$), 136.5 (s, *p*-Ar-C$_{Mes}$), 135.5 (s, *o*-Ar-C$_{Mes}$), 134.1 (d, $^2J_{CP}$ = 16.3 Hz, *o*-Ar-C$_{Ph}$), 131.4 (d, J_{CP} = 13.2 Hz, *o*-Ar-C$_{Ph}$), 128.8 (s, *m*-Ar-C$_{Mes}$), 128.3 (s, m-Ar-C$_{Mes}$), 127.9 (m, *m*-Ar-C$_{Ph}$, *p*-Ar-C$_{Ph}$), 127.4 (d, $^3J_{CP}$ = 8.1 Hz, *m*-Ar-C$_{Ph}$), 127.3 (s, p-Ar-C$_{Ph}$) 119.8 (s, N*C*CN), 117.0 (d, $^3J_{CP}$ = 7.2 Hz, NC*C*N), 54.3 (d, $^1J_{CP}$ = 24.0 Hz, N*C*P), 21.5 (s, *p*-Me$_{Mes}$), 20.6 (s, *o*-Me$_{Mes}$), 18.9 (s, *o*-Me$_{Mes}$).

³¹P{¹H} NMR (162 MHz, C$_6$D$_6$, RT): δ 66.2 (s).

Elemental analysis calcd (%) for C$_{50}$H$_{52}$N$_4$P$_2$Ru: C, 68.87; H, 6.01; N, 6.43. Found: C, 69.14; H, 6.39; N, 6.12.

MS (LIFDI) *m/z* (%): 872 (100) [**21**]$^+$.

5.2.20 Synthesis of **23**

$$\text{Mes} - \overset{+}{N} \diagup\!\!\diagdown N \diagup\!\!\diagup \overset{+}{N}H_3 \quad \overset{-}{Br} \quad \overset{-}{Br}$$
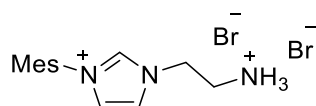
Chemical Formula: $C_{14}H_{21}Br_2N_3$
Molecular Weight: 391,15 g mol^{-1}

2-bromoethylamine hydrobromide (5.50 g, 26.8 mmol, 1.00 eq.) and K_2CO_3 (7.42 g, 53.7 mmol, 2.00 eq.) are added to a stirred solution of **1** (5.00 g, 26.8 mmol, 1.00 eq.) in toluene (120 mL). The reaction mixture is stirred for 1 d at 120 °C. After cooling to RT, the suspension is filtered, and the residue is suspended and stirred DCM (in 150 mL) for one hour. The suspension is filtered, the residue is washed with DCM (3 · 50 mL) and dried under reduced pressure. The off-white product is dissolved in DMF (100 mL), filtered and precipitated with Et_2O. **23** is obtained as a colorless powder in 95% (7.90 g) yield.

^{1}H-NMR (400 MHz, DMSO-d_6, 298 K): δ (ppm): 9.57 (s, 1H, NC*H*N), 8.36 (bs, 3H, N*H*$_3$), 8.21 (t, $^3J_{HH}$ = 1.8 Hz, 1H, NC*H*C*H*N), 7.98 (t, $^3J_{HH}$ = 1.8 Hz, 1H, NC*H*C*H*N), 7.13 (s, 2H, Ar-H$_{Mes}$), 4.62 (t, $^3J_{HH}$ = 6.1 Hz, 2H, NC*H*$_2$CH$_2$N), 3.53 (t, $^3J_{HH}$ = 6.1 Hz, 2H, NCH$_2$C*H*$_2$N), 2.32 (s, 3H, Ar-Me$_{Mes}$), 2.07 (s, 6H, Ar-Me$_{Mes}$).

5.2.21 Synthesis of **24**
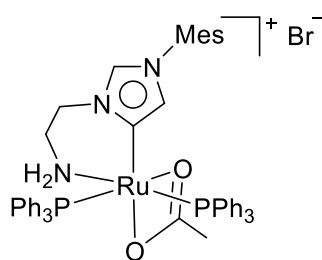
Chemical Formula: $C_{52}H_{52}N_2BrO_2P_2Ru$

Molecular Weight: 979,92 g mol^{-1}

6 (500 mg, 672 µmol, 1.00 eq.), **23** (342 mg, 874 µmol, 1.30 eq.) and K_2CO_3 (92.9 mg, 672 µmol, 1.00 eq.) are suspended in MeOH (20 mL) and stirred at 60 °C for 30 min. The resulting yellow suspension is filtered, and the solvent of the filtrate is evaporated under reduced pressure. The resulting yellow solid is dissolved in DCM (5 mL), filtered, and precipitated with 20 mL *n*-pentane. **24** is not obtained purely due to the presence of decomposition products.

^{1}H-NMR (400 MHz, CD_2Cl_2, 298 K): δ (ppm): 9.04 (s, 1H), 7.39 (t, $^3J_{HH}$ = 7.4 Hz, 3H), 7.22 (t, $^3J_{HH}$ = 7.6 Hz, 9H), 7.10 (t, $^3J_{HH}$ = 8.8 Hz, 6H), 7.04 (t, $^3J_{HH}$ = 7.4 Hz, 6H), 6.98 (s, 1H), 6.88 (t, $^3J_{HH}$ = 8.8 Hz, 7H), 5.27 (d, $^3J_{HH}$ = 1.6 Hz, 1H), 4.54-4.37 (m, 2H), 3.47-3.37 (m, 2H), 3.11 (bs, 1H), 2.72 (bs, 1H), 2.31 (s, 3H), 2.23 (s, 3H), 1.62 (s, 3H), 1.18 (s, 3H).

^{31}P-NMR (162 MHz, CD_2Cl_2, 298 K): δ (ppm): 56.1 (d, $^2J_{PP}$ = 32.8 Hz, 1P), 52.6 (d, $^2J_{PP}$ = 32.8 Hz, 1P).

5.3 Catalytic Reactions

5.3.1 TH / No sampling

In a typical experiment, the reactors are charged with ^{i}PrOH (4.9 mL), acetophenone (500 µmol) and the catalyst (0.1 mol%). The mixture is heated to 100 °C for 1 min and a 0.1 M solution of NaO^{i}Pr in ^{i}PrOH (100 µL, 10 µmol, 2 mol%) is added to the stirred mixture. At the required reaction times, the reactors are cooled using an ice bath. 500 µL aliquots are mixed with 100 µl of a solution of nitrobenzene in ^{i}PrOH (25.0 mg/mL). The mixture is then filtered over a short pad of silica and analyzed by gas chromatography.

5.3.2 TH / Sampling with Syringe

In a typical experiment, the reactor is charged with the catalyst (0.01 mol%) taken from a 1.00 mg/mL stock solution in DCM and dried under reduced pressure. ^{i}PrOH (9.6 mL) and the substrate (1.00 mmol) are added and the mixture is stirred and heated to the desired temperature for 2 min. The reaction is started by addition of a 0.1 M solution of NaO^{i}Pr in ^{i}PrOH (200 µL, 20.0 µmol, 2 mol%). At the required reaction times, aliquots of 0.5 mL are taken with a syringe and quenched in a cooled solution (0 °C) of diethyl ether. The samples are filtered over a short pad of silica and analyzed by gas chromatography.

5.3.3 TH / Fast Sampling with Teflon Cannula

In a typical experiment, the reactor is charged with the catalyst (0.01 mol%) taken from a 1.00 mg/mL stock solution in DCM and dried under reduced pressure. ^{i}PrOH (9.6 mL) and the substrate (1.00 mmol) are added and the mixture is stirred and heated to the desired temperature for 2 min. The reaction is started by addition of a 0.1 M solution of NaO^{i}Pr in ^{i}PrOH (200 µL, 20.0 µmol, 2 mol%). An argon overpressure of 0.2 mbar is applied and a teflon cannula is poked through the septum in order to have a constant argon counterflow. At the required reaction times, the cannula is shortly dipped into the reaction mixture and aliquots of about 0.2 mL are pumped through it according to the overpressure in the reactor. The samples are directly quenched in a cooled solution (0 °C) of diethyl ether. The samples are filtered over a short pad of silica and analyzed by gas chromatography.

5.3.4 Catalytic Oppenauer-type Oxidation

In a typical experiment, the reactor is charged with the catalyst taken from a 1.00 mg/mL stock solution in DCM and dried under reduced pressure. KO^{t}Bu (2 mol%), *tert*-butanol (4.6 mL) and the substrate 0.5 mmol are added and the mixture is stirred and heated to the desired temperature for 2 min. The reaction is started by addition of acetone (218 µL, 6.00 eq). At the required reaction times, aliquots of 0.3 mL are taken with a syringe and quenched in cooled (0 °C) diethyl ether. The samples are filtered over a short pad of silica and analyzed by gas chromatography. In the case of cholesterol as the

substrate, larger aliquots are taken and analyzed by ^{1}H NMR spectroscopy after evaporation of the solvent.

5.3.5 Neat catalytic Oppenauer-type Oxidation

In a typical experiment, the reactor is charged 380 µL of a 2.00 mg/mL stock solution of the catalyst in DCM. The solvent is removed under reduced pressure and the degassed alcohol (1.47 mmol) and KO^{t}Bu (2 mol%, 3.30 mg) are added. After stirring the mixture at 40 °C for 1 min, acetone (2.00 eq, 218 µl) is added as the reaction starter. Samples of 50µl are taken after at the required reaction times and quenched in cooled (0 °C) diethyl ether. The samples are filtered over a short pad of silica and analyzed by gas chromatography.

5.4 Single Crystal X-Ray Structure Determination.

5.4.1 General data.

X-ray crystallographic data were collected on different single crystal x-ray diffractometers with the following setups: [147]

1) a CCD detector (Bruker APEX II, κ-CCD), an FR591 rotating anode and a MONTEL mirror optic using the APEX2 software package

2) a CCD detector (Bruker APEX II, κ-CCD), a fine-focus sealed tube and a Triumph monochromator using the APEX2 software package

3) a CMOS detector (Bruker APEX III, κ-CMOS), a TXS rotating anode and a Helios optic using the APEX3 software package

4) a CMOS detector (Bruker APEX III, κ-CMOS), an IMS microsource and a Helios optic using the APEX3 software package

All measurements used MoK$_\alpha$ radiation (λ = 0.71073 Å). The measurements were performed on single crystals coated with perfluorinated ether. The crystal was fixed on top of a glass fiber or kapton micro sampler and frozen under a stream of cold nitrogen. A matrix scan was used to determine the initial lattice parameters. Reflections were corrected for Lorentz and polarisation effects, scan speed, and background using SAINT.[148] Absorption corrections, including odd and even ordered spherical harmonics were performed using SADABS.[148] Space group assignments were based upon systematic absences, E statistics, and successful refinement of the structures. Structures were solved by direct methods (SHELXS) or charge flipping (SHELXT) with the aid of successive difference Fourier maps, and were refined against all data using SHELXL-2014 in conjunction with SHELXLE.[149, 150] H atoms were calculated in ideal positions as follows: Methyl H atoms were refined as part of rigid rotating groups, with a C-H distance of 0.98 Å and U$_{iso(H)}$ = 1.5·U$_{eq(C)}$. Other H atoms were placed in calculated positions and refined using a riding model, with methylene and aromatic C-H distances of 0.99 Å and 0.95 Å, respectively, other C-H distances of 1.00 Å and U$_{iso(H)}$ = 1.2·U$_{eq(C)}$. Non-H atoms were refined with anisotropic displacement parameters. Full-matrix least-squares refinements were carried out by minimizing $\Sigma w(F_o^2 \ F_c^2)^2$ with SHELXL weighting scheme.[150] Neutral atom scattering factors for all atoms and anomalous dispersion corrections for the non-H atoms were taken from *International Tables for Crystallography*.[151] A split layer refinement was used for the disordered acetate and dppe ligand in the case of **14** and the disordered Ir(cod)Cl-moiety in the case of **17** and additional SIMU, DELU, RIGU and SAME restraints were employed to ensure convergence within chemically reasonable limits, if necessary. The unit cell of **7** contains four molecules of tetrahydrofuran and the unit cell of **15** contains

eight molecules of diethyl ether which were treated as a diffuse contribution to the overall scattering without specific atom positions by SQUEEZE/PLATON.[152] Images of the crystal structures were generated with Mercury.[153] CCDC 1860098-1860101 contain the supplementary crystallographic data for this paper. These data can be obtained free of charge *via* www.ccdc.cam.ac.uk/data_request/cif, or by emailing data_request@ccdc.cam.ac.uk, or by contacting The Cambridge Crystallographic Data Centre, 12 Union Road, Cambridge CB2 1EZ, UK; fax: +44 1223 336033.

5.4.2 Detailed crystallographic data.

5.4.2.1 Crystallographic Data of Complex 9 (CCDC 1860098).

Sample and Crystal Data

Chemical formula	$C_{62}H_{68}Cl_5IrN_4O_2P_2Ru$
Formula weight	1433.66 g mol^{-1}
Temperature	123(2) K
Wavelength	0.71073 Å
Crystal size	0.035 mm × 0.204 mm × 0.240 mm
Crystal habit	Fluorescent intense orange plate
Crystal System	Triclinic
Space group	P −1
Unit cell dimensions	a = 10.8823(5) Å, b = 14.2847(7) Å, c = 20.7956(10) Å, α = 78.593(2) °, β = 81.810(2) °, γ = 70.502(2) °
Volume	2976.9(2) Å^3
Z	2
Density (calculated)	1.599 g cm^{-3}
Absorption coefficient	2.812 mm^{-1}
F(000)	1440

Data Collection and Structure Refinement

Diffractometer	Bruker Kappa Apex II CCD
Radiation Source	FR591 rotating anode, Mo
Theta range for data collection	1.69 to 25.35 °
Index ranges	−12≤h≤13, −17≤k≤17, −25≤l≤25

Reflections collected	100492
Independent reflections	10875 [R(int) = 0.0345]
Coverage of independent reflections	99.8%
Max. and min. transmission	0.9080 and 0.5520
Data / restraints / parameters	10875 / 0 / 701
Goodness-of-fit on F^2	1.043
Δ/σ_{max}	0.001
Final R indices (8880 data; I>2σ(I))	R_1 = 0.0269, wR_2 = 0.0682
Final R indices (all data)	R_1 = 0.0308, wR_2 = 0.0711
Largest diff. max. min.	1.44 and −0.96 e$Å^{-3}$

5.4.2.2 Crystallographic Data of Complex **14** (CCDC 1860101).

Sample and Crystal Data	
Chemical formula	$C_{64.05}H_{74.12}BrN_2O_{4.51}P_3Ru$
Formula weight	1218.10 g mol^{-1}
Temperature	100(2) K
Wavelength	0.71073 Å
Crystal size	0.149 mm × 0.209 mm × 0.230 mm
Crystal habit	Clear yellow fragment
Crystal System	Monoclinic
Space group	P 1 2$_1$/c 1
Unit cell dimensions	a = 11.7840(15) Å, b = 20.151(3) Å, c = 26.982(4) Å, α = 90 °, β = 102.446(8) °, γ = 90 °
Volume	6256.6(14) Å^3
Z	4
Density (calculated)	1.293 g cm^{-3}
Absorption coefficient	1.013 mm^{-1}
F(000)	2531

Data Collection and Structure Refinement	
Diffractometer	Bruker Kappa Apex II CCD
Radiation Source	TXS rotating anode, Mo
Theta range for data collection	2.16 to 25.35 °
Index ranges	$-14 \leq h \leq 14, -24 \leq k \leq 24, -32 \leq l \leq 32$
Reflections collected	121874
Independent reflections	11452 [R(int) = 0.0491]

Coverage of independent reflections	99.9%
Max. and min. transmission	0.8640 and 0.8000
Data / restraints / parameters	11452 / 180 / 710
Goodness-of-fit on F^2	1.052
Δ/σ_{max}	0.001
Final R indices (8880 data; I>2σ(I))	R_1 = 0.0383, wR_2 = 0.1074
Final R indices (all data)	R_1 = 0.0440, wR_2 = 0.1118
Largest diff. max. min.	1.204 and −0.880 eÅ^{-3}

5.4.2.3 Crystallographic Data of Complex **15** (CCDC 1860099).

Sample and Crystal Data	
Chemical formula	$C_{54}H_{53}AgBrN_2O_2P_3Ru$
Formula weight	1143.74 g mol^{-1}
Temperature	100(2) K
Wavelength	0.71073 Å
Crystal size	0.263 mm × 0.330 mm × 0.432 mm
Crystal habit	Clear yellow fragment
Crystal System	Monoclinic
Space group	P 1 2$_1$/c 1
Unit cell dimensions	a = 15.193(3) Å, b = 14.891(3) Å, c = 26.067(4) Å, α = 90 °, β = 92.246(8) °, γ = 90 °
Volume	5893(2) Å^3
Z	4
Density (calculated)	1.289 g cm^{-3}
Absorption coefficient	1.384 mm^{-1}
F(000)	2312

Data Collection and Structure Refinement	
Diffractometer	Bruker D8 Kappa Apex II
Radiation Source	Fine-focus sealed tube, Mo
Theta range for data collection	1.92 to 25.02 °
Index ranges	-18≤h≤18, -17≤k≤17, -31≤l≤31
Reflections collected	93474
Independent reflections	10401 [R(int) = 0.0394]
Coverage of independent reflections	100.0%

Max. and min. transmission	0.7120 and 0.5860
Data / restraints / parameters	10401 / 488 / 764
Goodness-of-fit on F^2	1.037
Δ/σ_{max}	0.001
Final R indices (8880 data; I>2σ(I))	R_1 = 0.0447, wR_2 = 0.1283
Final R indices (all data)	R_1 = 0.0534, wR_2 = 0.1352
Largest diff. max. min.	0.821 and −2.364 eÅ^{-3}

5.4.2.4 Crystallographic Data of Complex **16**.

Sample and Crystal Data	
Chemical formula	$C_{58}H_{63}AgClN_2O_3P_3Ru$
Formula weight	1173.40 g mol^{-1}
Temperature	100(2) K
Wavelength	0.71073 Å
Crystal size	0.118 mm × 0.134 mm × 0.196 mm
Crystal habit	Yellow fragment
Crystal System	Monoclinic
Space group	P 1 21/c 1
Unit cell dimensions	a = 15.0653(15) Å, b = 14.8221(13)Å,
	c = 25.870(3) Å, α = 90 °, β = 92.312(3) °, γ = 90 °
Volume	5772(1) Å^3
Z	4
Density (calculated)	1.350 g cm^{-3}
Absorption coefficient	0.773 mm^{-1}
F(000)	2408

Data Collection and Structure Refinement	
Diffractometer	Bruker Kappa Apex II CCD
Radiation Source	FR591 rotating anode, Mo
Theta range for data collection	2.46 to 25.35 °
Index ranges	$-18 \leq h \leq 18$, $-17 \leq k \leq 17$, $-31 \leq l \leq 31$
Reflections collected	157726
Independent reflections	10560 [R(int) = 0.0316]
Coverage of independent reflections	99.9%

Max. and min. transmission	0.9140 and 0.8630
Data / restraints / parameters	10560 / 826 / 824
Goodness-of-fit on F^2	1.159
Δ/σ_{max}	0.001
Final R indices (8880 data; $I>2\sigma(I)$)	$R_1 = 0.0365$, $wR_2 = 0.0814$
Final R indices (all data)	$R_1 = 0.0408$, $wR_2 = 0.0834$
Largest diff. max. min.	0.798 and -0.967 eÅ^{-3}

5.4.2.5 Crystallographic Data of Complex **17** (CCDC 1860101).

Sample and Crystal Data

Chemical formula	$C_{62}H_{65}ClIrN_2O_2P_3Ru$
Formula weight	1291.79 g mol^{-1}
Temperature	100(2) K
Wavelength	0.71073 Å
Crystal size	0.094 mm × 0.225 mm × 0.256 mm
Crystal habit	Clear yellow fragment
Crystal System	Triclinic
Space group	P −1
Unit cell dimensions	a = 12.0683(8) Å, b = 13.5766(10) Å,
	c = 18.7301(13) Å, α = 76.489(2) °,
	β = 83.192(2) °, γ = 77.258(2) °
Volume	2903.2(4) Å^3
Z	2
Density (calculated)	1.478 g cm^{-3}
Absorption coefficient	2.722 mm^{-1}
F(000)	1300

Data Collection and Structure Refinement

Diffractometer	Bruker D8 Venture Duo IMS
Radiation Source	IMS microsource, Mo
Theta range for data collection	2.24 to 26.02 °
Index ranges	$-14 \leq h \leq 14$, $-16 \leq k \leq 16$, $-23 \leq l \leq 23$
Reflections collected	100821
Independent reflections	11416 [R(int) = 0.0408]

Coverage of independent reflections	99.9%
Max. and min. transmission	0.7840 and 0.5430
Data / restraints / parameters	11416 / 375 / 744
Goodness-of-fit on F^2	1.091
Δ/σ_{max}	0.001
Final R indices (8880 data; $I>2\sigma(I)$)	$R_1 = 0.0340$, $wR_2 = 0.0772$
Final R indices (all data)	$R_1 = 0.0389$, $wR_2 = 0.0799$
Largest diff. max. min.	2.274 and -1.036 eÅ^{-3}

5.4.2.6 Crystallographic Data of Complex **18 (**CCDC 1936771).

Sample and Crystal Data	
Chemical formula	$C_{55.90}H_{60.83}BrCl_{3.82}N_4O_2P_2Ru$
Formula weight	1199.13 g mol^{-1}
Temperature	100(2) K
Wavelength	0.71073 Å
Crystal size	0.150 mm × 0.207 mm × 0.245 mm
Crystal habit	Clear yellow fragment
Crystal System	Monoclinic
Space group	P 1 21/n 1
Unit cell dimensions	a = 12.4759(10) Å, b = 19.5565(15) Å, c = 23.6332(19) Å, α = 90 °, β = 104.776(2) °, γ = 90 °
Volume	5575.5(8) Å^3
Z	4
Density (calculated)	1.429 g cm^{-3}
Absorption coefficient	1.282 mm^{-1}
F(000)	2457

Data Collection and Structure Refinement	
Diffractometer	Bruker D8 Venture Duo IMS
Radiation Source	IMS microsource, Mo
Theta range for data collection	2.27 to 25.03 °
Index ranges	−14≤h≤14, −23≤k≤23, −28≤l≤28
Reflections collected	129622
Independent reflections	9848 [R(int) = 0.0511]

Coverage of independent reflections	99.9%
Max. and min. transmission	0.8310 and 0.7440
Data / restraints / parameters	9848 / 111 / 753
Goodness-of-fit on F^2	1.248
Δ/σ_{max}	0.002
Final R indices (8880 data; I>2σ(I))	R_1 = 0.0648, wR_2 = 0.1313
Final R indices (all data)	R_1 = 0.0702, wR_2 = 0.1332
Largest diff. max. min.	2.319 and $-$1.058 eÅ^{-3}

5.4.2.7 Crystallographic Data of Complex **20** (CCDC 1936772).

Sample and Crystal Data	
Chemical formula	$C_{104}H_{112}N_8P_4Ru_2$
Formula weight	1800.03 g mol^{-1}
Temperature	100(2) K
Wavelength	0.71073 Å
Crystal size	0.059 mm × 0.089 mm × 0.170 mm
Crystal System	triclinic
Space group	P −1
Unit cell dimensions	a = 11.7066(4) Å, b = 19.2827(5) Å, c = 20.5490(7) Å, α = 103.0290(10) °, β = 92.5120(10) °, γ = 90.7780(10) °
Volume	4513.6(2) Å^3
Z	2
Density (calculated)	1.324 g cm^{-3}
Absorption coefficient	0.458 mm^{-1}
F(000)	1880

Data Collection and Structure Refinement	
Diffractometer	Bruker D8 Venture
Radiation Source	TXS rotating anode, Mo
Theta range for data collection	2.08 to 25.01 °
Index ranges	−13≤h≤13, −22≤k≤22, −24≤l≤24
Reflections collected	185271
Independent reflections	15878 [R(int) = 0.0771]
Coverage of independent reflections	99.8%

Max. and min. transmission	0.9730 and 0.9260
Data / restraints / parameters	15878 / 211 / 1172
Goodness-of-fit on F^2	1.019
Δ/σ_{max}	0.002
Final R indices (8880 data; I>2σ(I))	R_1 = 0.0288, wR_2 = 0.0631
Final R indices (all data)	R_1 = 0.0433, wR_2 = 0.0680
Largest diff. max. min.	0.940 and −0.457 eÅ^{-3}

5.4.2.8 Crystallographic Data of Complex **21**.

Sample and Crystal Data

Chemical formula	$C_{53}H_{59}N_4O_2P_2Ru$
Formula weight	915.05 g mol^{-1}
Temperature	100(2) K
Wavelength	0.71073 Å
Crystal size	0.074 mm × 0.125 mm × 0.152 mm
Crystal habit	Clear yellow fragment
Crystal System	Monoclinic
Space group	P 1 21/n 1
Unit cell dimensions	a = 10.998(8) Å, b = 18.491(13) Å,
	c = 23.171(17) Å, α = 90 °,
	β = 99.88(2) °, γ = 90 °
Volume	4642.(6) Å^3
Z	4
Density (calculated)	1.309 g cm^{-3}
Absorption coefficient	0.447 mm^{-1}
F(000)	1916

Data Collection and Structure Refinement

Diffractometer	Bruker D8 Venture
Radiation Source	TXS rotating anode, Mo
Theta range for data collection	2.20 to 25.03 °
Index ranges	$-13 \leq h \leq 13, -22 \leq k \leq 22, -27 \leq l \leq 27$
Reflections collected	130843
Independent reflections	8179 [R(int) = 0.0950]

Coverage of independent reflections	99.9%
Max. and min. transmission	0.9680 and 0.9350
Data / restraints / parameters	8179 / 2 / 555
Goodness-of-fit on F^2	1.113
Δ/σ_{max}	0.001
Final R indices (8880 data; I>2σ(I))	R_1 = 0.0421, wR_2 = 0.1034
Final R indices (all data)	R_1 = 0.0621, wR_2 = 0.1146
Largest diff. max. min.	0.697 and −0.540 eÅ^{-3}

5.4.2.9 Crystallographic Data of Complex **24**.

Sample and Crystal Data	
Chemical formula	$C_{55}H_{58}BrCl_6N_3O_2P_2Ru$
Formula weight	1248.66 g mol^{-1}
Temperature	100(2) K
Wavelength	0.71073 Å
Crystal size	0.081 mm × 0.160 mm × 0.563 mm
Crystal habit	Clear yellow fragment
Crystal System	Monoclinic
Space group	P −1
Unit cell dimensions	a = 13.8255(6) Å, b = 14.2018(7) Å, c = 14.8115(7) Å, α = 106.002(2) °, β = 91.124(2) °, γ = 91.004(2) °
Volume	2794.2(2) Å^3
Z	2
Density (calculated)	1.484 g cm^{-3}
Absorption coefficient	1.383 mm^{-1}
F(000)	1272

Data Collection and Structure Refinement	
Diffractometer	Bruker D8 Venture
Radiation Source	TXS rotating anode, Mo
Theta range for data collection	2.29 to 25.35 °
Index ranges	−16≤h≤16, −17≤k≤17, −17≤l≤17
Reflections collected	87726
Independent reflections	10219 [R(int) = 0.0629]

Coverage of independent reflections	99.9%
Max. and min. transmission	0.8960 and 0.5100
Data / restraints / parameters	10219 / 75 / 663
Goodness-of-fit on F^2	1.009
Δ/σ_{max}	0.032
Final R indices (8880 data; I>2σ(I))	$R_1 = 0.0256$, $wR_2 = 0.0668$
Final R indices (all data)	$R_1 = 0.0319$, $wR_2 = 0.0699$
Largest diff. max. min.	0.645 and −1.654 eÅ^{-3}

5.5 Buried Volume Calculations

In order to determine the buried volume of compound **3** and **4** DFT calculations were performed using Gaussian-16[154] with the pure functional B97[155] and Grimme's D3BJ dispersion[156]. The double-ζ basis set def2-SVP[157] is applied for all atoms and Ru is treated by the Stuttgart-Dresden effective core potential[158] as implemented in Gaussian. No symmetry or internal coordinate constraints were used during optimization. The reported geometries are true ground states verified by the absence of negative eigenvalues in the vibrational frequency calculations. The buried volume is calculated by the SambVca tool[159] using scaled Van-der-Waals radii (1.17) and a sphere radius of 3.5 and 5 Å respectively. Hydrogens are neglected and the acetate in compound **3** and the hydrides in **4** are removed.

6. References

1.   J. W. Erisman, M. A. Sutton, J. Galloway, Z. Klimont and W. Winiwarter, *Nat. Geosci.*, 2008, **1**, 636-639.
2.   W. Crookes, *Science*, 1898, **8**, 561-575.
3.   F. Haber and R. LeRossignol, Making ammonia, Badische Anilin- & Soda-Fabrik AG, Germany, US971501, 1910.
4.   *Catalyst Market Size, Share & Trends Analysis Report*, grandviewresearch.com/industry-analysis/catalyst-market, accessed 10 June 2019.
5.   C. Han, E. Sahle-Demessie, A. Shah, S. Nawaz, L.-u. Rahman, N. McGuinness, S. Pillai, H. Choi, D. Dionysiou and M. Nadagouda, in *Sustainable Catalysis: Energy-Efficient Reactions and Applications*, eds. R. Luque and F. L.-Y. Lam, Wiley-VCH Verlag GmbH & Co. KGaA, Weinheim, Germany, 2018.
6.   R. Schlögl, in *Handbook of Heterogeneous Catalysis*, Wiley-VCH Verlag GmbH & Co. KGaA, Weinheim, Germany, 2nd edn., 2008.
7.   J. A. Dumesic, G. W. Huber and M. Boudart, in *Handbook of Heterogeneous Catalysis*, Wiley-VCH Verlag GmbH & Co. KGaA, Weinheim, Germany, 2008.
8.   W. A. Herrmann and B. Cornils, *Angew. Chem., Int. Ed.*, 1997, **36**, 1048-1067.
9.   B. Cornils and W. A. Herrmann, in *Applied Homogeneous Catalysis with Organometallic Compounds*, Wiley-VCH Verlag GmbH, Weinheim, Germany, 2008, pp. 1-27.
10.   O. Roelen, Chemische Verwertungsgesellschaft mbH, Oberhausen, DE 849.548 (9381 1952).
11.   R. Noyori and S. Hashiguchi, *Acc. Chem. Res.*, 1997, **30**, 97-102.
12.   F. E. Hahn and M. C. Jahnke, *Angew. Chem., Int. Ed.*, 2008, **47**, 3122-3172.
13.   M. N. Hopkinson, C. Richter, M. Schedler and F. Glorius, *Nature*, 2014, **510**, 485-496.
14.   A. Igau, H. Grutzmacher, A. Baceiredo and G. Bertrand, *J. Am. Chem. Soc.*, 1988, **110**, 6463-6466.
15.   A. J. Arduengo, III, R. L. Harlow and M. Kline, *J. Am. Chem. Soc.*, 1991, **113**, 361-363.
16.   H.-W. Wanzlick and E. Schikora, *Chemische Berichte*, 1961, **94**, 2389-2393.
17.   K. Öfele, *J. Organometal. Chem.*, 1968, **12**, 42-43.
18.   H. W. Wanzlick and H. J. Schoenherr, *Angew. Chem., Int. Ed.*, 1968, **7**, 141-142.
19.   M. Albrecht, *Adv. Organomet. Chem.*, 2014, **62**, 111-158.
20.   P. L. Arnold and S. Pearson, *Coord. Chem. Rev.*, 2007, **251**, 596-609.
21.   R. H. Crabtree, *Coord. Chem. Rev.*, 2013, **257**, 755-766.
22.   O. Schuster, L. Yang, H. G. Raubenheimer and M. Albrecht, *Chem. Rev.*, 2009, **109**, 3445-3478.
23.   J. B. Waters and J. M. Goicoechea, *Coord. Chem. Rev.*, 2015, **293-294**, 80-94.
24.   C. E. Ellul, M. F. Mahon, O. Saker and M. K. Whittlesey, *Angew. Chem., Int. Ed.*, 2007, **46**, 6343-6345.
25.   S. Gründemann, A. Kovacevic, M. Albrecht, J. W. Faller Robert and H. Crabtree, *Chem. Commun.*, 2001, 2274-2275.
26.   G. A. Filonenko, E. Cosimi, L. Lefort, M. P. Conley, C. Coperet, M. Lutz, E. J. M. Hensen and E. A. Pidko, *ACS Catal.*, 2014, **4**, 2667-2671.
27.   S. Saha, T. Ghatak, B. Saha, H. Doucet and J. K. Bera, *Organometallics*, 2012, **31**, 5500-5505.
28.   L. Benhamou, J. Wolf, V. Cesar, A. Labande, R. Poli, N. Lugan and G. Lavigne, *Organometallics*, 2009, **28**, 6981-6993.
29.   A. Prades, M. Viciano, M. Sanau and E. Peris, *Organometallics*, 2008, **27**, 4254-4259.
30.   W. A. Herrmann, M. Elison, J. Fischer, C. Köcher and G. R. J. Artus, *Angew. Chem., Int. Ed.*, 1995, **34**, 2371-2374.
31.   W. A. Herrmann, *Angew. Chem., Int. Ed.*, 2002, **41**, 1290-1309.
32.   R. H. Grubbs, A. G. Wenzel, D. J. O'Leary and E. Khosravi, in *Catalyst Development and Mechanism*, ed. R. H. Grubbs, WIley-VCH Verlag GmbH & Co. KGaA, Weinheim, Germany, 2015.

33. G. C. Vougioukalakis and R. H. Grubbs, *Chem. Rev.*, 2010, **110**, 1746-1787.
34. L. Benhamou, E. Chardon, G. Lavigne, S. Bellemin-Laponnaz and V. Cesar, *Chem. Rev.*, 2011, **111**, 2705-2733.
35. O. Kühl, *Chem. Soc. Rev.*, 2007, **36**, 592-607.
36. T. Dröge and F. Glorius, *Angew. Chem., Int. Ed.*, 2010, **49**, 6940-6952.
37. H. V. Huynh, *Chem. Rev.*, 2018, **118**, 9457-9492.
38. S. Hameury, P. de Fremont and P. Braunstein, *Chem. Soc. Rev.*, 2017, **46**, 632-733.
39. K. Riener, S. Haslinger, A. Raba, M. P. Högerl, M. Cokoja, W. A. Herrmann and F. E. Kühn, *Chem. Rev.*, 2014, **114**, 5215-5272.
40. O. Kühl, in *Functionalised N-Heterocyclic Carbene Complexes*, John Wiley & Sons, Ltd, 2010, pp. 39-53.
41. A. T. Normand and K. J. Cavell, *Eur. J. Inorg. Chem.*, 2008, 2781-2800.
42. M. Hollering, D. T. Weiss, M. J. Bitzer, C. Jandl and F. E. Kühn, *Inorg. Chem.*, 2016, **55**, 6010-6017.
43. M. J. Bitzer, F. E. Kühn and W. Baratta, *J. Catal.*, 2016, **338**, 222-226.
44. M. J. Bitzer, A. Pöthig, C. Jandl, F. E. Kühn and W. Baratta, *Dalton Trans.*, 2015, **44**, 11686-11689.
45. L. Pardatscher, M. J. Bitzer, C. Jandl, J. W. Kück, R. M. Reich, F. E. Kühn and W. Baratta, *Dalton Trans.*, 2019, **48**, 79-89.
46. J. Witt, A. Pöthig, F. E. Kühn and W. Baratta, *Organometallics*, 2013, **32**, 4042-4045.
47. P. Braunstein and F. Naud, *Angew. Chem., Int. Ed.*, 2001, **40**, 680-699.
48. P. L. Arnold, S. A. Mungur, A. J. Blake and C. Wilson, *Angew. Chem., Int. Ed.*, 2003, **42**, 5981-5984.
49. S. A. Mungur, S. T. Liddle, C. Wilson, M. J. Sarsfield and P. L. Arnold, *Chem. Commun.*, 2004, 2738-2739.
50. D. S. McGuinness and K. J. Cavell, *Organometallics*, 2000, **19**, 741-748.
51. K. Riener, M. J. Bitzer, A. Pöthig, A. Raba, M. Cokoja, W. A. Herrmann and F. E. Kühn, *Inorg. Chem.*, 2014, **53**, 12767-12777.
52. E. Aldeco-Perez, A. J. Rosenthal, B. Donnadieu, P. Parameswaran, G. Frenking and G. Bertrand, *Science*, 2009, **326**, 556-559.
53. P. L. Arnold and S. T. Liddle, *Organometallics*, 2006, **25**, 1485-1491.
54. A. El-Hellani and V. Lavallo, *Angew. Chem., Int. Ed.*, 2014, **53**, 4489-4493.
55. Y. Wang, M. Y. Abraham, R. J. Gilliard, Jr., P. Wei, J. C. Smith and G. H. Robinson, *Organometallics*, 2012, **31**, 791-793.
56. Y. Wang, Y. Xie, M. Y. Abraham, P. Wei, H. F. Schaefer III, P. v. R. Schleyer and G. H. Robinson, *J. Am. Chem. Soc.*, 2010, **132**, 14370-14372.
57. D. R. Armstrong, S. E. Baillie, V. L. Blair, N. G. Chabloz, J. Diez, J. Garcia-Alvarez, A. R. Kennedy, S. D. Robertson and E. Hevia, *Chem. Sci.*, 2013, **4**, 4259-4266.
58. M. R. Crittall, C. E. Ellul, M. F. Mahon, O. Saker and M. K. Whittlesey, *Dalton Trans.*, 2008, 4209-4211.
59. A. A. Danopoulos, D. Pugh and J. A. Wright, *Angew. Chem., Int. Ed.*, 2008, **47**, 9765-9767.
60. S. Kronig, E. Theuergarten, C. G. Daniliuc, P. G. Jones and M. Tamm, *Angew. Chem., Int. Ed.*, 2012, **51**, 3240-3244.
61. A. Krüger, E. Kluser, H. Müller-Bunz, A. Neels and M. Albrecht, *Eur. J. Inorg. Chem.*, 2012, **2012**, 1394-1402.
62. R. A. Musgrave, R. S. P. Turbervill, M. Irwin and J. M. Goicoechea, *Angew. Chem., Int. Ed.*, 2012, **51**, 10832-10835.
63. R. A. Musgrave, R. S. P. Turbervill, M. Irwin, R. Herchel and J. M. Goicoechea, *Dalton Trans.*, 2014, **43**, 4335-4344.
64. C. Pranckevicius and D. W. Stephan, *Chem. – Eur. J.*, 2014, **20**, 6597-6602.
65. U. J. Scheele, S. Dechert and F. Meyer, *Chem. – Eur. J.*, 2008, **14**, 5112-5115.

66. Y. Wang, Y. Xie, M. Y. Abraham, R. J. Gilliard, P. Wei, C. F. Campana, H. F. Schaefer III, P. v. R. Schleyer and G. H. Robinson, *Angew. Chem., Int. Ed.*, 2012, **51**, 10173-10176.

67. J. B. Waters, R. S. P. Turbervill and J. M. Goicoechea, *Organometallics*, 2013, **32**, 5190-5200.

68. S. Sabater, J. A. Mata and E. Peris, *Chem. - Eur. J.*, 2012, **18**, 6380-6385.

69. S. Sabater, J. A. Mata and E. Peris, *Organometallics*, 2012, **31**, 6450-6456.

70. S. Sabater, J. A. Mata and E. Peris, *Eur. J. Inorg. Chem.*, 2013, **2013**, 4764-4769.

71. S. Sabater, J. A. Mata and E. Peris, *Nat. Commun.*, 2013, **4**, 2553.

72. A. Zanardi, R. Corberan, J. A. Mata and E. Peris, *Organometallics*, 2008, **27**, 3570-3576.

73. A. Zanardi, J. A. Mata and E. Peris, *Organometallics*, 2009, **28**, 1480-1483.

74. A. Zanardi, J. A. Mata and E. Peris, *J. Am. Chem. Soc.*, 2009, **131**, 14531-14537.

75. A. Zanardi, J. A. Mata and E. Peris, *Chem. – Eur. J.*, 2010, **16**, 10502-10506.

76. A. Zanardi, J. A. Mata and E. Peris, *Chem. – Eur. J.*, 2010, **16**, 13109-13115.

77. S. Gonell, M. Poyatos, J. A. Mata and E. Peris, *Organometallics*, 2012, **31**, 5606-5614.

78. E. Mas-Marza, J. A. Mata and E. Peris, *Angew. Chem., Int. Ed.*, 2007, **46**, 3729-3731.

79. J. A. Mata, F. E. Hahn and E. Peris, *Chem Sci*, 2014, **5**, 1723-1732.

80. S. Diez-Gonzalez, N. Marion and S. P. Nolan, *Chem. Rev.*, 2009, **109**, 3612-3676.

81. E. Peris, *Chem. Rev.*, 2018, **118**, 9988-10031.

82. D. Wang and D. Astruc, *Chem. Rev.*, 2015, **115**, 6621-6686.

83. D. A. Hey, R. M. Reich, W. Baratta and F. E. Kühn, *Coord. Chem. Rev.*, 2018, **374**, 114-132.

84. H. Meerwein and R. Schmidt, *Justus Liebigs Ann. Chem.*, 1925, **444**, 221-238.

85. W. Ponndorf, *Angew. Chem.*, 1926, **39**, 138-143.

86. A. Verley, *Bull. Soc. Chim. Fr.*, 1925, **37**, 537-542.

87. C. F. de Graauw, J. A. Peters, H. van Bekkum and J. Huskens, *Synthesis*, 1994, 1007-1017.

88. Y. M. Y. Haddad, H. B. Henbest, J. Husbands and T. R. B. Mitchell, *Proc. Chem. Soc.*, 1964, 361.

89. M. J. Trocha-Grimshaw and H. B. Henbest, *Chem. Commun.*, 1967, 544.

90. Y. Sasson and J. Blum, *Tetrahedron Lett.*, 1971, 2167-2170.

91. Y. Sasson and J. Blum, *J. Org. Chem.*, 1975, **40**, 1887-1896.

92. R. L. Chowdhury and J. E. Bäckvall, *J. Chem. Soc., Chem. Commun.*, 1991, 1063-1064.

93. C. Gunanathan and D. Milstein, *Chem. Rev.*, 2014, **114**, 12024-12087.

94. G. Chelucci, S. Baldino and W. Baratta, *Coord. Chem. Rev.*, 2015, **300**, 29-85.

95. S. Facchetti, V. Jurcik, S. Baldino, S. Giboulot, H. G. Nedden, A. Zanotti-Gerosa, A. Blackaby, R. Bryan, A. Boogaard, D. B. McLaren, E. Moya, S. Reynolds, K. S. Sandham, P. Martinuzzi and W. Baratta, *Organometallics*, 2016, **35**, 277-287.

96. W. Baratta and P. Rigo, *Eur. J. Inorg. Chem.*, 2008, 4041-4053.

97. F. Foubelo, C. Najera and M. Yus, *Tetrahedron: Asymmetry*, 2015, **26**, 769-790.

98. A. C. Hillier, H. M. Lee, E. D. Stevens and S. P. Nolan, *Organometallics*, 2001, **20**, 4246-4252.

99. M. Albrecht, J. R. Miecznikowski, A. Samuel, J. W. Faller and R. H. Crabtree, *Organometallics*, 2002, **21**, 3596-3604.

100. A. A. Danopoulos, S. Winston and W. B. Motherwell, *Chem. Commun.*, 2002, 1376-1377.

101. M. Poyatos, J. A. Mata, E. Falomir, R. H. Crabtree and E. Peris, *Organometallics*, 2003, **22**, 1110-1114.

102. W. Baratta, J. Schuetz, E. Herdtweck, W. A. Herrmann and P. Rigo, *J. Organomet. Chem.*, 2005, **690**, 5570-5575.

103. S. Gladiali and R. Taras, in *Modern Reduction Methods*, Wiley-VCH Verlag GmbH & Co. KGaA, Weinheim, Germany, 2008, pp. 135-157.

104. R. Noyori, M. Yamakawa and S. Hashiguchi, *J. Org. Chem.*, 2001, **66**, 7931-7944.

105. S. E. Clapham, A. Hadzovic and R. H. Morris, *Coord. Chem. Rev.*, 2004, **248**, 2201-2237.

106. A. Aranyos, G. Csjernyik, K. J. Szabo and J.-E. Bäckvall, *Chem. Commun.*, 1999, 351-352.

107. J.-E. Bäckvall, *J. Organomet. Chem.*, 2002, **652**, 105-111.

108. Y. R. S. Laxmi and J.-E. Bäckvall, *Chem. Commun.*, 2000, 611-612.

109. H. O. House, *Modern Synthetic Reactions (The Organic Chemistry Monograph Series). 2nd ed*, Benjamin, 1972.

110. C. R. Graves, B.-S. Zeng and S. T. Nguyen, *J. Am. Chem. Soc.*, 2006, **128**, 12596-12597.
111. T. Ooi, T. Miura, Y. Itagaki, H. Ichikawa and K. Maruoka, *Synthesis*, 2002, 279-291.
112. R. V. Oppenauer, *Recl. Trav. Chim. Pays-Bas Belg.*, 1937, **56**, 137-144.
113. G. Z. Wang and J. E. Bäckvall, *J. Chem. Soc., Chem. Commun.*, 1992, 337-339.
114. M. L. S. Almeida, M. Beller, G. Z. Wang and J. E. Bäckvall, *Chem. – Eur. J.*, 1996, **2**, 1533-1536.
115. M. L. S. Almeida, P. Kocovsky and J. E. Bäckvall, *J. Org. Chem.*, 1996, **61**, 6587-6590.
116. S. Gauthier, R. Scopelliti and K. Severin, *Organometallics*, 2004, **23**, 3769-3771.
117. C. S. Yi, T. N. Zeczycki and I. A. Guzei, *Organometallics*, 2006, **25**, 1047-1051.
118. W. M. Du, L. D. Wang, P. Wu and Z. K. Yu, *Chem. – Eur. J.*, 2012, **18**, 11550-11554.
119. S. Manzini, C. A. Urbina-Blanco and S. P. Nolan, *Organometallics*, 2013, **32**, 660-664.
120. C. M. Nicklaus, P. H. Phua, T. Buntara, S. Noel, H. J. Heeres and J. G. de Vries, *Adv. Synth. Catal.*, 2013, **355**, 2839-2844.
121. S. Manzini, J. A. Fernandez-Salas and S. P. Nolan, *Acc. Chem. Res.*, 2014, **47**, 3089-3101.
122. Q. Wang, W. Du, T. Liu, H. Chai and Z. Yu, *Tetrahedron Lett.*, 2014, **55**, 1585-1588.
123. R. Labes, C. Battilocchio, C. Mateos, G. R. Cumming, O. de Frutos, J. A. Rincon, K. Binder and S. V. Ley, *Org. Process Res. Dev.*, 2017, **21**, 1419-1422.
124. C. K. Hill and J. F. Hartwig, *Nat. Chem.*, 2017, **9**, 1213-1221.
125. F. Hanasaka, K.-i. Fujita and R. Yamaguchi, *Organometallics*, 2004, **23**, 1490-1492.
126. A. N. Ajjou and J.-L. Pinet, *Can. J. Chem.*, 2005, **83**, 702-710.
127. K. Fujita and R. Yamaguchi, *Synlett*, 2005, 560-571.
128. F. Hanasaka, K.-i. Fujita and R. Yamaguchi, *Organometallics*, 2006, **25**, 4643-4647.
129. M. G. Coleman, A. N. Brown, B. A. Bolton and H. Guan, *Adv. Synth. Catal.*, 2010, **352**, 967-970.
130. S. A. Moyer and T. W. Funk, *Tetrahedron Lett.*, 2010, **51**, 5430-5433.
131. K.-i. Fujita, T. Yoshida, Y. Imori and R. Yamaguchi, *Org. Lett.*, 2011, **13**, 2278-2281.
132. T. C. Johnson, G. J. Clarkson and M. Wills, *Organometallics*, 2011, **30**, 1859-1868.
133. A. Quintard and J. Rodriguez, *Angew. Chem., Int. Ed.*, 2014, **53**, 4044-4055.
134. Y. Nishibayashi, A. Yamauchi, G. Onodera and S. Uemura, *J. Org. Chem.*, 2003, **68**, 5875-5880.
135. Y. Zhao and S. R. Gilbertson, *Org. Lett.*, 2014, **16**, 1033-1035.
136. A. Plikhta, A. Pöthig, E. Herdtweck and B. Rieger, *Inorg. Chem.*, 2015, **54**, 9517-9528.
137. R. W. Mitchell, A. Spencer and G. Wilkinson, *Dalton Trans.*, 1973, 846-854.
138. J. Wolf, A. Labande, J.-C. Daran and R. Poli, *J. Organomet. Chem.*, 2006, **691**, 433-443.
139. C. Yang, H. M. Lee and S. P. Nolan, *Org. Lett.*, 2001, **3**, 1511-1514.
140. M. V. Baker, D. H. Brown, R. A. Haque, B. W. Skelton and A. H. White, *Dalton Trans.*, 2004, 3756-3764.
141. H. M. J. Wang and I. J. B. Lin, *Organometallics*, 1998, **17**, 972-975.
142. J. Heinze, *Angew. Chem., Int. Ed.*, 1984, **23**, 831-847.
143. L. Pardatscher, B. J. Hofmann, P. J. Fischer, S. M. Hölzl, R. M. Reich, F. E. Kühn and W. Baratta, Unpublished Results, Manuscript in Preparation.
144. R. Buhaibeh, O. A. Filippov, A. Bruneau-Voisine, J. Willot, C. Duhayon, D. A. Valyaev, N. Lugan, Y. Canac and J.-B. Sortais, *Angew. Chem., Int. Ed.*, 2019, Ahead of Print.
145. M. Käß, J. Hohenberger, M. Adelhardt, E. M. Zolnhofer, S. Mossin, F. W. Heinemann, J. Sutter and K. Meyer, *Inorg. Chem.*, 2014, **53**, 2460-2470.
146. W. L. F. Armarego and C. Chai, *Purification of Laboratory Chemicals, 5th Edition*, Butterworth-Heinemann, 2003.
147. *APEX suite of crystallographic software, APEX 2, version 2008.4*, APEX 2, Version 2014-9.0 and APEX 3, Version 2015-5.2, Bruker AXS Inc., Madison, Wisconsin, USA, 2014/2015.
148. V. A. a. A. a. S. SAINT, Versions 2014/5 and 2016/2, Bruker AXS Inc., Madison, Wisconsin, USA, 2014/2016.
149. C. B. Hübschle, G. M. Sheldrick and B. Dittrich, *J. Appl. Crystallogr.*, 2011, **44**, 1281-1284.
150. G. M. Sheldrick, *Acta Cryst. C*, 2015, **71**, 3-8.

151. *International Tables for Crystallography*, A. J. Wilson, Ed.; Kluwer Academic Publishers: Dordrecht, The Nederlans, 1992; Vol. C, Tables 6.1.1.4 (pp 500-502), 4.2.6.8 (pp 219-222), and 4.2.4.2 (pp 193-199).

152. A. L. Spek, *Acta Cryst. C*, 2015, **71**, 9-18.

153. C. F. B. Macrae, I. J.; Chisholm, J. A.; Edgington, P. R.; McCabe, P.; Pidcock, E.; Rodriguez-Monge, L.; Taylor, R.; van de Streek, J.; Wood, P. A., *J. Appl. Cryst.*, 2008, **41**, 466-470.

154. M. J. Frisch, G. W. Trucks, H. B. Schlegel, G. E. Scuseria, M. A. Robb, J. R. Cheeseman, G. Scalmani, V. Barone, G. A. Petersson, H. Nakatsuji, X. Li, M. Caricato, A. V. Marenich, J. Bloino, B. G. Janesko, R. Gomperts, B. Mennucci, H. P. Hratchian, J. V. Ortiz, A. F. Izmaylov, J. L. Sonnenberg, Williams, F. Ding, F. Lipparini, F. Egidi, J. Goings, B. Peng, A. Petrone, T. Henderson, D. Ranasinghe, V. G. Zakrzewski, J. Gao, N. Rega, G. Zheng, W. Liang, M. Hada, M. Ehara, K. Toyota, R. Fukuda, J. Hasegawa, M. Ishida, T. Nakajima, Y. Honda, O. Kitao, H. Nakai, T. Vreven, K. Throssell, J. A. M. Jr., J. E. Peralta, F. Ogliaro, M. J. Bearpark, J. J. Heyd, E. N. Brothers, K. N. Kudin, V. N. Staroverov, T. A. Keith, R. Kobayashi, J. Normand, K. Raghavachari, A. P. Rendell, J. C. Burant, S. S. Iyengar, J. Tomasi, M. Cossi, J. M. Millam, M. Klene, C. Adamo, R. Cammi, J. W. Ochterski, R. L. Martin, K. Morokuma, O. Farkas, J. B. Foresman and D. J. Fox, *Wallingford*, CT, 2016.

155. S. Grimme, *Journal of Computational Chemistry*, 2006, **27**, 1787-1799.

156. S. Grimme, S. Ehrlich and L. Goerigk, *Journal of Computational Chemistry*, 2011, **32**, 1456-1465.

157. A. Schäfer, H. Horn and R. Ahlrichs, *The Journal of Chemical Physics*, 1992, **97**, 2571-2577.

158. A. Bergner, M. Dolg, W. Küchle, H. Stoll and H. Preuß, *Molecular Physics*, 1993, **80**, 1431-1441.

159. L. Falivene, R. Credendino, A. Poater, A. Petta, L. Serra, R. Oliva, V. Scarano and L. Cavallo, *Organometallics* 2016, **35**, 2286-2293.

Complete List of Publications

3. *Cationic abnormal N-heterocyclic carbene ruthenium complexes as suitable precursors for the synthesis of heterobimetallic compounds*
    L. Pardatscher, M. J. Bitzer, C. Jandl, J. W. Kück, R. M. Reich, F. E. Kühn and W. Baratta, *Dalton Trans.* **2019**, *48*, 79-89.

2. Abnormal N-heterocyclic carbenes as ligands in catalytic transfer hydrogenation and as central modules in heterobimetallic complexes
    L. Pardatscher, M. Bitzer, R. M. Reich, W. Baratta and F. Kühn
    Talk, 256th National Meeting and Exposition of the American Chemical Society, Boston, Massachusetts, USA

1. Hydrogen Production and Storage on a Formic Acid/Bicarbonate Platform using Water-Soluble N-Heterocyclic Carbene Complexes of Late Transition Metals
    D. Jantke[#], **L. Pardatscher**[#], M. Drees, M. Cokoja, W. A. Herrmann, F. E. Kühn, *ChemSusChem* **2016**, *9*, 2849-2854
    [#] these authors contributed equally to this work
    This publication was already published during the master's thesis.

Eidesstattliche Erklärung

Ich erkläre an Eides statt, dass ich die bei der promotionsführenden Einrichtung

TUM Graduate School

der TUM zur Promotionsprüfung vorgelegte Arbeit mit dem Titel:

Abnormal N-Heterocyclic Carbene Ligands in Heterobimetallic Complexes and Ruthenium Catalyzed Hydrogen Transfer Reactions

in <u>Fakultät für Chemie, Molekulare Katalyse</u>

   Fakultät, Institut, Lehrstuhl, Klinik, Krankenhaus, Abteilung

unter der Anleitung und Betreuung durch: <u>Prof. Dr. Fritz E. Kühn</u> ohne sonstige Hilfe erstellt und bei der Abfassung nur die gemäß § 6 Ab. 6 und 7 Satz 2 angebotenen Hilfsmittel benutzt habe.

☒ Ich habe keine Organisation eingeschaltet, die gegen Entgelt Betreuerinnen und Betreuer für die Anfertigung von Dissertationen sucht, oder die mir obliegenden Pflichten hinsichtlich der Prüfungsleistungen für mich ganz oder teilweise erledigt.

☒ Ich habe die Dissertation in dieser oder ähnlicher Form in keinem anderen Prüfungsverfahren als Prüfungsleistung vorgelegt.

☐ Die vollständige Dissertation wurde in _____ veröffentlicht. Die promotionsführende Einrichtung

_____

hat der Veröffentlichung zugestimmt.

☒ Ich habe den angestrebten Doktorgrad noch nicht erworben und bin nicht in einem früheren Promotionsverfahren für den angestrebten Doktorgrad endgültig gescheitert.

☐ Ich habe bereits am _____ bei der Fakultät für _____ der

Hochschule _____ unter

Vorlage einer Dissertation mit dem Thema _____

_____ die

Zulassung zur Promotion beantragt mit dem Ergebnis: _____

Die öffentlich zugängliche Promotionsordnung der TUM ist mir bekannt, insbesondere habe ich die Bedeutung von § 28 (Nichtigkeit der Promotion) und § 29 (Entzug des Doktorgrades) zur Kenntnis genommen. Ich bin mir der Konsequenzen einer falschen Eidesstattlichen Erklärung bewusst.

Mit der Aufnahme meiner personenbezogenen Daten in die Alumni-Datei bei der TUM bin ich

☒ einverstanden,   ☐ nicht einverstanden.

Garching bei München, 08.07.2019, Lorenz Pardatscher